Spring 1-1-2017

Nonlinear Dispersive Elastic Waves in Solids: Exact, Approximate, and Numerical Solutions

Romik Khajehtourian
University of Colorado at Boulder, r.khajehtourian@gmail.com

Nonlinear Dispersive Elastic Waves in Solids: Exact, Approximate, and Numerical Solutions

by

Romik Khajehtourian

B.S., Mechanical Engineering, University of Sistan and Baluchestan, 2007

M.S., Aerospace Engineering, Sharif University of Technology, 2011

M.S., Applied Mathematics, University of Colorado Boulder, 2017

A thesis submitted to the

Faculty of the Graduate School of the

University of Colorado in partial fulfillment

of the requirements for the degree of

Doctor of Philosophy

Smead Department of Aerospace Engineering Sciences

2017

This thesis entitled:
Nonlinear Dispersive Elastic Waves in Solids: Exact, Approximate, and Numerical Solutions
written by Romik Khajehtourian
has been approved for the Smead Department of Aerospace Engineering Sciences

Professor Mahmoud I. Hussein (Chair)

Professor Mark Ablowitz

Professor Alireza Doostan

Professor John Evans

Professor Carlos Felippa

Professor Mark Hoefer

Date

The final copy of this thesis has been examined by the signatories, and we find that both the content and the form meet acceptable presentation standards of scholarly work in the above mentioned discipline.

Khajehtourian, Romik (Ph.D., Aerospace Engineering Sciences)

Nonlinear Dispersive Elastic Waves in Solids: Exact, Approximate, and Numerical Solutions

Thesis directed by Professor Mahmoud I. Hussein

Wave motion lies at the heart of many disciplines in the physical sciences and engineering. For example, problems and applications involving light, sound, heat, or fluid flow are all likely to involve wave dynamics at some level. A particular class of problems is concerned with the propagation of elastic waves in a solid medium, such as a fiber-reinforced composite material responding to vibratory excitations, or soil and rock admitting seismic waves moments after the onset of an earthquake, or phonon transport in a semiconducting crystal like silicon. Regardless of the type of wave, the dispersion relation provides a fundamental characterization of the elastodynamic properties of the medium.

The first part of the dissertation examines the propagation of a large-amplitude elastic wave in a one-dimensional homogeneous medium with a focus on the effects of inherent nonlinearities on the dispersion relation. Considering a thin rod, where the thickness is small compared to the wavelength, an exact, closed-form formulation is presented for the treatment of two types of nonlinearity in the strain-displacement gradient relation: Green-Lagrange and Hencky. The derived relation is then verified by direct time-domain simulations, examining both instantaneous dispersion (by direct observation) and short-term, pre-breaking dispersion (by Fourier transformation). A high-order perturbation analysis is also conducted yielding an explicit analytical space-time solution, which is shown to be spectrally accurate. The results establish a perfect match between theory and simulation and reveal that regardless of the strength of the nonlinearity, the dispersion relation fully embodies all information pertaining to the nonlinear harmonic generation mechanism that unfolds as an arbitrary-profiled wave evolves in the medium.

In the second part of the dissertation, the analysis is extended to a continuous periodic thin rod exhibiting multiple phases or embedded local resonators. The extended method, which

is based on a standard transfer-matrix formulation augmented with a nonlinear enrichment at the constitutive material level, yields an approximate band structure that is accurate to an amplitude that is roughly one eighth of the unit cell length. This approach represents a new paradigm for examining the balance between periodicity and nonlinearity in shaping the nature of wave motion.

Dedicated to my parents,

Goharik and Avetis

Acknowledgements

First of all, I would like to express my greatest debt of gratitude to my adviser Professor Mahmoud I. Hussein for his great support throughout the research and also for taking the time and putting the effort in teaching and educating me about different aspects of research and academia. He has been a great role model to me, and has provided constant encouragement throughout the course of my graduate studies. I am very grateful to him for directing me to become a better researcher.

I would also like to convey my deepest gratitude to my dissertation committee members, Professor Carlos Felippa who has been one of the best teachers I have ever had, Professor Mark Ablowitz and Professor Mark Hoefer for the fruitful discussions that we had together throughout the last three years, Professor Alireza Doostan and Professor John Evans for their consistent support. I wish to express my gratitude to all the professors whose courses I have taken during my time at CU-Boulder. I am also very grateful for the support I received from the NSF CAREER Grant No. 1254931.

I would like to express my gratitude to my colleagues at CU-Boulder for the in-depth discussions that helped in shaping the work and their valuable comments on the manuscript. Thank you Dimitri, Hossein, Clémence, Michael, and Osama.

I want to extend a special thanks to my friends Hamid, Farhad, Azadeh, and Arash who made my time in Boulder very memorable. We have traveled very long miles and have seen all colors of Colorado together. I owe a happy hour or two to you.

Finally, the greatest thanks of all goes to my wonderful parents Goharik and Avetis, my caring

sisters, Greta and Elena, my supporting brothers, Roberto and Vahe, and the next generation of artists and scientists in our family, Dion, Stephanie and Maya. Nothing would have been possible without your support and love.

Contents

Figures

Figure

Chapter 1

Introduction

1.1 Elastic waves

There are many different types of waves in nature and wave motion has been an overlapping theme throughout physics since the early days of Newton and Maxwell. Study of waves exists in nearly all of the traditional branches of physics: mechanics, electromagnetism, thermofluids, quantum mechanics, to name a few. Wave propagation in solid materials is a topic of interest in mechanics with a number of engineering applications. The study of structures and materials involving elastic wave phenomena includes, but not limited to, the fields of seismology, e.g. the study of earthquakes and the propagation of elastic waves through the Earth, crack propagation in rocks, ultrasonics, response to impact loads, and vibrational excitations in structures. For an arbitrary transient load, the fundamental characteristics of the response can be predicted by elastodynamic analysis by considering only a small portion of the medium through which an excitation will propagate. To motivate our discussion, consider the 1D linear wave equation

$$\frac{\partial^2 u}{\partial t^2} = c^2 \frac{\partial^2 u}{\partial x^2}, \tag{1.1}$$

and its general solution

$$u(x,t) = f(x \pm ct), \tag{1.2}$$

which represents waves of displacement u propagating with velocity c in the positive and negative x directions as a function of time t. The quasi-static velocity of a wave is determined by the physical

properties of the medium through which it propagates. In the case of wave propagation in a one-dimensional (1D) solid material, $c = \sqrt{Y/\rho}$, where Y is the modulus of elasticity or rigidity and ρ is the density.

Equation (1.1) represent both longitudinal and transverse waves with the value of the elasticity modulus being defined accordingly. In longitudinal waves, the particles of the medium vibrate in the direction of the wave propagation such as primary waves in earthquakes. In transverse waves, the particles of the medium vibrate perpendicular to the direction of the wave propagation, such as shear waves in an earthquake or vibratory waves in a taut string. Only longitudinal waves can propagate in liquids and gases, which are elastic with respect to volume but not with respect to shape. Sound pressure waves are an example of this class of wave motion.

The harmonic elastic wave solution, Eq. (1.2), is characterized by the amplitude, phase, frequency and wavelength. A special feature of elastic waves governed by Eq. (1.1) is that their phase and group velocities are independent of the wave amplitude and geometry. In these waves, the elongation of the medium is small and the displacement is related to the strain through an infinitesimal strain gradient. Also, strain is a linear function of the stress, that is Hooke's law. When the elongation becomes relatively large, however, then the displacements exceed the infinitesimal strain limits and the strain-displacement relationship can be defined by one of the Seth-Hill's finite-strain measures. In this case, there will be one or more additional terms in the Eq. (1.1) accounting for the finite deformation [1]. Similarly, one may consider a highly elastic material such as rubber. When stresses grow large, the deformation in this case exceeds what is predicted by Hooke's law, even with geometrically small deformations. In this case, Eq. (1.1) will again have additional terms, now accounting for the material nonlinearity. Geometric and/or material nonlinearity causes the phase and group velocities to be dependent on the wave amplitude.

Mathematically, the wave equation is classified under the category of hyperbolic equations in the theory of linear partial differential equations (PDEs). Hyperbolic equations are among the most challenging to solve since sharp changes in their solutions remain and can reflect off boundaries. This is unlike, for example, the heat equation, where solutions are smooth as long as the initial

conditions are smooth. This added complexity naturally reflects in the analytical or numerical treatment needed to obtain a solution.

In this dissertation, nonlinear dispersive elastic waves in solids are studied in depth. Emphasis is placed on longitudinal waves. However, the main concepts and formulations may easily be extended to transverse waves. A major part of this report is devoted to the notion of an amplitude-dependent nonlinear dispersion relation in an elastic medium. Amplitude-dependent waves are analyzed by the three classical categories of analysis: analytical and exact, analytical and approximate, and numerical.

1.2 Dispersion in elastic media

In this section, we present a brief introduction to dispersion in a linear system, a periodic rod, and a nonlinear system, a homogeneous rod. In the linear system, the effect of periodicity is introduced by the Transfer Matrix (TM) method, an implicit way of calculating dispersion for periodic media. In the nonlinear system, a nonlinear strain-displacement relationship, i.e., finite deformation, alters Eq. (1.1) allowing us to derive the corresponding explicit dispersion relation in each homogeneous medium forming the periodic unit cell.

1.2.1 Linear dispersion relation, e.g., from periodicity

Bloch's theorem [2] provides the underlying mathematical framework for obtaining the elastic band structure (i.e., dispersion curves) for a periodic material. There are several approaches for applying the theorem to a unit cell modeled as a continuum. Here, we briefly describe the TM method (for a background on the method and further details, see Refs. [3–5]).

We begin our dynamic analysis of a periodic material with the equation of motion stated in Eq. (1.1). As mentioned earlier, we restrict ourselves to a 1D model, e.g., a thin rod, for which the equation of motion is the same as Eq. (1.1). For simplicity, we assume that the cross-sectional area of the rod is non-varying with x. We consider a homogeneous, linearly elastic 1D rod of infinite extent (having no global boundaries at which waves may reflect), and apply a plane wave solution

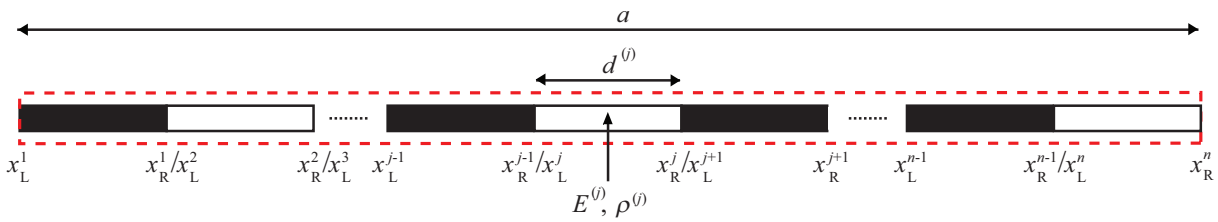

Figure 1.1: Continuous model of a one-dimensional two-phased phononic crystal viewed as a periodic thin rod.

of the form

$$u(x,t) = A\mathrm{e}^{\mathrm{i}(\kappa x - \omega t)}, \tag{1.3}$$

where A is the wave amplitude, κ is the wave number, ω is the temporal frequency of the traveling wave, and $\mathrm{i} = \sqrt{-1}$. Here, we make another assumption about the cross-sectional dimensions of the rod, namely, that they are much smaller than the wavelengths of all waves considered in the analysis. Substituting Eq. (1.3) into Eq. (1.1) provides the linear dispersion relation

$$E\kappa^2 = \rho\omega^2. \tag{1.4}$$

This approach may also be applied to heterogeneous media provided the heterogeneity is periodic. In this case, we refer to Eq. (1.3) as Bloch's theorem [where $A = A(x,\kappa)$], and it suffices to analyze only a single unit cell representing the unique segment that is repeated to generate the periodic medium and to apply periodic boundary conditions to this segment. In Fig. 1.1, we present a simple bi-material model of a 1D phononic crystal in the form of a layered periodic rod (where the unit cell is enclosed in a red dashed box). The spatial lattice spacing of the 1D periodic material is denoted by the constant a. The same analysis may also be applied to a unit cell with a stepwise varying cross-sectional area, but this case will not be considered here.

For an arbitrary homogeneous layer j in the unit cell, the associated material properties, which are constant, are denoted as $E^{(j)}$ and $\rho^{(j)}$. The longitudinal velocity in layer j is therefore $c^{(j)} = \sqrt{E^{(j)}/\rho^{(j)}}$. The layer is bordered by layer $j-1$ on the left and layer $j+1$ on the right. Denoting the thickness of an arbitrary layer by $d^{(j)}$, the cell length is $a = \sum_{j=1}^{n} d^{(j)}$ for a unit cell with n layers. Following this notation, the solution to Eq. (1.1) is formed from the superposition of

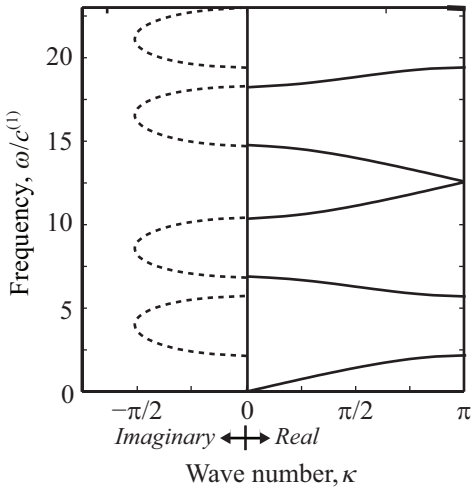

Figure 1.2: Frequency band structure for a 1D phononic crystal. Solid curves represent pass bands, and dashed curves represent stop-bands.

forward (transmitted) and backward (reflected) traveling waves with a harmonic time dependence,

$$u(x,t) = [A_+^{(j)} \mathrm{e}^{\mathrm{i}\kappa^{(j)}x} + A_-^{(j)} \mathrm{e}^{-\mathrm{i}\kappa^{(j)}x}]\mathrm{e}^{-\mathrm{i}\omega t}, \tag{1.5}$$

where $\kappa^{(j)} = \omega/c^{(j)}$ is the layer wave number. We can use Eq. (1.5) to form the TM and solve an eigenvalue problem to get the structure band of the system. For details see Ref. [5]. To demonstrate the effect of periodicity, we consider the same geometric features as the periodic bi-material rod in Fig. 1.1 and the following ratio of material properties: $c^{(2)}/c^{(1)} = 2$ and $\rho^{(2)}/\rho^{(1)} = 3$. Furthermore, we consider a bi-layered unit cell in which $d^{(2)} = d^{(1)}$. The results are shown in Fig. 1.2 for a phononic crystal of size $a = 1$.

1.2.2 Linear dispersion relation, e.g., from lateral inertia

The equation of motion for a 1D nonlinear homogeneous thin rod under uniaxial stress can be derived by Hamilton's Principle (Fig. 1.3). Hamilton's Principle requires a functional of the Lagrangian density $\mathcal{L}$ (which contains the medium's elastic dynamic information) to reach its minimum value, that is

$$\delta \int_{t_0}^{t} \mathcal{L} dt = 0. \tag{1.6}$$

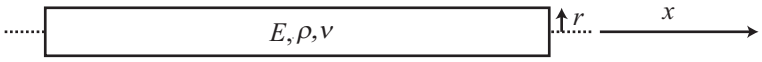

Figure 1.3: Continuous model of a 1D homogeneous medium with infinite length.

The Lagrangian is formed by $\mathcal{L} = \mathcal{T} - \mathcal{U}$. Here we do not account for external non-conservative forces and moments. The symbols $\mathcal{T}$ and $\mathcal{U}$ denote the kinetic and elastic strain energy densities of the system, respectively. Considering infinitesimal strain $\epsilon = \partial u\ \partial x$, the density of the kinetic energy of longitudinal motion is

$$\mathcal{T} = \frac{1}{2}\rho(\frac{\partial u}{\partial t})^2 + \frac{1}{2}\rho\nu^2 r^2(\frac{\partial^2 u}{\partial x t})^2, \tag{1.7}$$

and the elastic strain energy density is

$$\mathcal{U} = \frac{1}{2}\sigma\epsilon. \tag{1.8}$$

For the stress-strain relation, we consider Hooke's law, i.e., $\sigma = E\epsilon$, where σ and ϵ are the uniaxial stress and finite strain, respectively.

If we substitute the Lagrangian density into the Euler-Lagrange equation with displacement u being a single function and time and position being the dual variables,

$$\frac{\partial}{\partial x}\frac{\partial \mathcal{L}}{\partial u_x} + \frac{\partial}{\partial t}\frac{\partial \mathcal{L}}{\partial u_t} - \frac{\partial^2}{\partial x \partial t}\frac{\partial \mathcal{L}}{\partial u_{xt}} = 0, \tag{1.9}$$

Eq. (1.1) becomes

$$\frac{\partial^2 u}{\partial t^2} = c^2\frac{\partial^2 u}{\partial x^2} + \nu^2 r^2 \frac{\partial^4 u}{\partial t t x x}, \tag{1.10}$$

where $(.)_{,x}$ denotes a partial derivative with respect to position. By solving this equation we obtain the exact dispersion relation,

$$\omega_{\text{li}} = \frac{\omega}{\sqrt{1 + \nu^2 r^2 \kappa^2}}. \tag{1.11}$$

where ω is the frequency based on infinitesimal strain,

$$\omega(\kappa) = c|\kappa|. \tag{1.12}$$

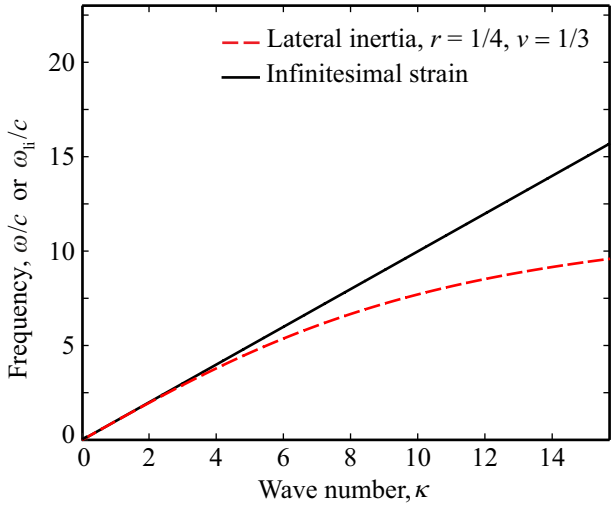

Figure 1.4: Frequency dispersion curves for a 1D homogeneous elastic medium. The lateral inertia dispersion relation is based on Eq. (1.11); the infinitesimal strain dispersion relation is based on Eq. (4.30).

By taking the limit, $\lim_{r\to 0}\omega_{\rm li}$, in Eq. (1.11), Eq. (1.12) is recovered which is the standard linear dispersion relation for a 1D homogeneous elastic medium or a thin rod [6]. Dispersion Curves for both infinitesimal and finite strains are shown in Fig. 1.4 .

1.2.3 Non-linear dispersion relation, e.g., from finite strain

Considering a thin rod (Fig. 1.3, when $r \to 0$), we again use Hamilton's Principle to derive he equation of motion. As an example, we consider the Green-Lagrange finite-strain relation from the Seth-Hill family of strains

$$\epsilon = \frac{\partial u}{\partial x} + \frac{1}{2}(\frac{\partial u}{\partial x})^2, \tag{1.13}$$

but upcoming derivations can extend to any other type of finite-strain measure. The density of the kinetic energy of longitudinal motion is

$$\mathcal{T} = \frac{1}{2}\rho(\frac{\partial u}{\partial t})^2, \tag{1.14}$$

and the elastic strain energy density is

$$\mathcal{U} = \frac{1}{2}E(\frac{\partial u}{\partial x})^2 + \frac{1}{2}E(\frac{\partial u}{\partial x})^3 + \frac{1}{8}E(\frac{\partial u}{\partial x})^4. \tag{1.15}$$

If we substitute the Lagrangian density into the Euler-Lagrange equation, Eq. (1.1) becomes

$$\frac{\partial^2 u}{\partial t^2} = c^2 \frac{\partial^2 u}{\partial x^2} + \frac{c^2}{2}\frac{\partial}{\partial x}(3(\frac{\partial u}{\partial x})^2 + (\frac{\partial u}{\partial x})^3). \tag{1.16}$$

Defining $\bar{u} = u_{,x}$ Eq. (1.16) becomes

$$\frac{\partial^2 \bar{u}}{\partial t^2} = c^2 \frac{\partial^2 \bar{u}}{\partial x^2} + \frac{c^2}{2}\frac{\partial^2}{\partial x^2}(3\bar{u}^2 + \bar{u}^3), \tag{1.17}$$

which is the equation of motion with respect to displacement gradient. Following the steps proposed in Ref. [1] we get the exact dispersion relation,

$$\omega_{\text{fin}}(\kappa; B) = \sqrt{\frac{2 + 3B|\kappa| + (B\kappa)^2}{2}}\omega. \tag{1.18}$$

By taking the limit, $\lim_{B\to 0} \omega_{\text{fin}}(\kappa; B)$, in Eq. (1.18), Eq. (1.12) is recovered which is the standard linear dispersion relation for a 1D homogeneous elastic medium or a thin rod [6]. Dispersion curves for both infinitesimal and finite strains are shown in Fig. 1.5. Later, in Section 2.2, we derive the exact dispersion relation considering both sources introduced in Sections 1.2.2 and 1.2.3. Also in Section 4.4 combining both effects of periodicity and nonlinearity introduced in Sections 1.2.1 and 1.2.3, respectively, are discussed.

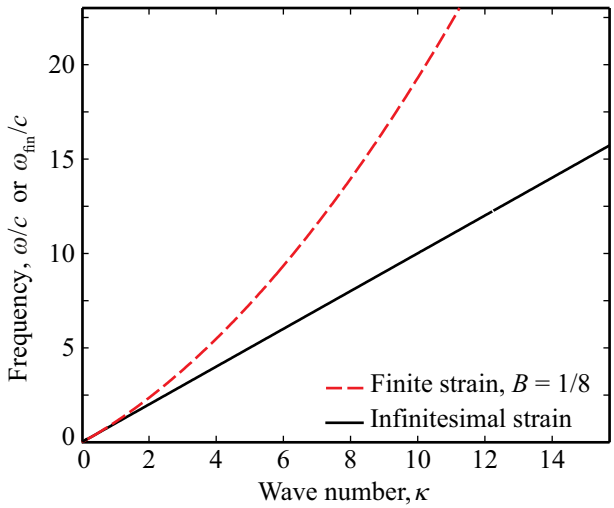

Figure 1.5: Frequency dispersion curves for a 1D homogeneous elastic medium [1]. The finite-strain dispersion relation is based on Eq. (1.18); the infinitesimal strain dispersion relation is based on Eq. (4.30).

1.3 Motivation

Aside from dissipation, the main factors that affect the propagation of elastic waves are nonlinearity and dispersion. Nonlinearity introduces harmonic generation where the energy of the primary mode transfers to other modes, representing sub or super harmonics of the primary mode. This causes sharp overfalls that appear in the moving wave profile. Linear dispersive effects, such as the presence of periodicity as discussed in Section 1.2.1, softens the wave profile due to the difference in the phase velocity of the various harmonic components. Nonlinearity and/or linear dispersive effects will cause a non-dispersive medium to become dispersive [1]. In this case, the relation between the frequency and the wavenumber is no longer a linear relation.

Most classical studies deal with dispersive media by employing perturbation techniques to explore the dispersion relation. Furthermore, often the effect of the dispersion is viewed as a linear effect which is a separate from the effects of nonlinearity. On the other hand, only a handful of theoretical studies on dispersive elastic media have been reported and still there is not a general framework to study dispersion due to nonlinear effects, especially for strong nonlinearity.

The goal of this dissertation is to establish a general analysis framework for the investigation of the effects of nonlinearity on the dispersion relation for elastic waves, with a focus on 1D problems. In addition to the development of exact solutions for several types of nonlinearity, perturbation and numerical analysis are also conducted to (1) verify the exact solutions, and (2) to gain further understanding of the *fundamental meaning of the concept of a nonlinear dispersion relation.* For example, how does the results of a direct numerical simulation, revealing nonlinear behavior in space and time, correlate with the corresponding nonlinear dispersion relation, especially when the nonlinearity is strong? How does the nonlinear dispersion relation implicitly capture information about both short term (instant) effects, and medium term (pre-breaking) effects, such as harmonic generation? The goal is also to extend the developed nonlinear formulation to periodic materials such as such as phononic crystals and locally resonant elastic metamaterials [7]. Lastly, the dissertation aims to discuss the possibility of extending the ideas and theory developed to other types of

nonlinear waves such as optical waves and shallow water waves.

1.4 Literature search

In the following subsections, a focused literature search is provided concerning dispersion in homogeneous elastic media among the broader field of physics, linear and nonlinear elastic phononic crystals, as well as metamaterials.

1.4.1 Dispersion in homogeneous media

Understanding of wave propagation is key to many branches of physics. In the study of waves, the knowledge of the wavevector-frequency dispersion relation provides valuable information that is often used to gain insights onto a range of properties [8]. While the vast majority of contemporary studies of dispersion are based on linear governing equations, there are studies that address the effects on the dispersion that arises from nonlinear quantities [9–12]. For an inherently nonlinear medium, as the wave amplitude becomes sufficiently large, the linearization procedure breaks down and nonlinear dispersion relations (NDR) are induced by interactions among waves. For example, nonlinear dispersion caused by weak turbulences is an ubiquitous phenomenon observed in various situations from fluid surface waves [13] to plasma waves [14]. In particular, the NDR for a thin vibrating plate under the Föppl-von Kármán equation is derived and investigated experimentally leading to corrections being added to the linear dispersion relation. [15–17]. Lee *et al* considered the Majda-McLaughlin-Tabak model of turbulent dynamics, omitted the linear term in the governing equations, and derived effective and approximate NDR to describe the dispersion arising merely due to the nonlinear terms [18]. Aside from weak turbulent theory, there are other origins which lead to NDR. Lie *et al* studied the weak nonlinearities of the wave equation under a nonlinear constitutive relation in 1D waveguides using the spectral finite element method [19]. Ganesh and Gonella analysed a 1D wave equation with weakly nonlinear stiffness in a periodic chain using a perturbation method [20]. In a recent study, Abedinnasab and Hussein derived the exact NDR for a thin rod accounting for both quadratic and cubic terms and omitting the Rayleigh-Love correction,

representing the wave equation under finite deformation [1].

1.4.2 Dispersion in phononic crystals and elastic metamaterials

Phononic crystals (PCs) are elastic materials with prescribed phonon wave propagation properties. While the term "phonon" is formally used in the physical sciences to describe vibration states in condensed matter at the atomic scale, in the present context, we use it to broadly describe elastic wave propagation modes. Like crystalline materials, a phononic material has local intrinsic properties and is therefore mathematically treated as a medium that is spatially extended to infinity. Compared to a homogeneous and geometrically uniform elastic continuum, a phononic material exhibits rich and unique dynamical properties due to the presence of some form of non-homogeneity and/or non-uniformity in either an ordered or disordered manner. In the ordered case, phononic materials are constructed from a repeated array of identical *unit cells* which enables the calculation of the elastic band structure for a given topological configuration. This direct exposure, and access, to the inherent dynamical properties of phononic materials has vigorously chartered a new direction in materials physics, at a multitude of scales, and has already begun to impact numerous applications ranging from vibration control [21,22], through subwavelength sound focusing [23,24] and cloaking [25,26], to reducing the thermal conductivity of semiconductors [27–29] and stabilizing a wall-bounded flow [30]. A discussion of applications and references are provided in Refs. [7,31,32], and recent special journal issues on the topic assemble some of the latest advances in the field [33,34].

For a given choice of unit-cell geometry and/or type and distribution of constituent materials, PCs can produce absolute band gaps due to Bragg scattering where acoustic/elastic waves are forbidden to propagate [35–37]. However, in order to open band gaps in the low frequency range of up to a few hundred kHz, the dimension of a periodic structure tends to be too large for a wide range of practical applications. This limitation may be overcome by using locally resonant elastic metamaterials (MMs), introduced by Liu et al. [38], in which band gaps may open up in the subwavelength regime and thus do not require the unit cell size to be on the order as the

wavelength. Within a band gap, for a PC or a MM, the wave energy is attenuated within only a small number of repeated unit cells. In addition to the possibility of subwavelength band gaps, MMs exhibit other unique physical properties that cannot be found in natural materials, such as negative properties [38–43]. A recent article and discussion in *Applied Mechanics Reviews* provide a broad review of PCs and MMs covering historical and recent developments as well as an outlook on future research directions [7, 44, 45].

The engineering of common structures such as rods, beams and plates with features, or microstructures, that house local resonators allows for the emergence of metamaterial behavior across the structure as a whole. This provides a promising avenue for vibration mitigation using low-frequency bands gaps and effective properties. In two-dimensional plate-like structures, this concept has been realized by embedding soft inclusions [46], erecting pillars [47–49], suspending heavy inclusions within a lattice [50], among other configurations [51]. In 1D structures, among the metamaterial configurations considered are three-phase rods [52], beams with resonating rings [53, 54], sandwich beams with internal mass-spring resonators [55], beams with side stubs [56, 57] and beams with small masses suspended on a membrane [58]. The band-gap formation mechanism in this class of 1D systems was studied analytically by Xiao et al. in the context of mass resonators attached to strings [59], rods [60] and beams [61]. In the case of rods, multi-degree-of-freedom resonators were considered to achieve a cluster of multiple subwavelength band gaps [60]. Liu and Hussein, on their part, investigated the effects of the various types and properties of periodicity on the frequency band structure considering flexural wave propagation in Euler and Timoshenko beams [62]. The conditions for transition between the Bragg scattering and the local resonance hybridization regimes have also been investigated in depth [62].

The majority of theoretical investigations of wave motion in elastic solids are based on linear analysis, that is, linear constitutive laws and linear strain-displacement relationships are assumed (see Refs. [63] and [64], and references therein). The incorporation of nonlinear effects, however, gives rise to a broader range of physical phenomena including amplitude-dependent elastic wave motion [65–69]. Capturing this property within the dispersion relation provides a general and

fundamental description of the nonlinear wave propagation characteristics. Abedinnasab and Hussein [1] derived exact dispersion relations for axial and flexural elastic wave motion in homogeneous rods and beams, respectively, under finite strain. The effects of nonlinearity have also been studied for other types of waves such as water waves [70, 71] and electrostatic and electromagnetic waves in plasmas [72, 73].

Finite-strain waves in elastic solids is a subset among the broader class of nonlinear waves. From a mathematical perspective, a formal treatment of finite strain requires the incorporation of a nonlinear strain tensor in setting up the governing equations of motion. Regardless of the type of nonlinearity, a common analysis framework has been one in which the dispersion is viewed to arise linearly, e.g., due to the presence of a microstructure or geometrical constraints, and that such dispersion may be balanced with nonlinear effects to allow for the generation of nonlinear traveling waves of fixed spatial profile such as shock waves and solitons [68, 69]. In contrast to this dispersion/non-linearity balancing framework where the focus is on finding these special types of waves and characterizing the amplitude-dependence, or wave-number-dependence, of their speeds, it has recently been shown that nonlinearity in itself may cause dispersion without the need for a linear dispersive mechanism [1, 18]. This perspective provides a motivation to derive dispersion relations that inherently embody the effects of the nonlinearities on the dispersion, i.e., amplitude-dependent relations for general wave motion that encompass both the frequency (or phase velocity) and the wave number.

Extending to periodic media, nonlinear PCs and MMs have received less attention due to the additional difficulties in modeling and characterization. Needless to say, there are unique opportunities associated with large motion in PCs and MMs, such as, for example, solitary wave tuning [74] and amplitude-dependent band-gap engineering [75]. Nonlinear dispersion relations appear in various contexts, for example, electronic waves in metals and semiconductors [76] and electromagnetic waves in PCs [77, 78]. In the context of nonlinear phononic materials, there are several studies that follow the premise of Bloch wave propagation analysis. These include investigations on systems exhibiting material nonlinearity, analyzed using the method of multiple scales [79–81], perturbation

analysis [75, 82], the harmonic balance method [83, 84], and the TM method in conjunction with a perturbation technique [85]. The effects of nonlinearity on the dynamics of periodic materials has also been explored in the context of atomic-scale models incorporating anharmonic potentials; see, for example, a recent paper focusing on phonon transport [86]. Concerning finite-strain dispersion in a layered elastic medium, this was recently investigated by Andrianov *et al.* [78] via a homogenization approach whereby the periodic unit cell was first homogenized as a linear medium and subsequently a finite-strain dispersion relation was derived for the averaged medium. This approach therefore does not retain the periodic character in the derived dispersion relation. On the experimental track, numerous studies have been conducted on nonlinear wave phenomena particularly in periodic granular chains, e.g., [74, 87]. It is evident that the effects of nonlinearity in phononic/granular materials could be utilized to enrich the design of devices in numerous engineering applications, such as for shock mitigation [88], tunable wave filtering [75], focusing [89] and rectification [90]. A recent study experimentally investigated vibrational waves in periodic strings [91]. In a recent investigation, we have studied the effect of finite deformation in 1D layered PCs using exact dispersion analysis in the different homogeneous layers and the standard TM method across the unit cell [92] and another study examining a 1D nonlinear elastic metamaterial [93].[1]

1.5 Thesis objectives

In this dissertation, nonlinear dispersive waves in solids are investigated. Nonlinear 1D models of homogeneous and phononic media are derived and followed by the development of exact, approximate, and numerical solutions. The main steps for accomplishing the desired goal are outlined as follows:

- Develop a framework for the derivation of the exact dispersion relation in 1D elastic media, considering any type of geometric or material nonlinearity.

[1] These studies form the foundation of Chapters 4 and 5 respectively.

- Derive an analytical spatial solution for nonlinear elastic waves in 1D homogeneous solids using high-order perturbation theory.
- Investigate the intrinsic harmonic generation mechanism in elastic solid media and establish a connection with the derived dispersion relation.
- Provide a formulation to allow the analysis to be extended to nonlinear 1D phononic crystals to 1D locally resonant elastic metamaterials.
- Develop finite element, finite difference, and spectral method codes for simulating nonlinear wave propagation in homogeneous and heterogeneous elastic solids.
- Investigate the possibility of expanding this framework into other types of nonlinear waves such as optical waves and water waves.

1.6 Overview

This dissertation focuses on wave propagation in 1D nonlinear dispersive elastic medium. It provides a rich collection of problems and the intent is to study the intrinsic dynamical properties of nonlinear elastic media under various circumstances. Chapter 1 provides an introduction to elastic wave propagation in general and an overview of a few example mechanisms that involve dispersion and nonlinearity. A brief literature review is provided and the framework of this dissertation is defined. Chapter 2 studies nonlinear dispersion relations for 1D homogeneous elastic media in the presence of linear dispersive mechanism (lateral inertia) and nonlinear dispersive mechanism (finite deformation). It focuses mainly on the connection between harmonic generation and dispersion. This chapter is an adaptation from a paper in preparation [94, 95]. Chapter 3 studies expanded nonlinear dispersion relations for 1D homogeneous elastic media derived by a higher order perturbation method. Using dispersion information, an analytical spatial solution has been derived as well. This chapter is also an adaptation from a paper in preparation [96]. Chapter 4 is a reprint of a submitted work that investigates phononic crystals, the band gap structure, and balancing of

dispersion due to nonlinearity and periodicity for 1D nonlinear phononic crystal. The preprint is available in Ref. [92]. Chapter 5 is a reprint of a published work that investigates the band gap structure for 1D nonlinear elastic metamaterials [93]. Finally, Chapter 6 presents an ongoing study and draws an outline for future plans.

Chapter 2

Unified theory of nonlinear dispersion and harmonic generation[1]

In this chapter, we report on an intriguing phenomenon concerning the connection between nonlinear dispersion relation and the evolution of nonlinear elastic waves in a homogeneous thick rod. Nonlinearities originating from two different forms of Seth-Hill finite-strain measures introduce amplitude-dependent dispersion relations which are verified using a Fourier spectral method followed by a wave number-frequency spectral (WFS) analysis. The evolution of large-amplitude waves consists of profile steepening and wave radiation in the opposite direction of propagation. This leads to the realization of harmonic generation which we demonstrate to correlate perfectly with the derived dispersion relation.

2.1 Introduction

Understanding of wave propagation is key to many branches of physics. In the study of waves, the knowledge of the wavevector-frequency dispersion relation provides valuable information that is often used to gain insights into a range of dynamical properties of the medium [97]. While the vast majority of contemporary studies of dispersion are based on linear governing equations, there are studies that address the effects on the dispersion that arises from nonlinear quantities [13,17,98]. In particular, nonlinear dispersion caused by weak turbulences is a ubiquitous phenomenon observed in various fields from vibrating plates [15] and plasma oscillations [14] to shallow waters [99]. For some of these systems, the predicted nonlinear dispersion relation (NDR) is compatible with results

[1] The material in this chapter is drawn from Ref. [94], a paper in preparation.

obtained from experiments [13, 16, 17] or from numerical simulations [14, 15, 18, 99, 100]. Although there is an agreement between theory, numerical simulations, and experiments, there are also limitations. In some of these cases, the compatibility is limited to only weak nonlinearities [13, 15–17]. Aside from weak turbulent theory, there are other origins which lead to nonlinear dispersion. For example, the NDR derived from the coupling of two water waves [101,102] or from dielectric medium nonlinearity of surface waves in left-handed materials [11].

In this chapter, we consider a one-dimensional (1D) thick rod with both linear and nonlinear dispersive mechanisms. We first demonstrate the possibility of qualitative changes in the dynamical behavior of an elastic medium purely due to nonlinear interactions, e.g., observation of dispersive behavior in an otherwise non-dispersive elastic medium. Particularly, we answer the important fundamental question of how for a nonlinear system, the nonlinear dispersion is connected to the generation of harmonics in the medium? This differs fundamentally from previous studies on weakly nonlinear models where the NDR is viewed as a single qualitative perturbation to the linear dispersion relation [17, 18]. For 1D elastic media in particular, a NDR for a thin rod under finite deformation is derived and verified numerically concerning the onset of dispersion [1]. In what follows, we present a theoretical framework to derive the NDR for 1D elastic waves in a thick rod containing both linear and nonlinear dispersive terms. Although this framework can be applied to PDEs nonlinearized due to different forms of nonlinearity sources, we limit our results to the Green-Lagrange strain (GLS) and the Hencky strain (HS) which are considered to be geometrical nonlinearities. The source of linear dispersive mechanism considered is lateral inertia. In case of neglecting the lateral inertia, the model is refereed as a thin rod. We demonstrate that the spectrum obtained by WFS analysis of the simulation data matches perfectly with the predicted dispersion relations. We show that a balance between a linear and a nonlinear dispersive mechanisms provides an opportunity to characterize solitons which is different from the conventional view, a balance between nonlinearity and dispersion [103, 104]. We further show that the values of WFS introduced by nonlinearities are strongly inductive of the harmonic generation, establishing a complete map connecting the space-time solution, the harmonic generation, and the NDR of the

system. Study of these waves and understanding the interaction between harmonic generation and NDR is key and provides new insights to any field involving wave motion, in particular nonlinear vibration analysis [105, 106], dislocation and crack dynamic analysis [107, 108], geophysical and seismic motion analysis [109, 110], material characterization and nondestructive evaluation [111], biomedical imaging [112], among others. Although in this chapter we discuss linearly dispersive media due to lateral inertia, but in principle the proposed framework is applicable to periodic media such as a phononic crystal [92], a nonlinear elastic metamaterial [93], or a 1D chain [20, 113], or others.

2.2 Nonlinear dispersion relation

Let us consider an infinite 1D rod with radius r and constant material properties under uniaxial stress $\sigma(x,t)$ and longitudinal displacements $u(x,t)$ at position x and time t. For such a medium, the governing equation can be obtained from the Hamilton's Principle $\delta\int_{t_0}^{t}\mathcal{L}\partial t = 0$. In the absence of external non-conservative forces and moments, the elastic Lagrangian density function, $\mathcal{L} = \mathcal{T} - \mathcal{U}$, summarizes the dynamics of the system via the kinetic and elastic strain energy densities, $\mathcal{T} = \rho\big((\partial_t u)^2 + \nu^2 r^2(\partial_{tx}^2 u)^2\big)/2$ and $\mathcal{U} = \sigma\epsilon/2$. Here ρ and ν are mass density and Poisson's ratio and uniaxial stress follows Hook's law $\sigma = E\epsilon$, where E is the elastic modulus. The finite strain ϵ describes the exact complete GLS and HS measures by $\epsilon = \partial_x u + (\partial_x u)^2/2$ and $\epsilon = \ln(1+\partial_x u)$, respectively. In these relations, $\partial_{(.)}u$ denotes the partial derivative of displacement with respect to (.). Applying $\mathcal{L}$ on the Euler-Lagrange equation $\partial_x(\partial_{\partial_x u}\mathcal{L}) + \partial_t(\partial_{\partial_t u}\mathcal{L}) = 0$, followed by defining $\bar{u} = \partial_x u$, result in the equation of motion with respect to displacement gradient in the general form of

$$\partial_{tt}\bar{u} - \partial_{xx}(\alpha\bar{u} + \beta\mathcal{N}(\bar{u}) + \gamma\partial_{tt}\bar{u}) = 0. \tag{2.1}$$

We determine the constants and nonlinear function of Eq. (2.1) by $\alpha = \beta = c^2$ and $\mathcal{N}(\bar{u}) = 3\bar{u}^2/2 + \bar{u}^3/2$ for the GLS measure, and $\alpha = 0$, $\beta = c^2$, and $\mathcal{N}(\bar{u}) = \ln(1+\bar{u})/(1+\bar{u})$ for the HS

measure. For both cases, $\gamma = r^2\nu^2$ and he velocity of sound is constant in the medium as is given by $c = \sqrt{E/\rho}$.

Assuming a thin rod, i.e. $r = 0$, Eq. (2.1) incorporates finite strain only in the wave equation and transforms the dynamics of the non-dispersive medium to a dispersive medium with a self-steepening character in the course of time evolution. However this system evolves differently depending on the type of finite strain measure introduced. Specifically, in the case of the GLS measure, waves with smaller wavelengths catch up with larger ones, leading to self steepening in the direction of propagation − hardening effect − and eventually forming a shock $\partial_x \bar{u} = -\infty$, while, in contrast, for the case of the HS measure, waves with larger wavelengths catch up with smaller ones, leading to self steepening in the opposite direction of propagation − softening effect [114]− and the formation of a shock $\partial_x \bar{u} = \infty$, as demonstrated in Fig. 2.1(a). Consider $m(x,t) < 0$ and $M(x,t) > 0$ to be the minimum and maximum value of $\partial_x \bar{u}$ as a function of time. There exist a finite bifurcation time τ_{B} when at least one point of the wave profile slope becomes vertical, $m \to -\infty$ and $M \to \infty$, and a shock forms at the leading edge in the GLS case and at the trailing edge in the HS case. These effects are shown in the inset of Fig. 2.1(a) by the corresponding characteristic lines. Analytically, one can determine the position and time of bifurcation by solving the following set of equations for a known solution, $\partial_{\bar{u}} x(\bar{u}) = 0$ (equivalent to $|\partial_x \bar{u}(x)| = \infty$), and $\partial_{\bar{u}\bar{u}} x(\bar{u}) = 0$ necessary to ensure the uniqueness of $\bar{u}(x)$.

To describe the dispersion in a convenient manner, it is appropriate to introduce a change of variables. This is accomplished by the transformation $\xi = \kappa x - \omega t$, so that Eq. (2.1) becomes

$$\omega^2 \partial_{\xi\xi} \bar{u} - \kappa^2 \partial_{\xi\xi} (\alpha \bar{u} + \beta \mathcal{N}(\bar{u}) + \omega^2 \gamma \partial_{\xi\xi} \bar{u}) = 0, \tag{2.2}$$

where κ and ω are the wave number and the frequency of the traveling wave. We solve this equation by setting the integration constants equal to zero to ensure the boundedness of the travelling wave solution at infinity for an initially bounded displacement field such as a sinusoidal displacement field with amplitude B. Following this change of variables, this initial displacement field essentially

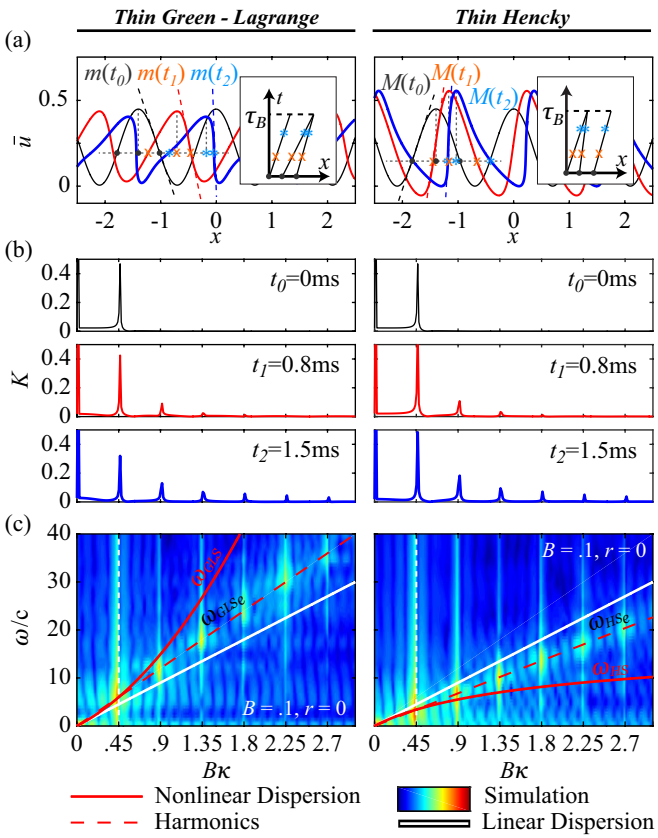

Figure 2.1: (color). Profile snap shots for three different times and their corresponding harmonics. (a) Profiles captured at $t_0 = 0$ ms, $t_1 = .8$ ms, and $t_2 = 1.5$ ms. Inset shows the characteristic lines of the corresponding wave. (b) Normalized distribution of the harmonics generated through time. (c) Wavenumber-frequency spectrum at t_2 represented by the logarithmic spectrum S^2 for the considered value of $\kappa_e = 4.5$.

corresponds to satisfying $\bar{u}(0) = B\kappa$ at $\xi = 0$, which if we apply to the solution of Eq. (2.2), we obtain the exact NDR respectively under GLS and HS measures as:

$$\omega_{\mathrm{GLS}} = c\kappa\sqrt{(2 + 3B\kappa + B^2\kappa^2)/(2 + 2\gamma\kappa^2)}, \tag{2.3}$$

and

$$\omega_{\mathrm{HS}} = c\kappa\sqrt{\ln(1 + B\kappa)/(B\kappa(1 + B\kappa)(1 + \gamma\kappa^2))}. \tag{2.4}$$

Indeed, the method we employed to derive these NDRs relies on the initial condition for Eq. (2.1). One can recover the linear dispersion relation, $\omega_{\mathrm{inf}} = c\kappa$, by applying $\lim_{B\to 0,\gamma\to 0}\omega_{\mathrm{GLS}}$ on Eq. (2.3) and $\lim_{B\to 0,\gamma\to 0}\omega_{\mathrm{HS}}$ on the Taylor series expansion of Eq. (2.4) [1, 11, 115].

2.3 Computational setup

In the following, we solve Eq. (2.1) using a spectral method for the spatial variable in conjunction with an efficient explicit time stepping method, and perform WFS analysis on the space-time solution to compare the corresponding wave number-frequency spectrum with the analytically derived NDRs in the Eqs. (2.3) and (2.4) [115]. To briefly summarize the computational setup, we prescribe a wave packet in a periodic domain. The dynamics of this packet is fully characterized by its amplitude B (arbitrary normalized) and excitation wave number κ_e. In principle, any wave packet with amplitude $\kappa_e B$, the condition used to derive the NDRs, can be used in these simulations. The space-time domain is defined by $-x^* < x \leq x^*$ (long enough to avoid any reflections from boundaries) with a grid spacing of $h = 1cm$, and $0 \leq t \leq t^*$ (t^* set at just before the breaking point of the wave profile) with a constant time stepping of $\Delta t = 1\mu$s. The material considered is aluminum which has properties, $\rho = 2700\text{kg/m}^3$, $\nu = .33$ and $E = 70\text{GPa}$. We display the results of the WFS analysis by the logarithmic value of the spectrum $S(\kappa, \omega) = \sum_{\kappa_e} \ln|s|$, scaled in the unit interval spanning the normalized axes of $B\kappa$ and ω/c.

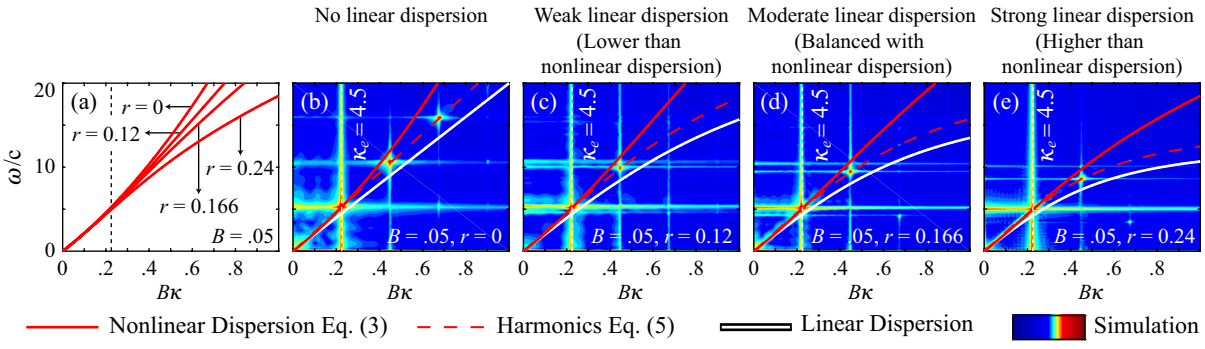

Figure 2.2: (color). Balance of linear and nonlinear dispersions. (a) Dispersive effects of increasing lateral inertia in the GLS model (Eq. (2.3)). Wave propagation and its corresponding WFS analyses. (b-e) The WFS analysis of the finite strain space-time solution represented by the logarithmic spectrum S for the mentioned κ_e values on the figure. Corresponding dispersion curves and harmonic generation paths are overlaid from Eqs. (2.3) and (2.5).

2.4 Observations

Any excitation, harmonic or in the form of a localized pulse, consists of a primary mode. Study of wave characteristics and their evolution in time, due to pure nonlinearities, reveals other modes in the spectrum get excited. To analyze further, first we choose a single mode harmonic excitation, $\bar{u}(x,t) = B\kappa_e(1+\cos(\kappa_e(x-ct))/2$ characterized by $B = .1$ and $\kappa_e = 4.5$ in a thin rod $r = 0$, simulate and present the results in Fig. 2.1. This wave packet evolves with time and as long as wave breaking is not reached, the nonlinear field obeys certain characteristics as dictated by the Eq. (2.1) (Fig. 2.1(a)). Performing Fourier analysis on the wave packet on the onset of excitation and two further times show the transition of energy, K, from the primary mode to the higher modes as shown in Fig. 2.1(b). The WFS analysis results corresponding to this excitation is also presented in Fig. 2.1(c). Both the infinitesimal dispersion relation and NDR are overlaid on the top of the spectrum in order to compare with the computational results. Differentiating between characterization parameters by keeping B constant and varying $\kappa_e = 4.5$ in the initial excitation pulse, we establish a connection between the harmonic generation mechanism and the NDR. In this case we evaluate Eqs. (2.3) and (2.4) at κ_e to take the form

$$\omega_{\mathrm{GLS_e}} = c\kappa\sqrt{(2+3B\kappa_e+B^2{\kappa_e}^2)/(2+2\gamma\kappa^2)}, \tag{2.5}$$

and

$$\omega_{\mathrm{HS_e}} = c\kappa\sqrt{\ln(1+B\kappa_e)/(B\kappa_e(1+B\kappa_e)(1+\gamma\kappa^2))}. \tag{2.6}$$

These relations predict the trajectories that the harmonic generation occurs along as shown with dashed lines. The brightened areas along the dashed lines confirms the accuracy of the theory in capturing the dynamical behavior of the system at the excited wave number κ_e. Intersections of this line with the κ_e values are exactly located on the NDRs. The secondary modes which align perfectly with the excited parts of the spectrum can be predicted by plugging integer multipliers of κ_e in κ of Eqs. (2.5) and (2.6).

Now we consider a thick rod under the GLS measure and propagate the same profile char-

acterized by $B = .05$ and $\kappa_e = 4.5$ with various thicknesses. As it is shown in Fig. 2.2, our theory can predict the simulations in the presence of linear and nonlinear dispersive mechanisms. Figure 2.2(d) in particular, shows a balance between the linear and nonlinear dispersions, for which, the red solid curve becomes a straight line, and wave profile propagate without any noticeable change in its shape acting as a soliton.

Next, we expand this concept and verify the NDR by superposing various excitations and their harmonic generation paths. But first we study the system at the infinitesimal limit. We simulate a localized pulse defined by $\bar{u}(x,t) = B\kappa_e(1+\text{sech}(\kappa_e(x-ct))/2$ over a long time domain with a relatively small amplitude of $B = .0005$ and $\kappa_e = 6$. This condition generates a non-dispersive wave in an almost non-dispersive medium. The linear dispersion relation, $\omega_{\text{inf}} = c\kappa$, can be recovered

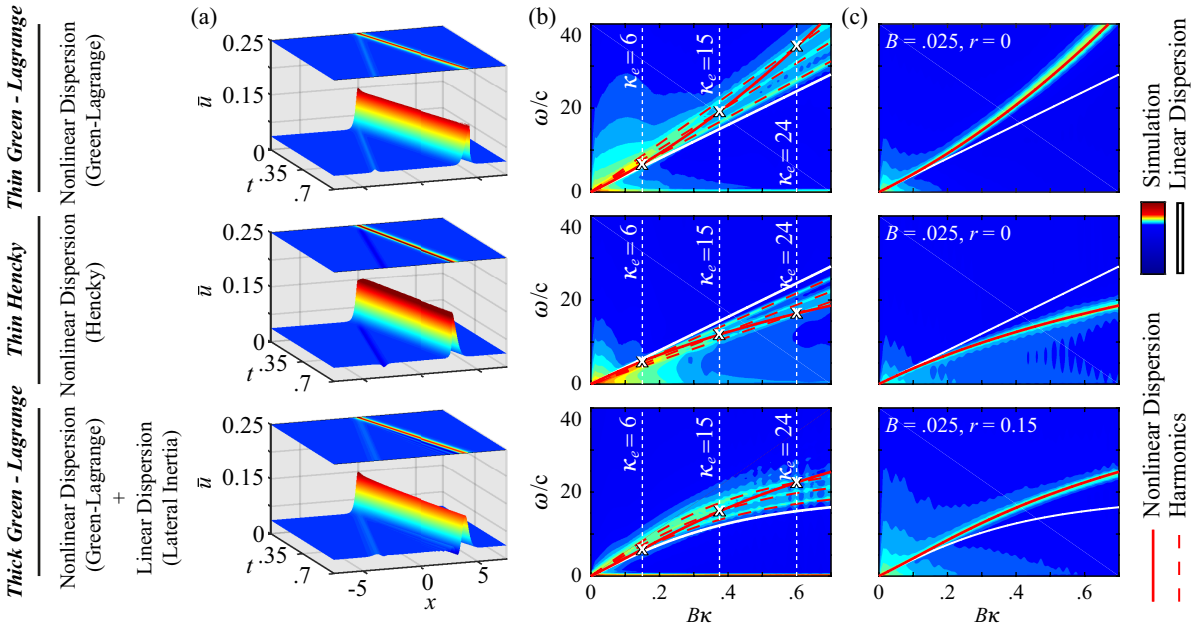

Figure 2.3: (color). Wave propagation and its corresponding WFS analyses (thin GLS, thin HS, and thick GLS models in first, second, and third rows, respectively). (a) Finite strain space-time solution. Here we have used $B = 0.025$ and $\kappa_e = 6$ to form the initial wave profile. Time and space units are [ms] and [m], respectively. (b) The WFS analysis of the finite strain space-time solution represented by the logarithmic spectrum S for the mentioned value of κ_es on the figure. Dashed curves corresponding to the harmonic generation paths are overlaid from Eqs. (2.5) and (2.6). (e) Superposition of WFS analyses by the logarithmic spectrum S for thirty distinct waves defined by the initial conditions of $B = 0.025$ and $\kappa_e = 1 : 30$. Also, corresponding dispersion curves from Eqs. (2.3) and (2.4) are overlaid.

from the NDRs by setting $B \to 0$ and $r \to 0$ [115].

In Fig. 2.3(a), we show the space-time solution of the same profile with $\kappa_e = 6$ and a $B = .025$. The initial wave packet propagates along the positive direction which is in sync with the initial velocity condition and at some point, a trailing wave radiates in the opposite direction. In addition, wave contour images are mapped to the top surface of the mesh confirming the gradual formation of shocks in agreement with the behavior explained in Fig. 2.1(a), at the leading and trailing edges of the wave packet for the GLS and HS measures, respectively. In Fig. 2.3(b), WFS results for a few distinct κ_e values are superposed. The path for the smallest κ_e corresponds to the space-time solution presented in Fig. 2.3(a). Finally, in Fig. 2.3(c), a superposition of the main modes for thirty distinct initial wave packets calculated from WFS analysis is presented. Initial wave packets share the same amplitude but different excitation wave numbers ranging from $\kappa_e = 1$ to $\kappa_e = 30$, with increments of 1. As a result, we see a perfect agreement between the numerically calculated wave number-frequency spectrum and the analytically predicted NDRs (Eqs. (2.3) and (2.4)). These NDRs show that the nonlinearity by itself causes wave dispersion, i.e., without the need for a linear dispersive mechanism. And most importantly, it shows that Eqs. (2.5) and (2.6) perfectly predict the harmonic generation lines.

2.5 Conclusions

In summary, we show here that setting the traveling wave phase condition to zero allows us to derive the relation for fully nonlinear dispersion of a traveling wave in an elastic medium and uncover fundamental nonlinear dynamical behaviors without directly solving the governing equations. We illustrate how the presented theory predicts the connection between the NDR and harmonic generation corresponding to purely nonlinear wave evolution and how it elucidates the harmonic generation mechanism within both linearly non-dispersive and linearly dispersive media. Our numerical approach of WFS analysis provides a direct confirmation of the theory.

Chapter 3

Spatial evolution of nonlinear elastic waves in a 1D thin rod by high-order perturbation theory[1]

In this chapter, we study expanded nonlinear dispersion relations for 1D homogeneous elastic media derived by the method of strained parameters. Neglecting any linear dispersive mechanism in the system, we focus on nonlinear dispersive mechanism, in particular, geometric nonlinearity in the form of finite deformation. Using dispersion information derived for these systems, an analytical spatial solution has been derived for each case.

3.1 Introduction

Nonlinear phenomena that appear in many areas of scientific fields such as optics, solid physics, plasma physics and fluid dynamics can be modeled by partial differential equations (PDEs). A broad class of analytical and numerical solution methods are used to handle these problems. However, the majority of these methods are suitable for linear and weakly nonlinear problems. In recent years, searching for traveling waves and soliton solutions of nonlinear systems have been pursued with some solid achievements [65, 97, 106, 116].

This chapter is devoted to the analysis of a one-dimensional elastic medium under finite deformation, in particular as modeled by the Green-Lagrange strain (GLS) and Hencky strain (HS) measures. The aim from this procedure is to obtain an approximation of the nonlinear dispersion relation leading to an analytical expression of a space-time solution.

[1] Most of the material in this chapter is taken from Ref. [96], a paper in preparation.

3.2 Expanded nonlinear dispersion relation

We consider a 1D elastic medium, with constant material properties and infinite length in both directions, admitting uniaxial stress $\sigma(x,t)$ and longitudinal displacements $u(x,t)$ at position x and time t. For such a medium, the governing equation can be obtained from the Hamilton's Principle $\delta \int_{t_0}^{t} \mathcal{L}\partial t = 0$. In the absence of external non-conservative forces and moments, the elastic Lagrangian density function, $\mathcal{L} = \mathcal{T} - \mathcal{U}$, summarizes the dynamics of the system via the kinetic and elastic strain energy densities, respectively,

$$\mathcal{T} = \rho(\partial_t u)^2/2, \tag{3.1}$$

and

$$\mathcal{U} = \sigma\epsilon/2, \tag{3.2}$$

where ρ is mass density and uniaxial stress follows Hook's law $\sigma = E\epsilon$, with E as the elastic modulus. The finite strain ϵ describes the exact complete GLS and HS measures by $\epsilon = \partial_x u + (\partial_x u)^2/2$ and $\epsilon = \ln(1 + \partial_x u)$, respectively. Applying $\mathcal{L}$ on the Euler-Lagrange equation

$$\partial_x(\partial_{\partial_x u}\mathcal{L}) + \partial_t(\partial_{\partial_t u}\mathcal{L}) = 0, \tag{3.3}$$

followed by defining $\bar{u} = \partial_x u$, result in the equation of motion with respect to displacement gradient in the general form of

$$\partial_{tt}\bar{u} - \partial_{xx}(\alpha\bar{u} + \beta\mathcal{N}(\bar{u})) = 0. \tag{3.4}$$

We determine the constants and nonlinear function of Eq. (3.4) by $\alpha = \beta = c^2$ and $\mathcal{N}(\bar{u}) = 3\bar{u}^2/2 + \bar{u}^3/2$ for the GLS measure, and $\alpha = 0$, $\beta = c^2$, and $\mathcal{N}(\bar{u}) = \ln(1+\bar{u})/(1+\bar{u})$ for the HS measure. The velocity of sound is constant in the medium as is given by $c = \sqrt{E/\rho}$.

Usually, the first effort in finding the nonlinear dispersion relation associated with a wave equation is through perturbation analyses. In the next two subsections we present a derivation of the extended nonlinear dispersion relation based on GLS and HS measures.

3.2.1 Expanded nonlinear dispersion relation: Green-Lagrange strain

Restating Eq. (3.4) with GLS constants gives

$$\bar{u}_{tt} = c^2\bar{u}_{xx} + (\frac{3}{2}c^2\bar{u}^2 + \frac{1}{2}c^2\bar{u}^3)_{xx}. \tag{3.5}$$

We aim to find the next approximation to the linear periodic wave train using the method of strained parameters assuming amplitude B is small [117]. The initial condition, $\bar{u}(B;0) = \kappa B$, suggests an expansion of the form

$$\omega(\kappa;B) = \sum_{n=0}^{N-1} B^n\omega_n(\kappa) + O(B^N), \tag{3.6}$$

$$\bar{u}(\zeta;B) = \sum_{n=1}^{N} B^n\bar{u}_n(\zeta) + O(B^{N+1}), \tag{3.7}$$

where

$$\zeta = \kappa x - \omega t. \tag{3.8}$$

Substituting this expansion into Eq. (3.5) and equating coefficients of like powers of B, for the first order we obtain

Order B:

$$\begin{aligned}(\omega_0{}^2 - c^2\kappa^2)\bar{u}_{1,\zeta\zeta} &= 0,\\ \omega_0 &= c\kappa,\end{aligned} \tag{3.9}$$

which is the infinitesimal dispersion relation. For the second order we have

Order B^2 :

$$\begin{aligned}(\omega_0{}^2 - c^2\kappa^2)\bar{u}_{2,\zeta\zeta} &= \kappa^2c^2(3/2\bar{u}_1^2)_{,\zeta\zeta} + 2\omega_0\omega_1\bar{u}_{1,\zeta\zeta},\\ 0 &= \kappa^2c^2 3/2\bar{u}_1^2 + 2\omega_0\omega_1\bar{u}_1 + s.t.\ ,\end{aligned} \tag{3.10}$$

and after removing secular terms and substituting $\bar{u}_1(0) = \kappa$, we get

$$\omega_1 = \frac{3c\kappa^2}{4}. \tag{3.11}$$

Now we use the results from the first two orders of frequency and form the third order equations as

Order B^3 :

$$(\omega_0{}^2 - c^2\kappa^2)\bar{u}_{3,\zeta\zeta} = \kappa^2 c^2(3\bar{u}_1\bar{u}_2 + 1/2\bar{u}_1^3)_{,\zeta\zeta} + 2\omega_0\omega_1\bar{u}_{2,\zeta\zeta} + (2\omega_0\omega_2 + \omega_1{}^2)\bar{u}_{1,\zeta\zeta},$$

$$0 = \kappa^2 c^2(3\bar{u}_1\bar{u}_2 + 1/2\bar{u}_1^3) + 2\omega_0\omega_1\bar{u}_2 + (2\omega_0\omega_2 + \omega_1{}^2)\bar{u}_1 + s.t.\ , \tag{3.12}$$

which upon substitution of $\bar{u}_2(0) = 0$, gives

$$\omega_2 = -\frac{c\kappa^3}{32}. \tag{3.13}$$

We can continue the same procedure for higher orders to get the corresponding terms of the frequency.

Order B^4 :

$$(\omega_0{}^2 - c^2\kappa^2)\bar{u}_{4,\zeta\zeta} = \kappa^2 c^2(3\bar{u}_1\bar{u}_3 + 3/2\bar{u}_2^2 + 3/2\bar{u}_1^2\bar{u}_2)_{,\zeta\zeta}$$

$$+2\omega_0\omega_2\bar{u}_{3,\zeta\zeta} + (2\omega_0\omega_2 + \omega_1{}^2)\bar{u}_{2,\zeta\zeta} + (2\omega_0\omega_3 + 2\omega_1\omega_2)\bar{u}_{1,\zeta\zeta},$$

$$0 = \kappa^2 c^2(3\bar{u}_1\bar{u}_3 + 3/2\bar{u}_2^2 + 3/2\bar{u}_1^2\bar{u}_2)$$

$$+2\omega_0\omega_2\bar{u}_3 + (2\omega_0\omega_2 + \omega_1{}^2)\bar{u}_2 + (2\omega_0\omega_3 + 2\omega_1\omega_2)\bar{u}_1 + s.t.\ . \tag{3.14}$$

Again after removing secular terms and substituting $\bar{u}_3(0) = 0$, we get

$$\omega_3 = \frac{3c\kappa^4}{128}. \tag{3.15}$$

Order B^5 :

$$(\omega_0{}^2 - c^2\kappa^2)\bar{u}_{5,\zeta\zeta} = \kappa^2 c^2(3\bar{u}_1\bar{u}_4 + 3\bar{u}_2\bar{u}_3 + 3/2\bar{u}_1^2\bar{u}_3 + 3/2\bar{u}_2^2\bar{u}_1)_{,\zeta\zeta}$$

$$+2\omega_0\omega_2\bar{u}_{4,\zeta\zeta} + (2\omega_0\omega_2 + \omega_1{}^2)\bar{u}_{3,\zeta\zeta} + (2\omega_0\omega_3 + 2\omega_1\omega_2)\bar{u}_{2,\zeta\zeta} + (2\omega_0\omega_4 + 2\omega_1\omega_3)\bar{u}_{1,\zeta\zeta},$$

$$0 = \kappa^2 c^2(3\bar{u}_1\bar{u}_4 + 3\bar{u}_2\bar{u}_3 + 3/2\bar{u}_1^2\bar{u}_3 + 3/2\bar{u}_2^2\bar{u}_1) + 2\omega_0\omega_2\bar{u}_4$$

$$+(2\omega_0\omega_2 + \omega_1{}^2)\bar{u}_3 + (2\omega_0\omega_3 + 2\omega_1\omega_2)\bar{u}_2 + (2\omega_0\omega_4 + 2\omega_1\omega_3)\bar{u}_1 + s.t.\ . \tag{3.16}$$

By substitution of $\bar{u}_4(0) = 0$ we get

$$\omega_4 = -\frac{37c\kappa^5}{2048}. \tag{3.17}$$

Therefore from Eq. (3.6), the frequency becomes

$$\omega(\kappa;B) = c\kappa + \frac{3c\kappa^2}{4}B - \frac{c\kappa^3}{32}B^2 + \frac{3c\kappa^4}{128}B^3 - \frac{37c\kappa^5}{2048}B^4 + \ldots, \tag{3.18}$$

which for small B is equivalent to Taylor expansion of

$$\omega(\kappa;B) = \sqrt{\frac{2+3B\kappa+(B\kappa)^2}{2}}c\kappa. \tag{3.19}$$

One can summarize all of the equations solved above into one general equation of order B^n as

Order B^n :

$$(\omega_0{}^2 - c^2\kappa^2)\bar{u}_{n,\zeta\zeta} = (3/2\sum_{i=0}^{n-1}\bar{u}_i\bar{u}_{n-i} + 1/2\sum_{i=1}^{n}\sum_{j=1}^{n}\bar{u}_i\bar{u}_j\bar{u}_{n-(i+j)})_{,\zeta\zeta} + \sum_{i=1}^{n-2}\omega_i{}^2\bar{u}_{n-2i,\zeta\zeta} + 2\sum_{i=0}^{n-2}\sum_{j=i+1}^{n-1}\omega_i\omega_j\bar{u}_{n-(i+j),\zeta\zeta}\ . \tag{3.20}$$

3.2.2 Expanded nonlinear dispersion relation: Hencky strain

The equation of motion for Hencky strain with respect to displacement gradient is

$$\bar{u}_{tt} = c^2(\frac{\ln(1+\bar{u})}{1+\bar{u}})_{xx} \tag{3.21}$$

which if we expand based on power series it becomes

$$\bar{u}_{tt} = c^2(\bar{u} - \frac{3\bar{u}^2}{2} + \frac{11\bar{u}^3}{6} - \frac{25\bar{u}^4}{12} + \frac{137\bar{u}^5}{60} + O(B^6))_{xx}, \tag{3.22}$$

where we assume amplitude B is small. Substituting Eqs. (3.6) and (3.7) into Eq. (3.22) and equating coefficients of like powers of B, we obtain

Order B:

$$(\omega_0{}^2 - c^2\kappa^2)\bar{u}_{1,\zeta\zeta} = 0,$$

$$\omega_0 = c\kappa. \tag{3.23}$$

Order B^2 :

$$(\omega_0{}^2 - c^2\kappa^2)\bar{u}_{2,\zeta\zeta} = \kappa^2c^2(-3/2\bar{u}_1^2)_{,\zeta\zeta} + 2\omega_0\omega_1\bar{u}_{1,\zeta\zeta},$$

$$0 = -3/2\kappa^2c^2\bar{u}_1^2 + 2\omega_0\omega_1\bar{u}_1 + s.t.\ . \tag{3.24}$$

After removing secular terms and substituting $\bar{u}_1(0) = \kappa$, we get

$$\omega_1 = -\frac{3c\kappa^2}{4}. \tag{3.25}$$

Order B^3 :

$$(\omega_0{}^2 - c^2\kappa^2)\bar{u}_{3,\zeta\zeta} = \kappa^2c^2(-3\bar{u}_1\bar{u}_2 + 11/6\bar{u}_1^3)_{,\zeta\zeta} + 2\omega_0\omega_1\bar{u}_{2,\zeta\zeta} + (2\omega_0\omega_2 + \omega_1{}^2)\bar{u}_{1,\zeta\zeta},$$

$$0 = \kappa^2c^2(-3\bar{u}_1\bar{u}_2 + 11/6\bar{u}_1^3) + 2\omega_0\omega_1\bar{u}_2 + (2\omega_0\omega_2 + \omega_1{}^2)\bar{u}_1 + s.t.\ . \tag{3.26}$$

By substitution of $\bar{u}_2(0) = 0$, we get

$$\omega_2 = \frac{61c\kappa^3}{96}. \tag{3.27}$$

Order B^4 :

$$(\omega_0{}^2 - c^2\kappa^2)\bar{u}_{4,\zeta\zeta} = \kappa^2c^2(-3\bar{u}_1\bar{u}_3 - 3/2\bar{u}_2^2 + 11/2\bar{u}_1^2\bar{u}_2 - 25/12\bar{u}_1^4)_{,\zeta\zeta}$$

$$+2\omega_0\omega_1\bar{u}_{3,\zeta\zeta} + (2\omega_0\omega_2 + \omega_1{}^2)\bar{u}_{2,\zeta\zeta} + (2\omega_0\omega_3 + 2\omega_1\omega_2)\bar{u}_{1,\zeta\zeta},$$

$$0 = \kappa^2c^2(-3\bar{u}_1\bar{u}_3 - 3/2\bar{u}_2^2 + 11/2\bar{u}_1^2\bar{u}_2 - 25/12\bar{u}_1^4)$$

$$+2\omega_0\omega_1\bar{u}_3 + (2\omega_0\omega_2 + \omega_1{}^2)\bar{u}_2 + (2\omega_0\omega_3 + 2\omega_1\omega_2)\bar{u}_1 + s.t.\ . \tag{3.28}$$

Again after removing secular terms and substituting $\bar{u}_3(0) = 0$, we get

$$\omega_3 = -\frac{217c\kappa^4}{384}. \tag{3.29}$$

Order B^5 :

$$(\omega_0{}^2 - c^2\kappa^2)\bar{u}_{5,\zeta\zeta} = \kappa^2c^2(-3\bar{u}_1\bar{u}_4 - 3\bar{u}_2\bar{u}_3 + 11/2\bar{u}_1^2\bar{u}_3 + 11/2\bar{u}_2^2\bar{u}_1 + 411/180\bar{u}_1^5 - 25/3\bar{u}_1^3\bar{u}_2)_{,\zeta\zeta}$$

$$+2\omega_0\omega_1\bar{u}_{4,\zeta\zeta} + (2\omega_0\omega_2 + \omega_1{}^2)\bar{u}_{3,\zeta\zeta} + (2\omega_0\omega_3 + 2\omega_1\omega_2)\bar{u}_{2,\zeta\zeta} + (2\omega_0\omega_4 + 2\omega_1\omega_3)\bar{u}_{1,\zeta\zeta},$$

$$0 = \kappa^2c^2(-3\bar{u}_1\bar{u}_4 - 3\bar{u}_2\bar{u}_3 + 11/2\bar{u}_1^2\bar{u}_3 + 11/2\bar{u}_2^2\bar{u}_1 + 411/180\bar{u}_1^5 - 25/3\bar{u}_1^3\bar{u}_2)$$

$$+(2\omega_0\omega_1 + \omega_1{}^2)\bar{u}_3 + (2\omega_0\omega_3 + 2\omega_1\omega_2)\bar{u}_2 + (2\omega_0\omega_4 + 2\omega_1\omega_3)\bar{u}_1 + s.t. \tag{3.30}$$

By substitution of $\bar{u}_4(0) = 0$ we get

$$\omega_4 = \frac{47551c\kappa^5}{92}. \tag{3.31}$$

Therefore from Eq. (3.6), the frequency becomes

$$\omega(\kappa;B) = c\kappa - \frac{3c\kappa^2}{4}B + \frac{61c\kappa^3}{96}B^2 - \frac{217c\kappa^4}{384}B^3 + \frac{47551c\kappa^5}{92160}B^4 + \ldots, \tag{3.32}$$

which for small B is equivalent to Taylor expansion of

$$\omega(\kappa;B) = \sqrt{\frac{\ln(1+B\kappa)}{B\kappa(1+B\kappa)}}c\kappa. \tag{3.33}$$

One can summarize all of the equations solved above into one general equation of order B^n as

Order B^n :

$$\begin{aligned}(\omega_0{}^2 - c^2\kappa^2)\bar{u}_{n,\zeta\zeta} = (-3/2!\sum_{i=0}^{n-1}\bar{u}_i\bar{u}_{n-i} + 11/3!\sum_{i=1}^{n}\sum_{j=1}^{n}\bar{u}_i\bar{u}_j\bar{u}_{n-(i+j)})_{,\zeta\zeta}\\ - 25/4!\sum_{i=1}^{n}\sum_{j=1}^{n}\sum_{k=1}^{n}\bar{u}_i\bar{u}_j\bar{u}_k\bar{u}_{n-(i+j+k)})_{,\zeta\zeta} + 137/5!\sum_{i=1}^{n}\sum_{j=1}^{n}\sum_{k=1}^{n}\sum_{l=1}^{n}\bar{u}_i\bar{u}_j\bar{u}_k\bar{u}_l\bar{u}_{n-(i+j+k+l)})_{,\zeta\zeta}\\ + \sum_{i=1}^{n-2}\omega_i{}^2\bar{u}_{n-2i,\zeta\zeta} + 2\sum_{i=0}^{n-2}\sum_{j=i+1}^{n-1}\omega_i\omega_j\bar{u}_{n-(i+j),\zeta\zeta}\ .\end{aligned} \tag{3.34}$$

Recalling the equation of motion for Hencky strain from chapter 2, we have

$$\bar{u}_{tt} = c^2(\frac{\ln(1+\bar{u})}{1+\bar{u}})_{xx}. \tag{3.35}$$

In order to apply the method of strained parameters, the logarithmic term should be expanded as a power series

$$\bar{u}_{tt} = c^2(\bar{u} - \frac{3\bar{u}^2}{2} + \frac{11\bar{u}^3}{6} - \frac{25\bar{u}^4}{12} + \frac{137\bar{u}^5}{60} + O(\bar{u}^6))_{xx}. \tag{3.36}$$

A comparison of exact and approximation dispersion relations are presented in Fig. 3.1. As expected, the correlation between these relations improves by increasing the order of terms considered in this perturbation analysis. In contrast, it gets worse for increasing the amplitude value.

To derive the expanded dispersion relation for a single mode harmonic excitation, one might use the same steps explained above, with the difference of introducing κ_e instead of κ in the initial conditions and get

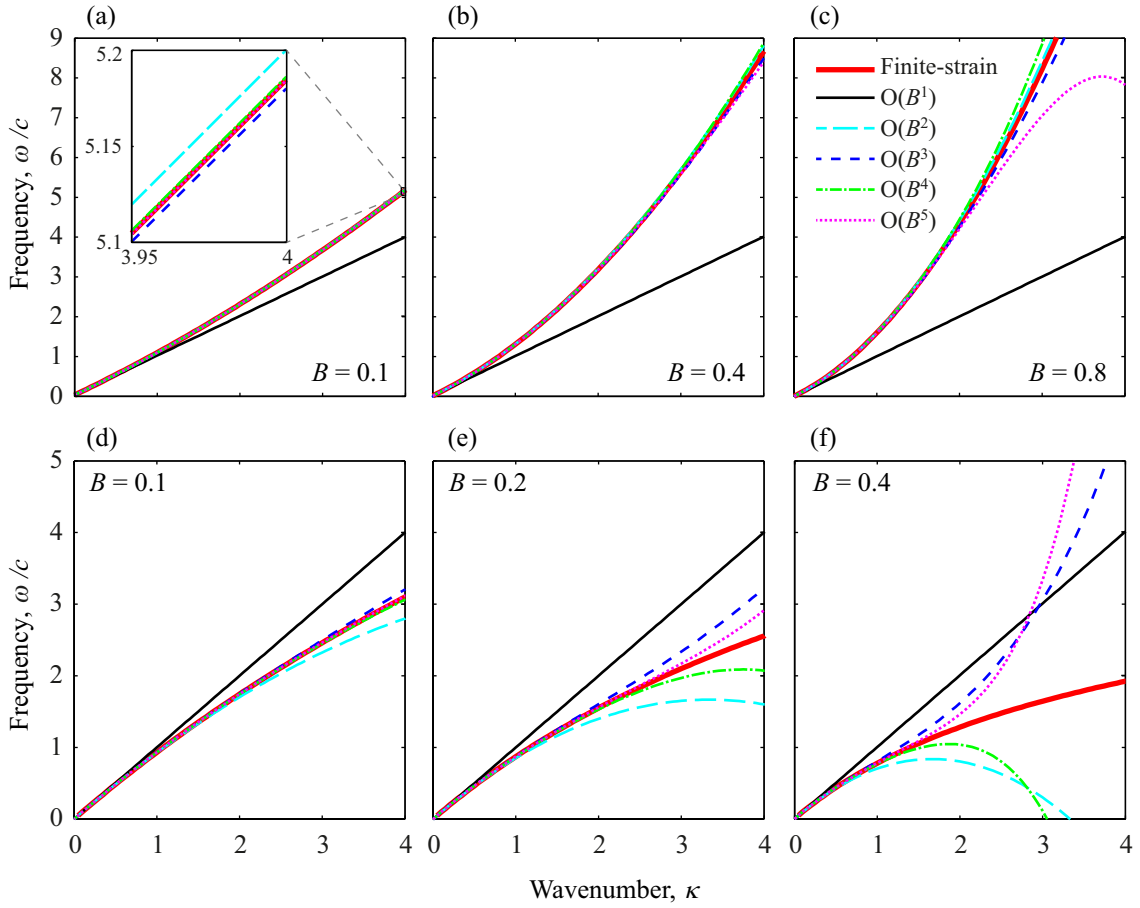

Figure 3.1: Frequency dispersion curves for a 1D homogeneous medium. (a-c) Green-Lagrange strain. (d-f) Hencky strain. The finite-strain dispersion relations are based on Eqs. (3.19) and (3.33). For comparison the first five orders from Eqs. (3.18) and (3.32) are overlaid.

$$\omega(\kappa,\kappa_e;B)=c\kappa+\frac{3c\kappa}{4}B\kappa_e-\frac{c\kappa}{32}B^2\kappa_e^2+\frac{3c\kappa}{128}B^3\kappa_e^3-\frac{37c\kappa}{2048}B^4\kappa_e^4+\ldots, \tag{3.37}$$

and

$$\omega(\kappa,\kappa_e;B)=c\kappa-\frac{3c\kappa}{4}B\kappa_e+\frac{61c\kappa}{96}B^2\kappa_e^2-\frac{217c\kappa}{384}B^3\kappa_e^3+\frac{47551c\kappa}{92160}B^4\kappa_e^4+\ldots, \tag{3.38}$$

which are direct expansions of Eqs. (2.5) and (2.6) in the case of thin rod.

The benefit of having an exact nonlinear dispersion relation for our systems is that we can characterize the accuracy limitations of the perturbation method for capturing the dispersion in these systems. It is well known that perturbation method breaks apart at large amplitudes and

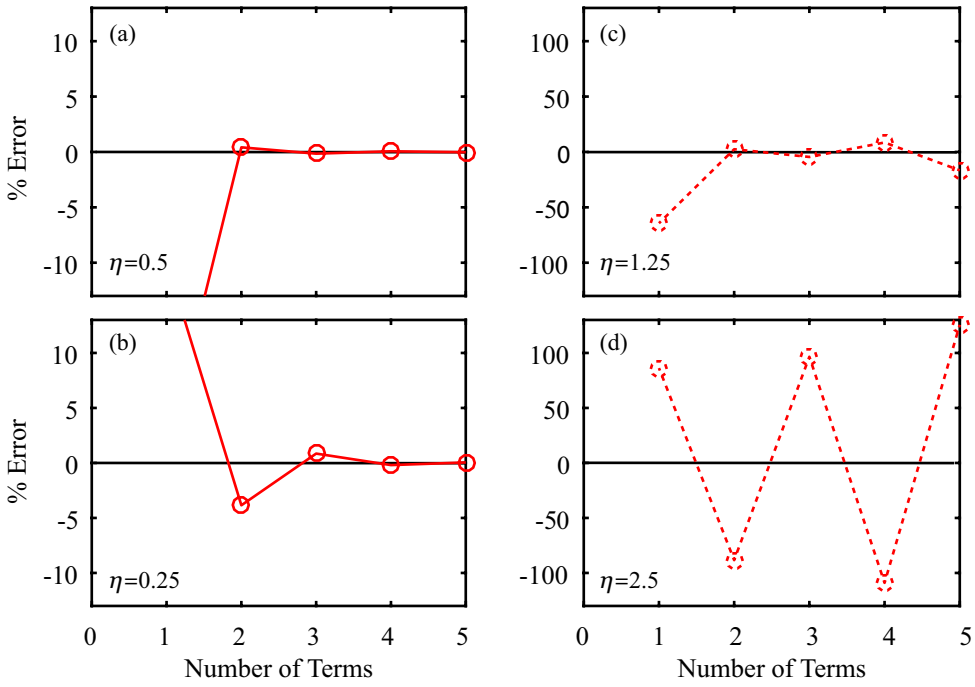

Figure 3.2: Limitation of perturbation theory in capturing dispersion. (a-b) Convergence of expanded dispersion relations (Eqs. (3.18) and (3.32)) to exact dispersion relations (Eqs. (3.19) and (3.33)) for Green Lagrange and Hencky strain, respectively. (c-d) An example of divergence for large values of η.

wave numbers. Defining a new parameter $\eta = B\kappa$, we combine the effect of both amplitude and wavenumber. As demonstrated in Fig. 3.2 for small values of this characterization number, convergence of the expanded dispersion relation to the exact dispersion relation is assured, while if we increase this value, perturbation theory falls apart and the expanded dispersion relation diverge from the exact one. Defining η^*, the limiting value of perturbation theory beyond which divergence happens, we find ${\eta^*}_5 = 1.28$ and ${\eta^*}_5 = 1.08$ for GLS and HS in the fifth order, respectively.

3.3 Space-time solution

So far we have shown how we can find the nonlinear dispersion relation for a thin elastic rod through a perturbation method. Now, we use our derived expanded NDR, Eq. (3.18), to solve Eq. (3.5) and obtain an analytical space-time solution. Recall that for longitudinal waves in a thin rod, the governing equation is of the classical form of Eq. (1.1). Consider now a thin rod of infinite

extent, $\infty < x < \infty$. Let the initial longitudinal displacement and velocity be prescribed along the entire rod by $u(x,0) = f(x)$ and $u_t(x,0) = g(x)$. The d'Alembert's solution to the homogeneous wave equation subject to general Cauchy initial conditions reads

$$u(x,t) = \frac{1}{2}\Big[f(x-ct) + f(x+ct)\Big] + \frac{1}{2c}\int_{x-ct}^{x+ct} g(s)ds. \tag{3.39}$$

If the wave equation becomes inhomogeneous with a forcing term of $q(x,t)$, the full solution of d'Alembert reads

$$u(x,t) = \frac{1}{2}\Big[f(x-ct) + f(x+ct)\Big] + \frac{1}{2c}\int_{x-ct}^{x+ct} g(s)ds + \frac{1}{2c}\int_0^t \int_{x-c(t-\tau)}^{x+c(t-\tau)} q(s,\tau)dsd\tau. \tag{3.40}$$

3.3.1 Space-time solution: Green-Lagrange strain

In what follows we consider Eq. (3.5) and assume that it has a solution of the form Eq. (3.7). Assuming that $\bar{u}(x,t)$ is an analytic function, the first order expansion can be represented by

$$\mathbf{B}: \begin{cases} \bar{u}_{1,tt} - v^2\bar{u}_{1,xx} = 0 \\ \bar{u}_1(x,0) = B\kappa_e(1+\operatorname{sech}(\kappa x))/2 \\ \bar{u}_{1,t}(x,0) = B{\kappa_e}^2 v \operatorname{sech}(\kappa x)\tanh(\kappa x)/2 \end{cases}, \tag{3.41}$$

which can be solved using Eq. (3.39) to find

$$\bar{u}_1(x,t) = B\kappa_e(1+\operatorname{sech}(\kappa(vt-x)))/2. \tag{3.42}$$

Setting up the next order we have

$$\mathbf{B^2}: \begin{cases} \bar{u}_{2,tt} - v^2\bar{u}_{2,xx} = 3v^2(\bar{u}_1\bar{u}_{1,x})_x \\ \bar{u}_2(x,0) = 0 \\ \bar{u}_{2,t}(x,0) = 0 \end{cases}, \tag{3.43}$$

which can be solved using Eq. (3.40) to find

$$\begin{aligned} \bar{u}_2(x,t) = &\frac{3B^2\kappa_e^2}{32}\Big(\operatorname{sech}(\kappa_e(x+vt))(2+\operatorname{sech}(\kappa_e(x+vt)))+ \\ &\operatorname{sech}(\kappa_e(x-vt))\big(-2-\operatorname{sech}(\kappa_e(x-vt))+ \\ &4vt\kappa_e(1+\operatorname{sech}(\kappa_e(x-vt)))\tanh(\kappa_e(x-vt))\big)\Big). \end{aligned} \tag{3.44}$$

Using Eq. (3.18), one can find $v = c$ and $v = c(1 + 3B\kappa_e/4)$ in Eqs. (3.42) and (3.44), respectively.

3.3.2 Space-time solution: Hencky strain

Similar to the previous subsection, we consider Eq. (3.22) and assume that it has a solution of the form Eq. (3.7). The first order expansion can be represented by

$$\mathbf{B}:\begin{cases}\bar{u}_{1,tt} - v^2\bar{u}_{1,xx} = 0\\ \bar{u}_1(x,0) = B\kappa_e(1+\operatorname{sech}(\kappa x))/2\\ \bar{u}_{1,t}(x,0) = B{\kappa_e}^2 v\operatorname{sech}(\kappa x)\tanh(\kappa x)/2\end{cases}, \tag{3.45}$$

with the solution of

$$\bar{u}_1(x,t) = B\kappa_e(1+\operatorname{sech}(\kappa(vt-x)))/2. \tag{3.46}$$

For the next order we have

$$\mathbf{B^2}:\begin{cases}\bar{u}_{2,tt} - v^2\bar{u}_{2,xx} = -3v^2(\bar{u}_1\bar{u}_{1,x})_x\\ \bar{u}_2(x,0) = 0\\ \bar{u}_{2,t}(x,0) = 0\end{cases}, \tag{3.47}$$

which can be solved to find

$$\begin{aligned}\bar{u}_2(x,t) = -\frac{3B^2\kappa_e^2}{32}\Big(&\operatorname{sech}(\kappa_e(x+vt))(2+\operatorname{sech}(\kappa_e(x+vt)))+\\ &\operatorname{sech}(\kappa_e(x-vt))\big(-2-\operatorname{sech}(\kappa_e(x-vt))+\\ &4vt\kappa_e(1+\operatorname{sech}(\kappa_e(x-vt)))\tanh(\kappa_e(x-vt))\big)\Big).\end{aligned} \tag{3.48}$$

Also, $v = c$ and $v = c(1 + 3B\kappa_e/4)$ in Eqs. (3.46) and (3.48), respectively.

Knowing $\bar{u}_1$ and $\bar{u}_2$ in both GLS and HS measures, we can plug them back in Eq. (3.7) to obtain the second order solution for the system. These solutions has been verified by obtaining the wavenumber-frequency spectrum from the corresponding spatiotemporal results.

Chapter 4

Finite-strain Bloch wave propagation by the transfer matrix method with nonlinear enrichment[1]

The introduction of nonlinearity alters the dispersion of elastic waves in solid media. In this chapter, we present an analytical formulation for the treatment of finite-strain Bloch waves in one-dimensional phononic crystals consisting of layers with alternating material properties. Considering longitudinal waves and ignoring lateral effects, the exact dispersion relation in each homogeneous layer is first obtained and subsequently used within the transfer matrix method to derive an approximate nonlinear dispersion relation for the overall periodic medium. The result is an amplitude-dependent elastic band structure that upon verification by numerical simulations is valid up to an amplitude-to-unit-cell length ratio of 1/8. The derived dispersion relation allows us to elucidate the interplay between the dispersion stiffening and softening effects that emerge due to the nonlinearity and the periodicity, respectively. For example, for a wave amplitude on the order of one eighth of the unit-cell size in a demonstrative structure, the two effects are practically in balance for wavelengths as small as roughly three times the unit-cell size.

4.1 Introduction

4.1.1 Phononic materials

Phononic materials are elastic materials with prescribed phonon wave propagation properties. While the term "phonon" is formally used in the physical sciences to describe vibration states

[1] This chapter is drawn from Ref. [92] and has been adapted to suit the style and the notation of the dissertation.

in condensed matter at the atomic scale, in the present context, we use it to broadly describe elastic wave propagation modes. Like crystalline materials, a phononic material has local intrinsic properties and is therefore mathematically treated as a medium that is spatially extended to infinity. Compared to a homogeneous and geometrically uniform elastic continuum, a phononic material exhibits rich and unique dynamical properties due to the presence of some form of non-homogeneity and/or non-uniformity in either an ordered or disordered manner. In the ordered case, phononic materials are constructed from a repeated array of identical *unit cells* which enables the calculation of the elastic band structure for a given topological configuration. This direct exposure, and access, to the inherent dynamical properties of phononic materials has vigorously chartered a new direction in materials physics, at a multitude of scales, and has already begun to impact numerous applications ranging from vibration control [21, 22], through subwavelength sound focusing [23, 24] and cloaking [25, 26], to reducing the thermal conductivity of semiconductors [27–29] and stabilizing a wall-bounded fluid flow [30]. A discussion of applications and references are provided in recent review articles [7, 31, 118] and books [32, 119, 120], and special journal issues on the topic assemble some of the latest advances in the field [33, 34, 121–125].

4.1.2 Elastic wave dispersion in the presence of nonlinearity

The majority of theoretical investigations of wave motion in elastic solids are based on linear analysis, that is, linear constitutive laws and linear strain-displacement relationships are assumed (see Refs. [63] and [64], and references therein). The incorporation of nonlinear effects, however, gives rise to a broader range of physical phenomena including amplitude-dependent elastic wave motion [65–69]. The effects of nonlinearity have also been studied for other types of waves such as water waves [70, 71] and electrostatic and electromagnetic waves in plasmas [72, 73].

Finite-strain waves in elastic solids is a subset among the broader class of nonlinear waves. From a mathematical perspective, a formal treatment of finite strain requires the incorporation of a nonlinear strain tensor in setting up the governing equations of motion. Regardless of the type of nonlinearity, a common analysis framework has been one in which the dispersion is viewed to

arise linearly, e.g., due to the presence of a microstructure or geometrical constraints, and that such dispersion may be balanced with nonlinear effects to allow for the generation of nonlinear traveling waves of fixed spatial profile such as shock waves and solitons [68, 69]. In contrast to this dispersion/non-linearity balancing framework where the focus is on finding these special types of waves and characterizing the amplitude-dependence, or wave-number-dependence, of their speeds, it has recently been shown that nonlinearity in itself may cause dispersion without the need for a linear dispersive mechanism [1, 18]. This perspective provides a motivation to derive dispersion relations that inherently embody the effects of the nonlinearities on the dispersion, i.e., amplitude-dependent relations for general wave motion that encompass both the speed (or frequency) and the wave number.

Extending to periodic media, nonlinear dispersion relations appear in various contexts, for example, electronic waves in metals and semiconductors [76] and electromagnetic waves in photonic crystals [77, 78]. In the context of nonlinear phononic materials, there are several studies that follow the premise of Bloch wave propagation analysis. These include investigations on systems exhibiting material nonlinearity, analyzed using the method of multiple scales [79–81], perturbation analysis [75, 82, 113, 126], the harmonic balance method [83, 84], and the transfer matrix (TM) method in conjunction with a perturbation technique [85]. The effects of nonlinearity on the dynamics of periodic materials has also been explored in the context of atomic-scale models incorporating anharmonic potentials; see, for example, a recent paper focusing on phonon transport [86]. Concerning finite-strain dispersion in a layered elastic medium, this was recently investigated by Andrianov *et al.* [78] via a homogenization approach whereby the periodic unit cell was first homogenized as a linear medium and subsequently a finite-strain dispersion relation was derived for the averaged medium. This approach therefore does not retain the periodic character in the derived dispersion relation. On the experimental track, numerous studies have been conducted on nonlinear wave phenomena particularly in periodic granular chains, e.g., [74, 87]. It is evident that the effects of nonlinearity in phononic/granular materials could be utilized to enrich the design of devices in numerous engineering applications, such as for shock mitigation [88], tunable wave

filtering [75], focusing [89] and rectification [90]. A more recent study experimentally investigated nonlinear vibrational waves in periodic strings [91]. The field of nonlinear elastic wave propagation continues to grow and branch into new directions, such as, for example, supratransmission in dissipative periodic structures [127] and the utilization of large-amplitude waves to create topologically protected edge states in two-dimensional lattices [128].

4.1.3 Overview

In this chapter, we present a theoretical treatment of elastic wave motion in phononic materials in the presence of nonlinearity, specifically the type arising from finite elastic strain. We consider *phononic crystals*, which is a class of phononic materials in which the prime dispersion mechanism is Bragg scattering [1] . For ease of exposition, we focus on a one-dimensional (1D) layered material model admitting only longitudinal displacements (which may also be viewed as a model for a periodic thin rod). Since the TM method provides the backbone of our approach, we first briefly overview it, in conjunction with Bloch's theorem [2], for the exact analysis of simple 1D linear phononic crystals (Section 4.2). We then review the treatment of geometric nonlinearity, i.e., finite strain, in the context of a homogeneous medium (Section 4.3.1). In Section 4.3.2, we combine the previous derivations, that is, we allow the finite-strain dispersion relation for a homogeneous medium to represent the motion characteristics in a single layer of a periodically layered 1D phononic crystal and subsequently incorporate this relation into the TM formalism. While the finite-strain dispersion within each layer is exact, the dispersion relation we obtain for the overall 1D phononic crystal represents an approximate solution. In Section 4.5, we verify the derived dispersion relation using brute-force space-time simulations followed by a Fourier transformation into the wave number-frequency domain. The simulations are also used to determine the upper limit of wave amplitude per unit-cell length for which the theory is accurate. Finally, we use our formulation to investigate the effects of geometric nonlinearity on the elastic band structure and Bloch mode

[1] A phononic material in general may be classified into two types, a phononic crystal and a locally resonant elastic metamaterial [7, 32]. In this work we focus on the former, but the mathematical treatment is also applicable to the latter [93].

shapes as a function of the wave amplitude and shed some light on the possibility of balancing the linear and nonlinear alterations to the dispersion relation to yield a solitary-like wave.

4.2 Wave propagation in 1D linear phononic crystals

Bloch's theorem [2] provides the underlying mathematical framework for obtaining the elastic band structure (i.e., dispersion curves) for a phononic crystal. There are several approaches for applying the theorem to a unit cell modeled as a continuum. In this work we utilize the TM method, which is described briefly below (for a background on the method and further details, see Refs. [3–5]).

We begin our dynamic analysis of a phononic crystal with the statement of the equation of motion. As mentioned earlier, we restrict ourselves to a 1D model, e.g., a thin rod, for which the equation of motion is

$$(Eu_{,x})_{,x} = \rho u_{,tt}, \tag{4.1}$$

where x, t, $u = u(x,t)$, $E = E(x)$ and $\rho = \rho(x)$ denote the position, time, displacement, material Young's modulus and material density, respectively. For simplicity, we assume that the cross-sectional area of the rod is non-varying with x.

Equation (4.1) may be used to study the propagation of elastic waves in various 1D media. In particular, we consider a homogeneous, linearly elastic 1D rod of infinite extent (having no boundaries at which waves may reflect), and apply a plane wave solution of the form

$$u(x,t) = A\mathrm{e}^{\mathrm{i}(\kappa x - \omega t)}, \tag{4.2}$$

where A is the wave amplitude, κ is the wave number, ω is the temporal frequency of the traveling wave, and $\mathrm{i} = \sqrt{-1}$. Here, we make another assumption about the cross-sectional dimensions of the rod, namely, that they are much smaller than the wavelengths of all waves considered in the analysis. Substituting Eq. (4.2) into Eq. (4.1) provides the linear dispersion relation

$$E\kappa^2 = \rho\omega^2. \tag{4.3}$$

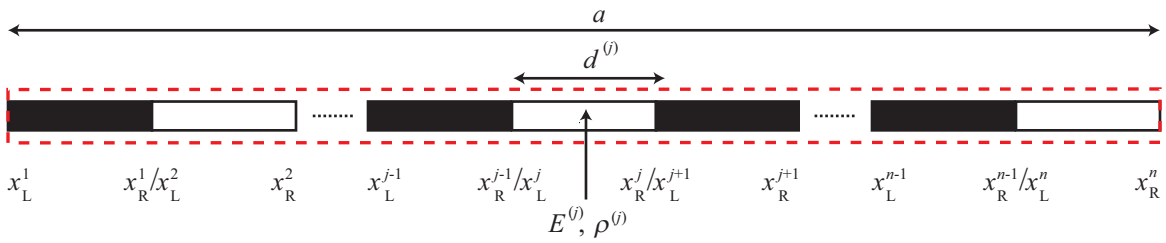

Figure 4.1: Continuous model of a 1D two-phased phononic crystal viewed as a periodic thin rod.

This approach may also be applied to heterogeneous media provided the heterogeneity is periodic. In this case, we refer to Eq. (4.2) as Bloch's theorem (where $A = A(x, \kappa)$), and it suffices to analyze only a single unit cell representing the unique segment that is repeated to generate the periodic medium and to apply periodic boundary conditions to this segment. In Fig. 4.1, we present a simple bi-material model of a 1D phononic crystal in the form of a layered periodic rod (where the unit cell is enclosed in a red dashed box). The spatial lattice spacing of the 1D phononic crystal is denoted by the constant a. The same analysis may also be applied to a unit cell with a stepwise varying cross-sectional area, but this case will not be considered here.

For an arbitrary homogeneous layer j in the unit cell, the associated material properties, which are constant, are denoted as $E^{(j)}$ and $\rho^{(j)}$. The longitudinal velocity in layer j is therefore $c^{(j)} = \sqrt{E^{(j)}/\rho^{(j)}}$. The layer is bordered by layer $j-1$ on the left and layer $j+1$ on the right. Denoting the thickness of an arbitrary layer by $d^{(j)}$, the cell length is $a = \sum_{j=1}^{n} d^{(j)}$ for a unit cell with n layers. Following this notation, the solution to Eq. (4.1) is formed from the superposition of forward (transmitted) and backward (reflected) traveling waves with a harmonic time dependence,

$$u(x,t) = [A_+^{(j)} \mathrm{e}^{\mathrm{i}\kappa^{(j)}x} + A_-^{(j)} \mathrm{e}^{-\mathrm{i}\kappa^{(j)}x}]\mathrm{e}^{-\mathrm{i}\omega t}, \tag{4.4}$$

where $\kappa^{(j)} = \omega/c^{(j)}$ is the layer wave number. The spatial components of Eq. (4.4) may be written along with those of the stress,

$$\sigma = E u_{,x}, \tag{4.5}$$

in compact form as

$$\begin{bmatrix} u(x) \\ \sigma(x) \end{bmatrix} = \begin{bmatrix} 1 & 1 \\ \mathrm{i}Z^{(j)} & -\mathrm{i}Z^{(j)} \end{bmatrix} \begin{bmatrix} A_+^{(j)} \mathrm{e}^{\mathrm{i}\kappa^{(j)}x} \\ A_-^{(j)} \mathrm{e}^{-\mathrm{i}\kappa^{(j)}x} \end{bmatrix} = \mathbf{H}_j \begin{bmatrix} A_+^{(j)} \mathrm{e}^{\mathrm{i}\kappa^{(j)}x} \\ A_-^{(j)} \mathrm{e}^{-\mathrm{i}\kappa^{(j)}x} \end{bmatrix},$$

where $Z^{(j)} = E^{(j)}\kappa^{(j)}$. There are two conditions that must be satisfied at the layer interfaces: (1) the continuity of displacement and (2) the continuity of stress. This allows for the substitution of the relation $x_R^{(j)} = x_L^{(j)} + d^{(j)}$ (where $x_R^{(j)}$ and $x_L^{(j)}$ denote the position of the right and left boundary, respectively, of layer j) into Eq. (4.6) and thus relating the displacement and stress at $x_L^{(j)}$ to those at $x_R^{(j)}$. Subsequently, by setting $x = x_L^{(j)}$ in Eq. (4.6), we get

$$\begin{bmatrix} u(x_R^{(j)}) \\ \sigma(x_R^{(j)}) \end{bmatrix} = \mathbf{H}_j \mathbf{D}_j \mathbf{H}_j^{-1} \begin{bmatrix} u(x_L^{(j)}) \\ \sigma(x_L^{(j)}) \end{bmatrix} = \mathbf{T}_j \begin{bmatrix} u(x_L^{(j)}) \\ \sigma(x_L^{(j)}) \end{bmatrix}, \tag{4.6}$$

where

$$\mathbf{D}_j = \begin{bmatrix} \mathrm{e}^{\mathrm{i}\kappa^{(j)}d^{(j)}} & 0 \\ 0 & \mathrm{e}^{-\mathrm{i}\kappa^{(j)}d^{(j)}} \end{bmatrix}, \tag{4.7}$$

and $\mathbf{T}_j$, the *transfer matrix* for layer j, has the expanded form

$$\mathbf{T}_j = \begin{bmatrix} \cos(\kappa^{(j)}d^{(j)}) & (1/Z^{(j)})\sin(\kappa^{(j)}d^{(j)}) \\ -Z^{(j)}\sin(\kappa^{(j)}d^{(j)}) & \cos(\kappa^{(j)}d^{(j)}) \end{bmatrix}. \tag{4.8}$$

As previously stated, Eq. (4.6) relates the displacement and stress at $x_L^{(j)}$ to those at $x_R^{(j)}$ of the same layer j. However, since the construction of the transfer matrix is valid for any layer and $x_L^{(j)} \equiv x_R^{(j-1)}$, the result in Eq. (4.6) can be extended recursively across several layers. In the interest of brevity, let $\mathbf{y}(.) = [\mathrm{u}(.)\ \sigma(.)]^{\mathrm{T}}$, thus,

$$\mathbf{y}(x_R^n) = \mathbf{T}_n \mathbf{T}_{n-1} \ldots \mathbf{T}_1 \mathbf{y}(x_L^1) = \mathbf{T}\mathbf{y}(x_L^1). \tag{4.9}$$

Ultimately, the displacement and stress at the left end of the first layer ($x = x_L^1$) in a unit cell are related to those at the right boundary of the nth layer ($x = x_R^n$) by the cumulative transfer matrix, $\mathbf{T}$.

Now we turn to Bloch's theorem, which states that the time harmonic response at a given point in a unit cell is the same as that of the corresponding point in an adjacent unit cell except for a phase difference of $e^{i\kappa a}$. This relation is given by $f(x+a) = e^{i\kappa a} f(x)$, which when applied to the states of displacement and stress across a unit cell gives

$$\mathbf{y}(x_R^n) = e^{i\kappa a}\mathbf{y}(x_L^1). \tag{4.10}$$

Combining Eqs. (4.9) and (4.10) yields the eigenvalue problem

$$[\mathbf{T} - \mathbf{I}\gamma]\mathbf{y}(x_L^1) = \mathbf{0}, \tag{4.11}$$

where $\gamma = e^{i\kappa a}$. The solution of Eq. (4.11), which appears in complex conjugate pairs, provides the dispersion relation $\kappa = \kappa(\omega)$ for the 1D phononic crystal. Real-valued wave numbers, calculated from γ using Eq. (4.12), support propagating wave modes, whereas imaginary wave numbers, extracted from γ using Eq. (4.13), represent spatially attenuating modes:

$$\kappa_{\mathrm{R}} = \frac{1}{a}\mathrm{Re}[\frac{1}{i}\ln\gamma], \tag{4.12}$$

$$\kappa_{\mathrm{I}} = \frac{1}{a}\mathrm{Im}[\frac{1}{i}\ln\gamma]. \tag{4.13}$$

4.3 Treatment of nonlinearity

We now provide a theoretical treatment of finite-strain dispersion; first we review the pre-requisite problem of a 1D homogeneous medium, and follow with the derivation for a 1D phononic crystal. In the homogeneous medium problem, the approach is exact regardless of the amplitude of the traveling wave, i.e., strong nonlinearities are treated exactly. In the subsequent derivation of the phononic crystal dispersion curves, the accuracy decreases with increasing wave amplitude.

4.3.1 Finite-strain waves in 1D homogeneous media

The equation of motion and finite-strain dispersion relation is reviewed here for 1D plane wave motion in a bulk homogeneous medium without consideration of lateral effects. In principle, this problem is equivalent to that of a slender rod. In the derivations, all terms in the nonlinear

strain tensor are retained and no high-order terms emerging from the differentiations are subsequently neglected. The reader is referred to Ref. [1] for more details as well as a validation of the theoretical approach by means of a comparison with a standard finite-strain numerical simulation of a corresponding 1D model with finite dimensions.

4.3.1.1 Equation of motion

Introducing u as the elastic longitudinal displacement, the exact complete Green-Lagrange strain field in our 1D model is given by

$$\epsilon = \frac{\partial u}{\partial s} + \frac{1}{2}(\frac{\partial u}{\partial s})^2, \tag{4.14}$$

where the first and second terms on the RHS represent the linear and nonlinear parts, respectively, and s is the Lagrangian longitudinal coordinate which is equal to x in Eq. (4.1).

Using Hamilton's principle, we write the equation of motion under longitudinal stress as

$$\int_0^t (\delta T - \delta U^e)\mathrm{d}t = 0, \tag{4.15}$$

where T and U^e denote kinetic and elastic potential energies, respectively. We note that no external nonconservative forces are permitted because of our interest in the free wave propagation problem. Furthermore, the effects of lateral inertia are neglected. The variation of kinetic energy is obtained using integration by parts and is given as

$$\delta T = -\rho A \int_0^l (u_{,tt}\delta u)\mathrm{d}s, \tag{4.16}$$

where l denotes the length of a portion of the 1D medium. Similarly, the variation of elastic potential energy is written as

$$\delta U^e = \int_0^l \int_A (\sigma \delta \epsilon)\mathrm{d}A\,\mathrm{d}s, \tag{4.17}$$

where σ is the longitudinal stress. We choose to base our analysis on the Cauchy stress and model the stress-strain relationship by Hooke's law, $\sigma = E\epsilon$. Using Eq. (4.17), and with the aid of

integration by parts, we can now write the variation of elastic potential energy as

$$\delta U^e = \int_0^l \{\frac{1}{2} EAh(h^2 - 1)\delta u'\}\mathrm{d}s, \tag{4.18}$$

where $u' = du/ds = u_{,s}$, and h is an agent variable defined as

$$h = 1 + u'. \tag{4.19}$$

Substitution of Eqs. (4.18) and (4.16) into Eq. (4.15) produces the exact finite-strain equation of motion as

$$\rho A u_{,tt} = \frac{1}{2} EA(3h^2 - 1)u''. \tag{4.20}$$

If the longitudinal deformation is infinitesimal, then u' is small and from Eq. (4.19), $h \approx 1$. Substitution of $h = 1$ into Eq. (4.20) leads to

$$\rho A u_{,tt} = EAu'', \tag{4.21}$$

which is the equation of motion describing infinitesimal longitudinal deformation.

4.3.1.2 Dispersion relation

Using Eq. (4.19), we rewrite Eq. (4.20) as

$$u_{,tt} - c^2 u'' = \frac{1}{2}\Big[c^2[3(u')^2 + (u')^3]\Big]', \tag{4.22}$$

where $c = \sqrt{E/\rho}$. Differentiation of Eq. (4.22) with respect to s gives

$$(u_{,tt})' - c^2 u^{(3)} = \frac{1}{2}\Big[c^2[3(u')^2 + (u')^3]\Big]''. \tag{4.23}$$

Defining $\bar{u} = u'$ gives

$$\bar{u}_{,tt} - c^2 \bar{u}_{,ss} = \frac{1}{2}\Big[c^2[3\bar{u}^2 + \bar{u}^3]\Big]_{,ss}, \tag{4.24}$$

and introducing a phase variable $z = |\kappa|s + \omega_{\text{fin}} t$, where ω_{fin} represents the wave frequency under finite strain, Eq. (4.24) becomes

$$\omega_{\text{fin}}^2 \bar{u}_{,zz} - c^2\kappa^2 \bar{u}_{,zz} = \frac{1}{2}\kappa^2\Big[c^2[3\bar{u}^2 + \bar{u}^3]\Big]_{,zz}. \tag{4.25}$$

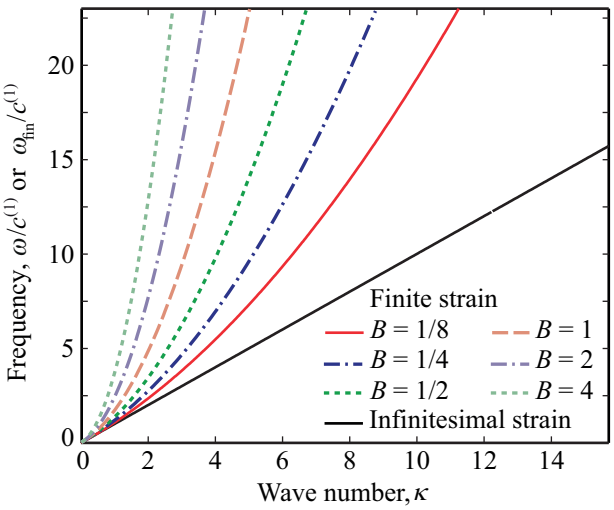

Figure 4.2: Frequency dispersion curves for a 1D homogeneous elastic medium [1]. The finite-strain dispersion relation is based on Eq. (4.29); the infinitesimal strain dispersion relation is based on Eq. (4.30).

Integrating Eq. (4.25) twice leads to

$$(\omega_{\text{fin}}^2 - c^2\kappa^2)\bar{u} - \frac{c^2\kappa^2}{2}[3\bar{u}^2 + \bar{u}^3] = 0, \tag{4.26}$$

where the nonzero constants of integration (in the form of polynomials in z) represent secular terms which we have set equal to zero to ensure that all waves remain bounded. Selecting the positive root of Eq. (4.26) we get

$$\bar{u}(z) = \frac{-3 + \sqrt{1 + 8\omega_{\text{fin}}^2/c^2\kappa^2}}{2}. \tag{4.27}$$

Since $\bar{u} = u_{,s}$, we recognize that $\bar{u} = |\kappa| u_{,z}$ and therefore Eq. (4.27) represents a first-order ordinary differential equation with z and u as the independent and dependent variables, respectively.

Now we return to Eq. (4.22) and consider for initial conditions a sinusoidal displacement field with amplitude B. This represents a fundamental harmonic signal for which we seek to characterize its dispersive behavior. In principle, any choice of the initial velocity field is permitted. Following the change of variables that has been introduced, we impose a balance between the spatial and temporal phase which allows us to set up the problem at $z = 0$. Thus we have the following

restrictions on the $\bar{u}(z)$ function given in Eq. (4.27):

$$\bar{u}(0) = |\kappa|B, \quad \bar{u}_{,z}(0) = 0. \tag{4.28}$$

These represent initial conditions in the wave phase, z, for Eq. (4.25) and allow for the introduction of the wave amplitude, B, into the formulation. Applying Eq. (4.28) to Eq. (4.27) enables us to use the latter to solve for ω_{fin} for a given value of κ. This leads to the exact dispersion relation,

$$\omega_{\text{fin}}(\kappa; B) = \sqrt{\frac{2 + 3B|\kappa| + (B\kappa)^2}{2}}\omega, \tag{4.29}$$

where ω is the frequency based on infinitesimal strain,

$$\omega(\kappa) = c|\kappa|. \tag{4.30}$$

By taking the limit, $\lim_{B\to 0} \omega_{\text{fin}}(\kappa; B)$, in Eq. (4.29) we recover Eq. (4.30) which is the standard linear dispersion relation for a 1D homogeneous elastic medium or a thin rod [6]. We note that Eq. (4.29) is a general nonlinear dispersion relation that is independent of the wave profile.

For demonstration, six amplitude-dependent finite-strain dispersion curves based on Eq. (4.29) are plotted in Fig. 4.2. These curves describe the fundamental dispersive properties that emerge due to the incorporation of finite strain. The curves demonstrate that nonlinearity by itself causes wave dispersion in an elastic medium, i.e., without the need for a linear dispersive mechanism. From a physical point of view one may envision an initial prescribed harmonic wave being set free at some point in time. The dispersion relation of Eq. (4.29) describes the frequency versus wave number relation for this wave as it disperses in the presence of amplitude-dependent finite strain. This concept was tested numerically and validated in Ref. [1]. Superimposed in Fig. 4.2 is the dispersion curve based on infinitesimal strain, i.e., Eq. (4.30). It is noted that the deviation between a finite-strain curve and the infinitesimal-strain curve increases with wave number, and the effect of the wave amplitude on this deviation is illustrated in the figure for six finite-strain cases where the value of B is doubled from one case to the other.

4.3.2 Finite-strain waves in 1D phononic crystals

The TM method is now used to obtain a dispersion relation for a 1D phononic crystal whose constituent materials are exhibiting finite-strain dispersion. The outcome is an approximate overall dispersion relation since the construction of the transfer matrix is based on a linear strain-displacement relationship [see Eq. (4.5) and (4.6)]. While not exact, this approach provides a quantitative prediction of the effects of nonlinearity on the location and size of band gaps and the values of the group velocity across the spectrum, all as a function of wave amplitude.

As presented in Section 4.2, the TM method is applicable in either the absence or presence of nonlinearity; the distinction is made in the definition of $\kappa^{(j)}$ in Eq. (4.4). For the linear problem, $\kappa^{(j)} = \kappa^{(j)}(\omega) = \omega/c^{(j)}$ as outlined earlier. A similar relationship between the jth-layer wave number and the finite-strain wave frequency, ω_{fin}, is now developed, i.e., $\kappa^{(j)} = \kappa^{(j)}(\omega_{\text{fin}})$.

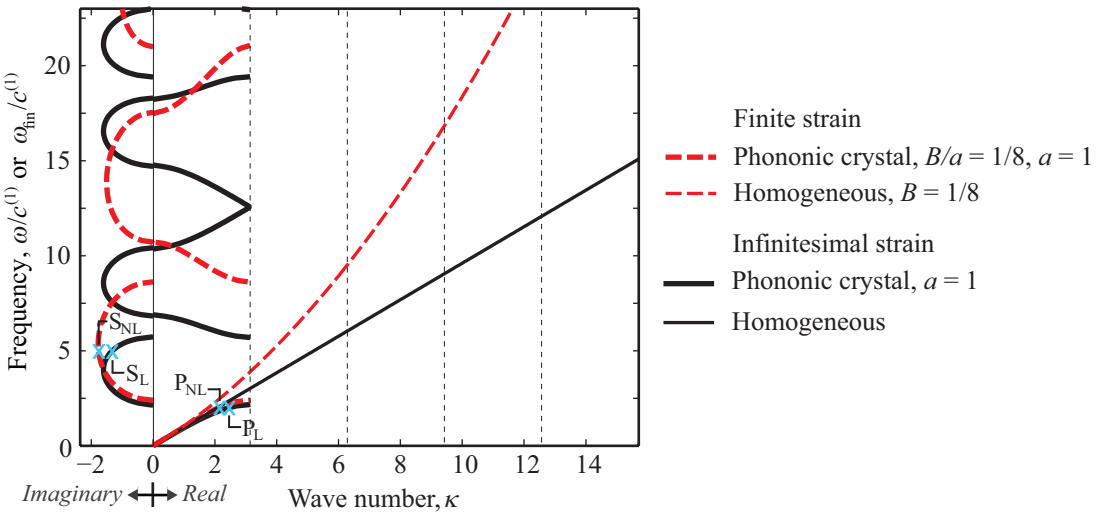

Figure 4.3: Frequency band structure for a 1D phononic crystal under finite strain [obtained using Eq. (4.33)]. For comparison, the dispersion curves under infinitesimal strain are included. Also, corresponding dispersion curves for a statically equivalent 1D homogeneous elastic medium are overlaid. The nonlinearity-induced shifting of the dispersion curves is marked at two frequencies. Points P_L and P_{NL} are at frequency $\omega/c^{(1)} = 2$ and lie on the first infinitesimal-strain and the first finite-strain pass-band branch, respectively. Points S_L and S_{NL} are at frequency $\omega/c^{(1)} = 5$ and lie on the first infinitesimal-strain and the first finite-strain stop-band branch, respectively.

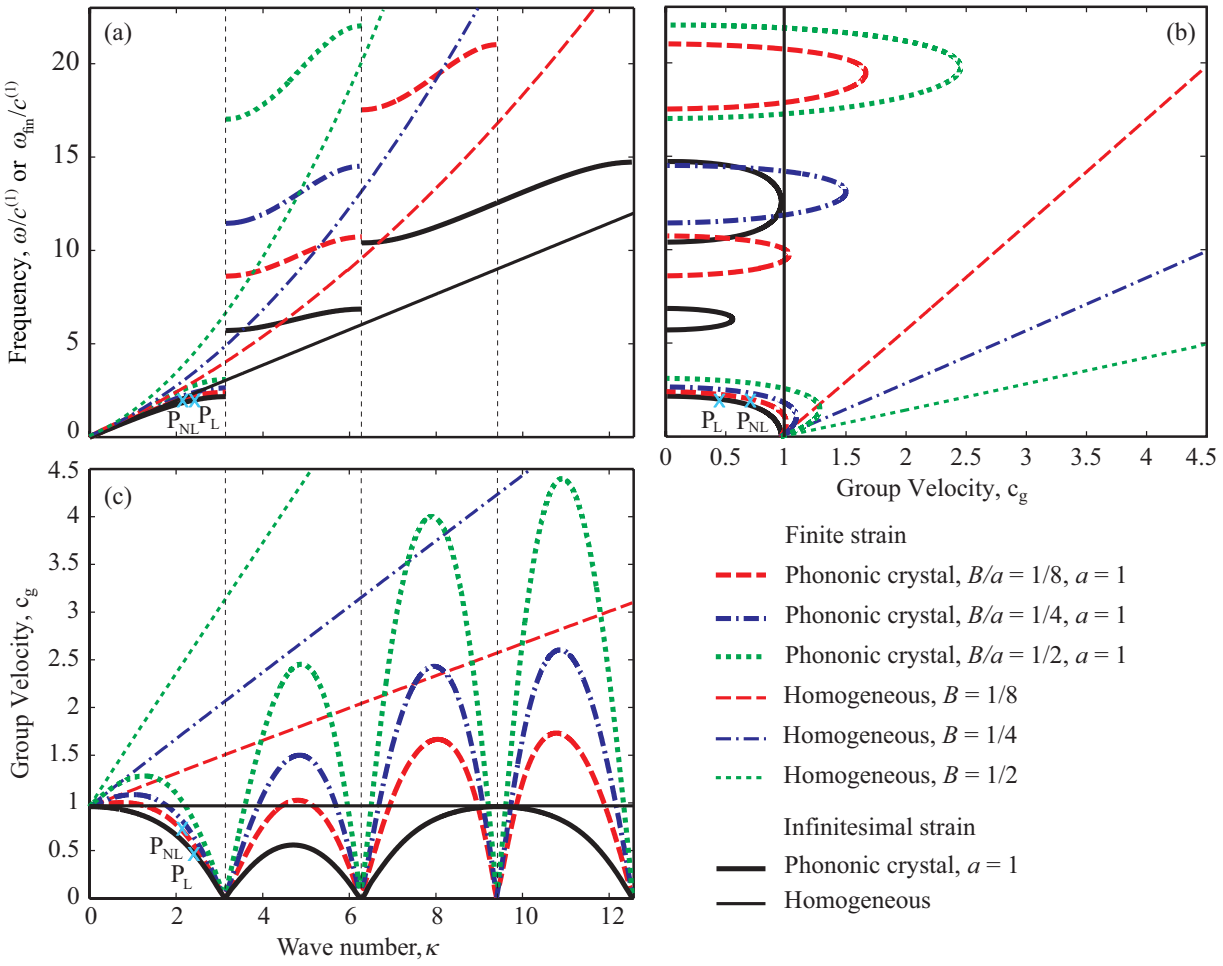

Figure 4.4: Effect of nonlinearity on the group velocity for the 1D phononic crystal and the statically equivalent 1D homogeneous elastic medium considered in Fig. 4.3. (a) unfolded frequency band structure, (b) frequency versus group velocity, (c) group velocity versus wave number. The nonlinearity-induced shifting of the dispersion curves at frequency $\omega/c^{(1)} = 2$ is noted.

First we rewrite Eq. (4.29) explicitly for layer j,

$$\omega_{\text{fin}} = c^{(j)}\kappa^{(j)}\sqrt{\frac{2+3B\kappa^{(j)}+[B\kappa^{(j)}]^2}{2}}, \tag{4.31}$$

which may be cast as the following 4th order characteristic equation:

$$[\kappa^{(j)}]^2(1+B\kappa^{(j)})(2+B\kappa^{(j)}) - 2\frac{\omega_{\text{fin}}^2}{[c^{(j)}]^2} = 0. \tag{4.32}$$

Solving Eq. (4.32) gives

$$\kappa_{1,2}^{(j)} = \frac{1}{12B}\Big(-9+P^{(j)} \mp \sqrt{Q^{(j)}-R^{(j)}}\Big), \tag{4.33a}$$

$$\kappa_{3,4}^{(j)} = -\frac{1}{12B}\Big(9+P^{(j)} \pm \sqrt{Q^{(j)}+R^{(j)}}\Big), \tag{4.33b}$$

where

$$P^{(j)} = \sqrt{\frac{33c^{(j)}A^{(j)}+12(4[c^{(j)}]^2-24B^2\omega_{\text{fin}}^2+[A^{(j)}]^2)}{c^{(j)}A^{(j)}}}, \tag{4.34a}$$

$$Q^{(j)} = \frac{66c^{(j)}A^{(j)}-48([c^{(j)}]^2-6B^2\omega_{\text{fin}}^2)-12[A^{(j)}]^2}{c^{(j)}A^{(j)}}, \tag{4.34b}$$

$$R^{(j)} = \frac{54\sqrt{3c^{(j)}A^{(j)}}}{\sqrt{11c_0^{(j)}A^{(j)}+4(4[c^{(j)}]^2+[A^{(j)}]^2-24B^2\omega_{\text{fin}}^2)}}, \tag{4.34c}$$

and

$$A^{(j)} = \left(-99B^2\omega_{\text{fin}}^2c^{(j)}+8[c^{(j)}]^3+3B\omega_{\text{fin}}\sqrt{(1536B^2+321[c^{(j)}]^2)B^2\omega_{\text{fin}}^4-48[c^{(j)}]^4}\right)^{\frac{1}{3}} . \tag{4.34d}$$

At this point, Eq. (4.33) is substituted into the $Z^{(j)} = E^{(j)}\kappa^{(j)}$ equations in the TM formulation presented in Section 4.2. This yields a nonlinear enriched eigenvalue problem that we may use to obtain an approximation of the finite-strain dispersion curves of a 1D phononic crystal [2] . While the technique is not limited to small values of B/a, its accuracy reduces as the strength of the nonlinearity increases. In Section 4.5, we numerically examine the accuracy as a function of B/a.

[2] This approach may in principle also be applied to other types of waves such as electromagnetic waves in a photonic crystal [129]. In that case, the nature of the nonlinearity will be different, but the process of enriching the TM formulation with a wavenumber that point-wise captures the nonlinear behavior will essentially be the same.

To demonstrate the effects of nonlinearity, we consider the same geometric features as the periodic bi-material rod in Fig. 4.1 and the following ratio of material properties: $c^{(2)}/c^{(1)} = 2$ and $\rho^{(2)}/\rho^{(1)} = 3$. Furthermore, we consider a bi-layered unit cell in which $d^{(2)} = d^{(1)}$. The results are shown in Fig. 4.3 for a phononic crystal of size $a = 1$ (arbitrary units) and a value of wave amplitude of $B/a = 1/8$. Superimposed, for comparison, are the dispersion curves on the basis of infinitesimal strain and the corresponding dispersion curves for an equivalent statically homogenized medium for which the speed of sound is c (obtained by the standard rule of mixtures). We observe in the figure that the finite-strain dispersion curves asymptotically converge to the infinitesimal and homogenized curves at long wavelengths as expected. We also note that the finite strain causes the dispersion branches to rise and the band-gap sizes to increase significantly−an attractive trait for many applications involving sound and vibration control. This behavior, however, is dependent on the type of nonlinearity considered.

The influence of the nonlinearity on the frequency-wave number relation naturally impacts the spectrum of group velocities, defined as

$$c_{\mathrm{g}} = \frac{\partial \omega_{\mathrm{fin}}(\kappa; B)}{\partial \kappa}. \tag{4.35}$$

In Fig. 4.4, we show the amplitude-dependent relationship between the frequency and the group velocity and between the group velocity and the wave number. The unfolded frequency band structure is also included for correlation. Most noticeable in this figure is the significant rise in the group velocity with amplitude. A similar rise takes effect for the phase velocity as well (not shown), indicating that with finite strain, the medium's permissible wave speeds are supersonic with respect to the nominal speeds under linear, infinitesimal strain. We also note that the homogenized medium's group velocity curves under finite strain are linear and exceed the maximum group velocity values for the corresponding phononic crystal; whereas, in contrast, the maximum group velocity in the infinitesimal-strain problem overlaps with the corresponding homogenized medium's horizontal group velocity line. This disparity may be a manifestation of the linear approximation inherent in the TM method. Thus the minimum distance between the maximum group velocity of a

phononic crystal and the corresponding homogenized medium's group velocity line may be viewed as a measure of accuracy for a given value of wave amplitude B/a. This conjecture is a subject for a future investigation.

In Fig. 4.5, we show three time snap shots of Bloch mode shapes corresponding to the pair of isofrequency pass-band points (top row) and the pair of isofrequency stop-band points (bottom row) marked in Fig. 4.3. The increase in the wavelength due to the nonlinearity at a given frequency, e.g., by comparing point P_{NL} to P_L, is observed in Fig. 4.5 in the form of a slight stretching of the waveform. The effect of the nonlinearity on the group velocity, as indicated in Fig. 4.4, is less obvious in the mode shape diagrams. The effect of the nonlinearity on stop-band stationery waves appears to be a smoothening of the spatial profile. A strengthening of the spatial attenuation is also observed and is consistent with the prediction in Fig. 4.3 at the selected frequency.

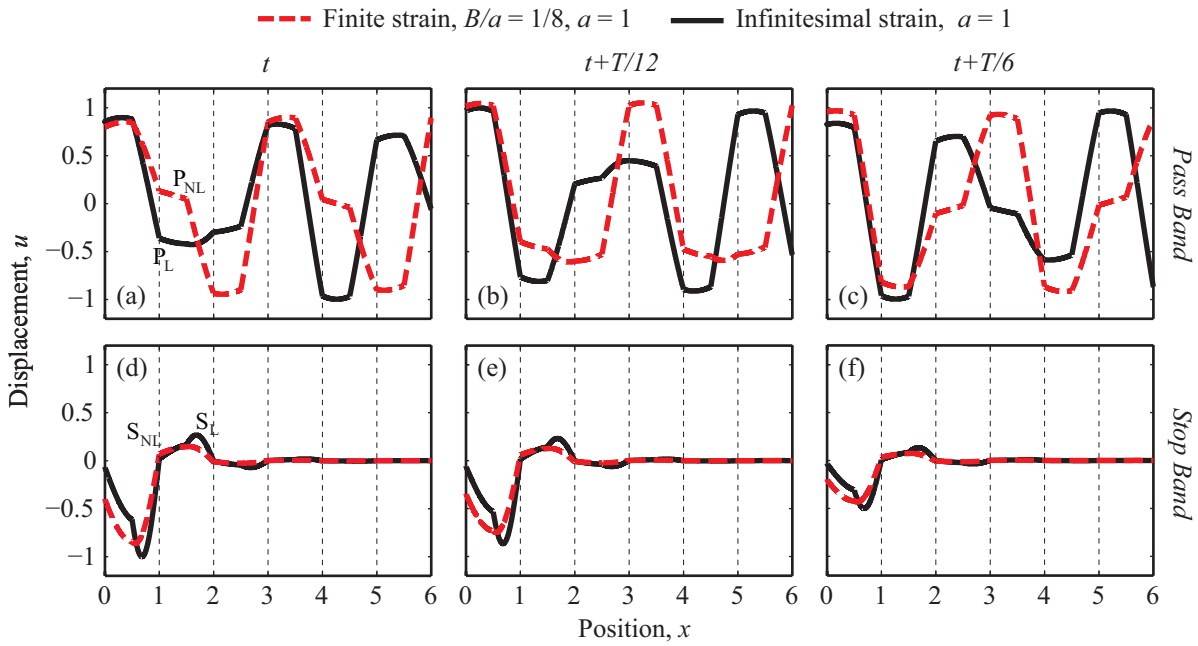

Figure 4.5: Three time snap shots of the Bloch mode shape over six unit cells corresponding to the four points P_L, P_{NL}, S_L, and S_{NL} marked in Fig. 4.3. The Bloch mode shape for points P_L and P_{NL} are shown in (a), (b), and (c), while the Bloch mode shapes for points S_L and S_{NL} are shown in (d), (e), and (f). Red dashed curves correspond to finite strain and black solid curves correspond to infinitesimal strain. Each pass-band and stop-band sets of curves are normalized with respect to the maximum displacement value of the infinitesimal strain case at time t.

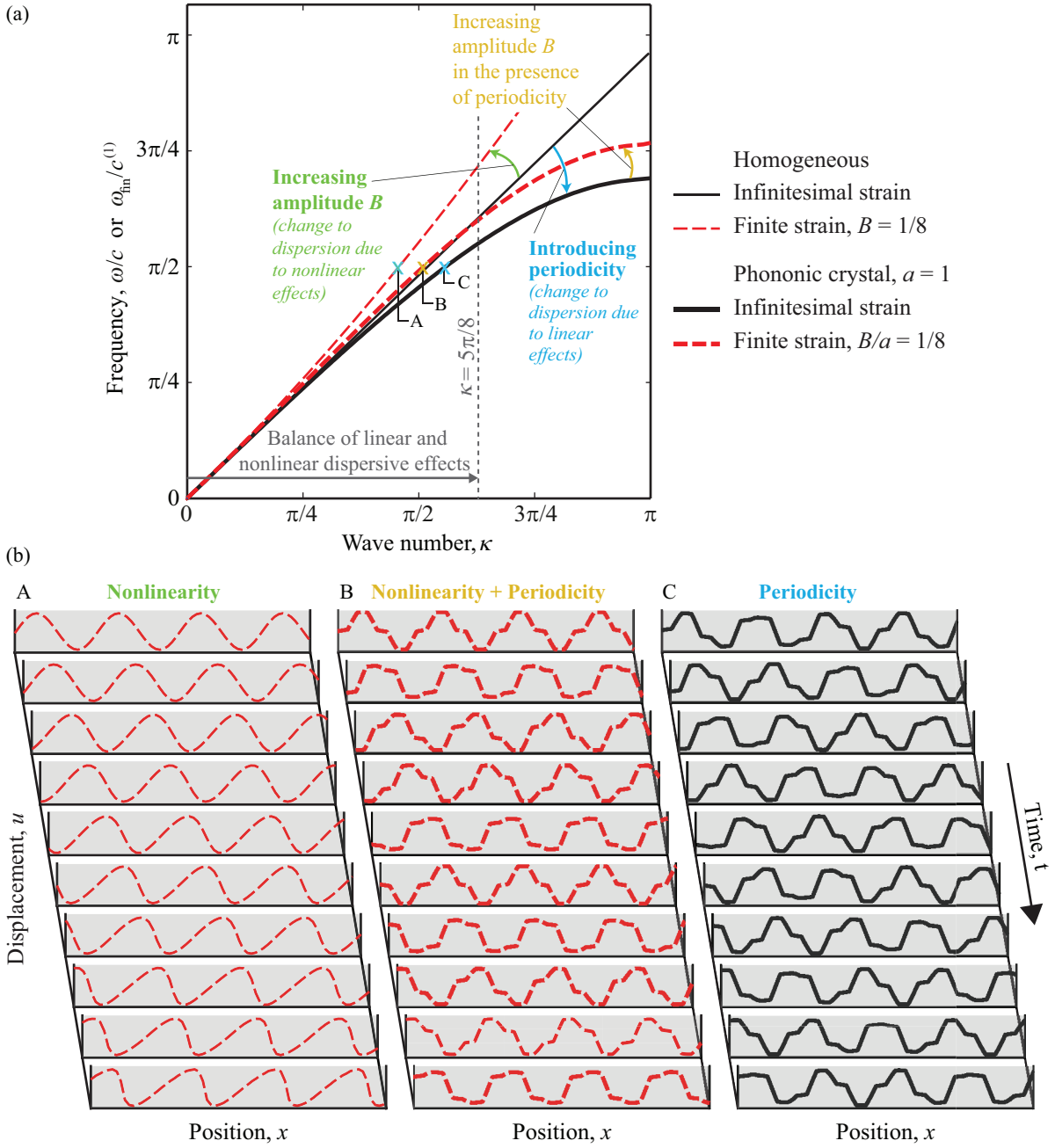

Figure 4.6: Illustration of the contrast between the effect of the periodicity on the dispersion as seen in the linear phononic crystal (see Section 4.2) versus the effect of the finite-strain nonlinearity on the dispersion which is here brought about by increasing the wave amplitude in a homogeneous medium with the same properties as a statically homogenized version of the phononic crystal (see Section 4.3.1). In the nonlinear phononic crystal considered in Section 4.3.2, the two opposing effects are simultaneously present and a balance may be practically realized up to a certain wave number. For a wave amplitude of $B/a = 1/8$, the two effects are approximately in balance up to $\kappa = 5\pi/8$ as shown in (a). The impact of this balance on the space-time displacement profile is demonstrated in (b). The A, B, and C profiles are obtained, respectively, by direct numerical integration, the present TM method with nonlinear enrichment, and the standard TM method.

4.4 Balance between Linear and Nonlinear Dispersion

In the literature, a common view is that nonlinearity of the type considered in this study tends to steepen, and subsequently narrow, a wave because large-amplitude constituent waves are able to catch up with slower low-amplitude ones; and, in contrast, dispersion causes a wave to widen its profile spatially because different constituent waves travel at different speeds [130]. Here, we view this problem from a different perspective. We consider the effect of the periodicity in altering the dispersion (which is a linear mechanism) and, in parallel, the effect of the nonlinearity in also altering the dispersion. In Fig. 4.6a, we reproduce the results displayed in Fig. 4.3 with a focus on the first Brillouin zone. The figure illustrates the two effects when taking place separately or in combination. In the structure considered, we observe that an amplitude of $B/a = 1/8$ allows the two effects to be practically in balance up to approximately $\kappa = 5\pi/8$, which corresponds to a wavelength as small as roughly three times the unit cell size. Such condition, in principle, brings rise to a solitary-type wave within this range of wavelengths.

This linear-nonlinear dispersion balancing phenomenon is elucidated further by plotting in Fig. 4.6b the mode shapes corresponding to Points A, B, and C marked in Fig. 4.6a. We observe in A that the finite strain steepens a sine wave until it eventually reaches the point of bifurcation (not shown). In contrast, in C we observe a linear wave with a spatially variant profile at each time step due to the periodically alternating material properties. In B, which corresponds to a balanced state, no wave profile steepening is observed (thus the wave is stabilized) and the spatial profile is now invariant at each time window.

4.5 Numerical verification

In this section, we conduct direct numerical simulations to verify the theory and determine the limits of its accuracy as the wave amplitude is increased. For this purpose and in the interest of simplicity, we consider a bi-material rod with the following material properties ratio: $c^{(2)}/c^{(1)} = 3/2$

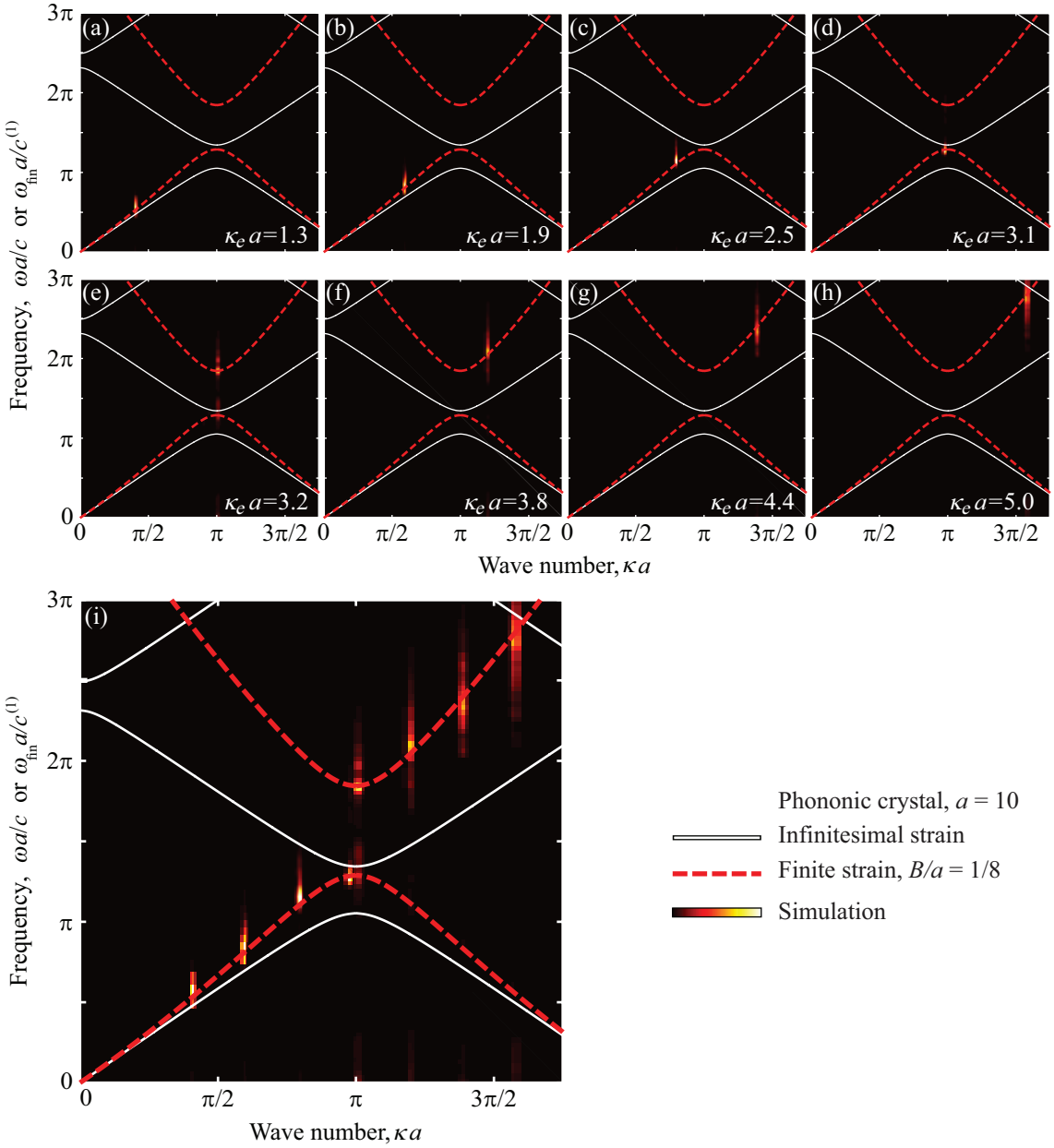

Figure 4.7: Numerical verification of the proposed TM method with nonlinear enrichment as applied to the 1D bi-material phononic crystal rod described in Section 4.5. (a)-(h) Finite-strain dispersion curves obtained by theory and simulation for a range of excitation wave numbers. (i) A superposition of the simulations spectra overlaid on the theoretical results. For comparison, the linear, infinitesimal-strain dispersion curves are also plotted.

and $\rho^{(2)}/\rho^{(1)} = 4/9$. The rod consists of 200 unit cells each consisting of two equal sized layers, and each unit cell has 25 grid points. A standard second-order finite-difference scheme is used to solve Eq. (4.24) with periodic boundary conditions applied. A prescribed sinusoidal displacement

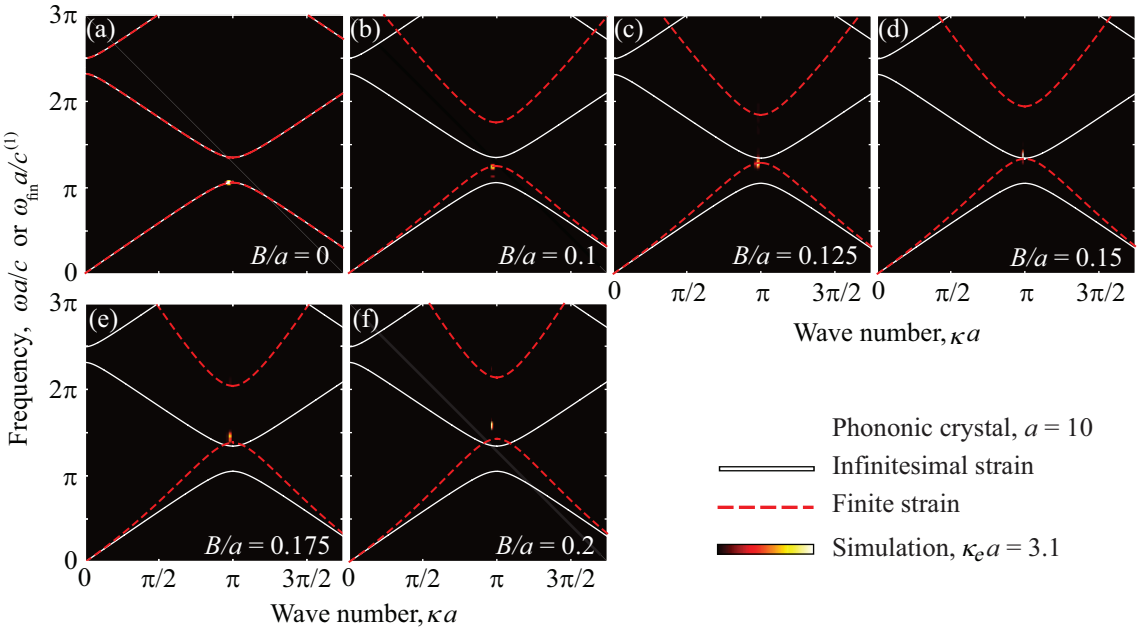

Figure 4.8: Examination of the limit on wave amplitude for obtaining accurate results by the proposed TM method with nonlinear enrichment. Similar to Figure 4.7, these results are for the 1D bi-material phononic crystal rod described in Section 4.5. For $\kappa_e a = 3.1$, the theoretical results breakdown when B/a exceeds 1/8. For comparison, the linear, infinitesimal-strain dispersion curves are also plotted.

gradient field with an initial amplitude of $|\kappa_e|B$ and wavenumber κ_e is applied across the length of the rod, i.e., $\bar{u}(x, t = 0) = |\kappa_e|B\sin(\kappa_e x)$. A constant time step of 10^{-3}(s) is used through the integrations sweep with a total time varying between 300(s) to 400(s) depending on the value of κ_e and the requirements for numerical stability. The space-time solution is then Fourier transformed to obtain an intensity distribution in the wave number-frequency domain. The results are shown in Fig. 4.7 for a unit cell of size $a = 10$ and wave amplitude of $B/a = 1/8$, considering eight different values of κ_e. Superimposed, for comparison, are the dispersion curves on the basis of finite as well as infinitesimal strains. A perfect agreement between the numerical wavenumber-frequency spectrum and the analytically predicted dispersion relation from Eq. (4.33) is clearly observed. Figure 4.8 shows the same set of results for $\kappa_e a = 3.1$ and for a range of values of B/a indicating that the present technique is accurate up to $B/a = 1/8$, i.e., for wave amplitudes that are between one sixth and one fifth of the unit cell length.

4.6 Conclusions

We have theoretically derived a wave number versus frequency finite-strain dispersion relation for Bloch wave propagation in a slender 1D phononic crystal (layered periodic elastic medium with a small cross section). The effect of finite strain has been incorporated exactly at the individual homogeneous layer level. Subsequently, the TM method has been applied to the unit cell to analytically provide an approximate nonlinear dispersion relation for the periodic medium. Thus this approach represents an application of the TM method with a nonlinear enrichment (in principle, it can be implemented for other types of waves such as nonlinear electromagnetic waves in a photonic crystal). Due to the assumption of a linear strain-displacement gradient relation in the TM method, the analysis becomes less accurate as the strength of the nonlinearity increases. Using brute-force numerical simulations, we demonstrated that the technique is accurate up to an amplitude that is roughly between one eight of the unit-cell length (see Fig. 4.8).

The results provide a quantitative prediction of the changes in the dispersion curves when periodicity and finite strain are introduced separately or in combination. In particular, we have shown that the wave amplitude could be chosen to create an approximate balance between the two effects up to a certain wave number, creating a solitary-type wave as illustrated in Fig. 4.6.

The dynamic behavior revealed by Eqs. (4.29) and (4.33) is based on our underlying assumption of Green-Lagrange strain at the homogeneous layer level. The same technique may be applied for a model with material nonlinearity in addition to the geometric nonlinearity. Specific choices of material and geometric nonlinearities could in principle lead to qualitatively different dispersion behavior, and thus it is necessary for future work to examine the problem experimentally to determine the most appropriate constitutive relation and strain measure guided by the theory presented in this chapter.

Chapter 5

Dispersion characteristics of a nonlinear elastic metamaterial[1]

In this chapter, we study wave dispersion in a one-dimensional nonlinear elastic metamaterial consisting of a thin rod with periodically attached local resonators. Our model is based on an exact finite-strain dispersion relation for a homogeneous solid, utilized in conjunction with the standard transfer matrix method for a periodic medium. The nonlinearity considered stems from large elastic deformation in the thin rod, whereas the metamaterial behavior is associated with the dynamics of the local resonators. We derive an approximate dispersion relation for this system and provide an analytical prediction of band-gap characteristics. The results demonstrate the effect of the nonlinearity on the characteristics of the band structure, including the size, location, and character of the band gaps. For example, large deformation alone may cause a pair of isolated Bragg-scattering and local-resonance band gaps to coalesce. We show that for a wave amplitude on the order of one-eighth of the unit cell size, the effect of the nonlinearity in the structure considered is no longer negligible when the unit-cell size is one-fourteenth of the wavelength or larger.

5.1 Introduction

5.1.1 Elastic metamaterials

Phononic crystals (PCs) are periodic materials with a spatial modulation of inertial and/or elastic properties. For a given choice of unit-cell geometry and/or type and distribution of constituent materials, PCs can produce absolute band gaps due to Bragg scattering where acous-

[1] This chapter is drawn from Ref. [93] and has been adapted to suit the style and the notation of the dissertation.

tic/elastic waves are forbidden to propagate [35–37]. However, in order to open band gaps in the low frequency range of up to a few hundred kHz, the dimension of a periodic structure tends to be too large for a wide range of practical applications. This limitation may be overcome by using locally resonant elastic metamaterials (MMs), introduced by Liu et al. [38], in which band gaps may open up in the subwavelength regime and thus do not require the unit cell size to be on the order as the wavelength. Within a band gap, for a PC or a MM, the wave energy is attenuated within only a small number of repeated unit cells. In addition to the possibility of subwavelength band gaps, MMs exhibit other unique physical properties that cannot be found in natural materials, such as negative properties [38–43]. A recent article and discussion in *Applied Mechanics Reviews* provide a broad review of PCs and MMs covering historical and recent developments as well as an outlook on future research directions [7, 44, 45].

The engineering of common structures such as rods, beams and plates with features, or microstructures, that house local resonators allows for the emergence of metamaterial behavior across the structure as a whole. This provides a promising avenue for vibration mitigation using low-frequency bands gaps and effective properties. In two-dimensional plate-like structures, this concept has been realized by embedding soft inclusions [46], erecting pillars [47–49], suspending heavy inclusions within a lattice [50], among other configurations. In one-dimensional (1D) structures, among the metamaterial configurations considered are three-phase rods [52], beams with resonating rings [53, 54], sandwich beams with internal mass-spring resonators [55], beams with side stubs [56, 57] and beams with small masses suspended on a membrane [58]. The band-gap formation mechanism in this class of 1D systems was studied analytically by Xiao et al. in the context of mass resonators attached to strings [59], rods [60] and beams [61]. In the case of rods, multi-degree-of-freedom resonators were considered to achieve a cluster of multiple subwavelength band gaps [60]. Liu and Hussein, on their part, investigated the effects of the various types and properties of periodicity on the frequency band structure considering flexural wave propagation in Euler and Timoshenko beams [62]. The conditions for transition between the Bragg scattering and the local resonance hybridization regimes have also been investigated in depth [59–62].

5.1.2 Elastic wave dispersion in the presence of nonlinearity

Wave motion in elastic solids is commonly studied in the context of linear theory whereby linear constitutive laws and linear strain-displacement relationships are assumed [63, 64]. The incorporation of nonlinearity, however, is necessarily incorporated whenever large deformations are to be accounted for [65,66,68,131]. In a nonlinear regime, the wave motion is amplitude-dependent. Capturing this property within the dispersion relation provides a general and fundamental description of the nonlinear wave propagation characteristics. Abedinnasab and Hussein [1] derived exact dispersion relations for axial and flexural elastic wave motion in homogeneous rods and beams under finite strain.

Nonlinear PCs and MMs have received even less attention due to the additional difficulties in modeling and characterization. Needless to say, there are unique opportunities associated with large motion in PCs and MMs, such as, for example, solitary wave tuning [74] and amplitude-dependent band-gap engineering [75]. Several approaches have been adopted from the nonlinear dynamics literature to treat this class of problems. For example, Manktelow et al. studied intensity-dependent dispersion of acoustic (and electromagnetic) waves in 1D weakly nonlinear periodic media using a perturbation method and a quasi-linear approach in conjunction with the Transfer Matrix (TM) method [85]. In a recent investigation, we have studied the effect of finite deformation in 1D layered PCs using exact dispersion analysis in the different homogeneous layers and the standard TM method across the unit cell [92].

5.1.3 Overview

The goal of this chapter is to examine the effect of nonlinearity, finite strain in particular, on the band-gap characteristics of a 1D MM consisting of a periodic suspension of masses connected via springs to a homogeneous elastic rod, as illustrated in Fig. 5.1. The nonlinearity considered arises from large elastic deformation in the rod, whereas the metamaterial behaviour is associated with the dynamics of the local resonators. Our model is based on embedding the exact finite-strain

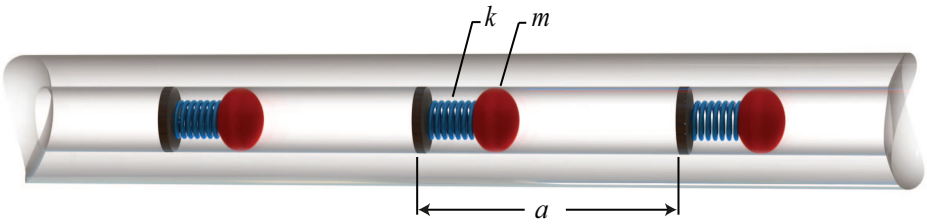

Figure 5.1: A finite section consisting of three unit cells of an infinite 1D nonlinear elastic MM.

dispersion relation for a 1D homogeneous rod [1] into the wavenumber variable in the standard TM method for a periodic elastic medium [5]. This approach has been applied earlier to a PC rod to examine the interplay between nonlinearity and periodicity [92]; here we apply it to a MM rod. We derive a dispersion relation for the system in Fig. 5.1 and provide an analytical prediction of various band-gap characteristics.

Since the TM method provides the backbone of the approach, we first briefly overview it, in conjunction with Bloch's theorem [2], for the exact analytical analysis of a simple 1D linear elastic MM (Section 5.2.1). Furthermore, we follow the analysis framework provided by Xiao et al. [59] which allows for the derivation of dispersion characteristics of the band gaps and presents physical models for equivalent finite structures (Section 5.2.2). This analysis places emphasis on the role of the resonator parameters. We then review the treatment of geometric nonlinearity, i.e., finite strain, in the context of a homogeneous medium following the theory proposed by Abedinnasab and Hussein [1] (Section 5.3.1). In Section 5.3.2, we combine the previous derivations. The homogeneous-medium finite-strain dispersion relation is used to represent the motion characteristics in the rod portion of the unit cell and is subsequently incorporated into the TM formalism in order to account for the local resonator within the unit cell. While the finite-strain dispersion relation for the bare rod is exact, the dispersion relation we obtain for the overall MM represents an approximate prediction due to an assumption of a linear relationship between the strain and the displacement gradient in the TM method. Finally, we use our formulation to investigate the effects of the nonlinearity on the band-structure characteristics and highlight the differences in the response compared to the corresponding linear model.

5.2 Dispersion characteristics of a 1D linear elastic metamaterial

The dispersion characteristics of periodic media are related to how waves interfere across unit cells with varying material and/or geometrical properties. Bloch's theorem [2] provides the mathematical framework for studying the dispersion, yielding a relationship between frequency and wavenumber (or wave vector) which when represented graphically displays the frequency band structure. We begin our dynamic analysis of a 1D MM with the statement of the equation of motion for longitudinal wave motion

$$(\sigma A)_{,x} + F = \rho A u_{,tt}, \tag{5.1}$$

where $\sigma = \sigma(x,t)$, $F = F(x,t)$, $u = u(x,t)$, $A = A(x)$ and $\rho = \rho(x)$ denote the stress, external body force (per unit length), displacement, cross sectional area, and material density, respectively. As indicated, the value of each of these quantities is dependent upon the position x along the axial direction and, with the exception of the area and density, time t. Differentiation with respect to position and/or time is denoted by the appropriate subscript following a quantity. For example, $(.)_{,x}$ indicates differentiation with respect to position while $(.)_{,tt}$ signifies double differentiation with respect to time. By considering free wave motion, $F = 0$, and a linearly elastic material, i.e., $\sigma = E u_{,x}$, where $E = E(x)$ is the Young's modulus of the material, we obtain

$$(E A u_{,x})_{,x} = \rho A u_{,tt}. \tag{5.2}$$

For a uniform, homogeneous rod of infinite extent (having no boundaries at which waves may reflect), we assume a plane wave solution of the form

$$u(x,t) = B\mathrm{e}^{\mathrm{i}(\kappa^* x - \omega t)}, \tag{5.3}$$

where B is the wave amplitude, κ^* is the wavenumber in the medium, ω is the temporal frequency of the traveling wave, and $\mathrm{i} = \sqrt{-1}$. Substituting Eq. (5.3) into Eq. (5.2) provides the linear dispersion relation

$$E\kappa^{*2} = \rho\omega^2. \tag{5.4}$$

This approach may be extended to heterogeneous and/or non-uniform media provided the heterogeneity and/or non-uniformity are/is periodic. In this case, it suffices to analyze only a single unit cell and apply the TM method along with Bloch's theorem. Figure 5.1 displays a simple model of a 1D MM with a spatial lattice spacing constant a.

5.2.1 Transfer matrix method

The TM method is commonly applied to a unit cell with different layers [5]. For the 1D MM we are considering, we will view the bare rod as a uniform and homogeneous single-layer unit cell and assume a solution to Eq. (5.2) consisting of a superposition of forward (transmitted) and backward (reflected) traveling waves with a harmonic time dependence,

$$u(x,t) = (B_+ \mathrm{e}^{\mathrm{i}\kappa^* x} + B_- \mathrm{e}^{-\mathrm{i}\kappa^* x})\mathrm{e}^{-\mathrm{i}\omega t}, \tag{5.5}$$

where B_+ and B_- are amplitudes of the forward and backward traveling waves, respectively. A state vector of the unit cell composed of spatial components of the displacement and the axial force (defined as $f = EAu_{,x}$) is written as

$$\mathbf{y}(x) = \begin{bmatrix} u(x) \\ f(x) \end{bmatrix} = \begin{bmatrix} 1 & 1 \\ \mathrm{i}Z & -\mathrm{i}Z \end{bmatrix} \begin{bmatrix} B_+ \mathrm{e}^{\mathrm{i}\kappa^* x} \\ B_- \mathrm{e}^{-\mathrm{i}\kappa^* x} \end{bmatrix} = \mathbf{H} \begin{bmatrix} B_+ \mathrm{e}^{\mathrm{i}\kappa^* x} \\ B_- \mathrm{e}^{-\mathrm{i}\kappa^* x} \end{bmatrix}, \tag{5.6}$$

where $Z = EA\kappa^*$. Using x_R and x_L to denote the position of the right and left boundaries of the unit cell, and recognizing that $x_\mathrm{R} = a + x_\mathrm{L}$, Eq. (5.6) becomes

$$\mathbf{y}(x_\mathrm{R}) = \begin{bmatrix} u(x_\mathrm{R}) \\ f(x_\mathrm{R}) \end{bmatrix} = \mathbf{H} \begin{bmatrix} \mathrm{e}^{\mathrm{i}\kappa^* a} & 0 \\ 0 & \mathrm{e}^{-\mathrm{i}\kappa^* a} \end{bmatrix} \begin{bmatrix} B_+ \mathrm{e}^{\mathrm{i}\kappa^* x_\mathrm{L}} \\ B_- \mathrm{e}^{-\mathrm{i}\kappa^* x_\mathrm{L}} \end{bmatrix}, \tag{5.7}$$

We rewrite Eq. (5.7) using Eq. (5.6) and define the transfer matrix as

$$\mathbf{U} = \mathbf{H} \begin{bmatrix} \mathrm{e}^{\mathrm{i}\kappa^* a} & 0 \\ 0 & \mathrm{e}^{-\mathrm{i}\kappa^* a} \end{bmatrix} \mathbf{H}^{-1} = \begin{bmatrix} \cos(\kappa^* a) & \dfrac{1}{Z}\sin(\kappa^* a) \\ -Z\sin(\kappa^* a) & \cos(\kappa^* a) \end{bmatrix}. \tag{5.8}$$

The transfer matrix, U, allows us to directly relate the plane wave solution from the left side of the unit cell to its right side,

$$\mathbf{y}(x_\mathrm{R}) = \mathbf{U}\mathbf{y}(x_\mathrm{L}). \tag{5.9}$$

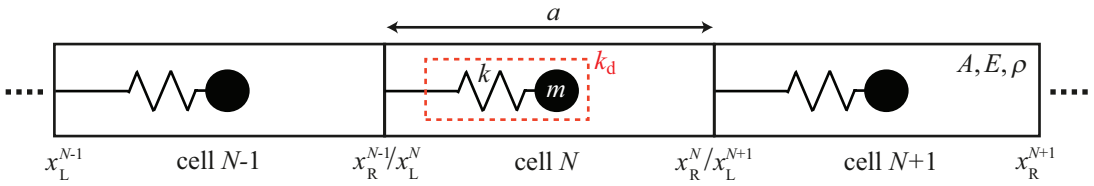

Figure 5.2: Graphical representation of 1D MM unit cell model: a homogeneous continuous rod with a single spring-mass resonator attached along the axial direction. The material properties and a labeling scheme are included.

To incorporate the contribution of the attached mass-spring oscillator we form the following matrix

$$\mathbf{P} = \begin{bmatrix} 1 & 0 \\ k_{\mathrm{d}} & 1 \end{bmatrix}, \tag{5.10}$$

where $k_{\mathrm{d}} = -(\omega^2 km)/(k - m\omega^2)$ represents the dynamic stiffness of a single degree-of-freedom oscillator with mass m and stiffness k. The total transfer matrix for the unit cell N may now be formed in the following manner:

$$\mathbf{y}(x_{\mathrm{L}}^{(N+1)}) = \mathbf{P}\mathbf{y}(x_{\mathrm{R}}^{(N)}) = \mathbf{P}\mathbf{U}\mathbf{y}(x_{\mathrm{L}}^{(N)}) = \mathbf{T}\mathbf{y}(x_{\mathrm{L}}^{(N)}). \tag{5.11}$$

Using Bloch's theorem we can also write

$$\mathbf{y}(x + a) = \mathrm{e}^{\mathrm{i}\kappa a}\mathbf{y}(x), \tag{5.12}$$

where κ is the wavenumber of a wave travelling along the 1D MM as a whole (rod and attached resonators). Using $x = x_{\mathrm{L}}$ as a reference point, and combining the TM method with the expression of Bloch's theorem, we obtain the eigenvalue problem

$$[\mathbf{T} - \mathrm{e}^{\mathrm{i}\kappa a}\mathbf{I}]\mathbf{y}(x_{\mathrm{L}}) = \mathbf{0}, \tag{5.13}$$

which may be rewritten as

$$\mathbf{T}(\omega)\mathbf{y}(x_{\mathrm{L}}) = \lambda\mathbf{y}(x_{\mathrm{L}}), \tag{5.14}$$

in which $\lambda = \mathrm{e}^{\mathrm{i}\kappa a}$ and $\mathbf{y}(x_{\mathrm{L}})$ are complex eigenvalues and eigenvectors, respectively. By solving the eigenvalue problem of Eq. (5.14), we generally obtain a complex conjugate pair of eigenvalues:

$$\lambda_1 = \mathrm{e}^{\mathrm{i}\kappa_1 a}, \quad \lambda_2 = \mathrm{e}^{\mathrm{i}\kappa_2 a}. \tag{5.15}$$

For any given ω, if κ is a solution so is $-\kappa$ which correspond to the propagation of a wave in the positive and negative directions, respectively. Thus $\kappa_1 = \kappa$ and $\kappa_2 = -\kappa$.

For convenience, a corresponding characteristic equation may be derived. From Eq. (5.11), the complete form of the transfer matrix of the unit cell is expressed as

$$\mathbf{T} = \begin{bmatrix} \cos(\kappa^* a) & \frac{1}{Z}\sin(\kappa^* a) \\ k_{\mathrm{d}}\cos(\kappa^* a) - Z\sin(\kappa^* a) & \frac{k_{\mathrm{d}}}{Z}\sin(\kappa^* a) + \cos(\kappa^* a) \end{bmatrix}, \tag{5.16}$$

from which we obtain the following dispersion relation in analytical form,

$$\cos\kappa a = \cos(\kappa^* a) + \frac{k_{\mathrm{d}}}{2Z}\sin(\kappa^* a), \tag{5.17}$$

which may be rewritten in non-dimensional form as

$$\cos\kappa a = \cos(\Omega\pi) + \frac{V}{2}\sin(\Omega\pi). \tag{5.18}$$

In Eq. (5.18), Ω denotes the non-dimensional frequency, defined as

$$\Omega = \frac{\kappa^* a}{\pi}, \tag{5.19}$$

and V denotes the non-dimensional dynamic stiffness of the resonator which is related to the resonator and rod parameters by

$$V = \frac{k_{\mathrm{d}}}{Z} = -\frac{\omega^2 km}{EA\kappa^*(k - m\omega^2)}. \tag{5.20}$$

Considering infinitesimal strain, we express κ^* in Eqs. (5.16)-(5.20) as a frequency-dependent function, $\hat{h}(\omega)$, based on the linear dispersion relation for the bare rod, which, from Eq. (5.4), is

$$\kappa^*_{\mathrm{inf}} = \hat{h}(\omega) = \omega/c, \tag{5.21}$$

where $c = \sqrt{E/\rho}$. When finite strain is considered, a new expression for κ^* is needed as described in Section 5.3.

5.2.2 Band gaps

In this section, we provide a brief formulation for the frequencies of the band-gap edges for the 1D MM following the approach of Xiao et al. [59] which was applied to the analogous problem of a string supporting a periodic array of local resonators. We use the dispersion analysis presented in the previous section to derive sets of equations to predict the frequencies of the stop- and pass-band edges. Free waves can propagate in this system when κ in Eq. (5.18) is pure real, for which the condition $-1 \leq \cos \kappa a \leq 1$ applies [132]. Thus the frequencies of the band-gap edges are governed by $\cos(\kappa a) = \pm 1$. Applying this condition to Eq. (5.18) we get

$$\cos(\Omega\pi) + \frac{V}{2}\sin(\Omega\pi) = \pm 1, \tag{5.22}$$

or equivalently

$$(\cos(\Omega\pi) + \frac{V}{2}\sin(\Omega\pi) - 1)(\cos(\Omega\pi) + \frac{V}{2}\sin(\Omega\pi) + 1) = 0, \tag{5.23}$$

which, in turn, is equivalent to

$$\sin\frac{\Omega\pi}{2}(V\sin\frac{\Omega\pi}{2} + 2\cos\frac{\Omega\pi}{2}) = 0, \tag{5.24a}$$

or

$$\cos\frac{\Omega\pi}{2}(V\cos\frac{\Omega\pi}{2} - 2\sin\frac{\Omega\pi}{2}) = 0. \tag{5.24b}$$

For convenience, the band-gap edge frequencies given by Eqs. (5.24a) and (5.24b) are labeled as Mode-A and Mode-B frequencies, respectively. These equations satisfy the following conditions

$$\sin\frac{\Omega\pi}{2} = 0, \tag{5.25a}$$

or

$$-2\cot\frac{\Omega\pi}{2} = V, \tag{5.25b}$$

for Mode A, and similarly

$$\cos\frac{\Omega\pi}{2} = 0, \tag{5.26a}$$

or

$$2\tan\frac{\Omega\pi}{2} = V, \tag{5.26b}$$

for Mode B. These relations are used to directly predict the frequencies of the band-gap edges. The band-gap edge frequencies governed by Eqs. (5.25a) and (5.26a) are independent of the resonator properties and are defined as

$$\Omega = n, \quad (n = 1, 2, 3, ...). \tag{5.27}$$

On the other hand, the band-gap edge frequencies governed by Eqs. (5.25b) and (5.26b) are affected by the resonator properties and thus correspond to the hybridized local resonance band gap.

By tuning the frequency in Eq. (5.21) to $\omega = \sqrt{k/m}$ and substituting back into Eq. (5.19) we get the non-dimensional resonance frequency

$$\Omega = \frac{a}{\pi}\sqrt{\frac{\rho}{E}}\sqrt{\frac{k}{m}}. \tag{5.28}$$

As noted in Refs. [[59]] and [[60]], the local resonance frequency may be exactly tuned to the Bragg conditions by equating Eq. (5.28) to Eq. (5.27). This yields an explicit formula for the resonator stiffness, k, that enables a complete coalescence between the hybridized local resonance band gap and the various Bragg-scattering band gaps; this formula is

$$k = \frac{E}{\rho a^2} m n^2 \pi^2, \quad (n = 1, 2, 3, ...). \tag{5.29}$$

A similar formula could be obtained for m in term of k. Upon reshuffling of parameters, Eq. (5.29) can be conveniently written as

$$\frac{1}{2\pi}\sqrt{\frac{k}{m}} = \frac{nc}{2a}, \quad (n = 1, 2, 3, ...), \tag{5.30}$$

where the left hand side represents the local-resonance frequency, while the right hand side represents the Bragg condition frequencies associated with the 1D periodic lattice. This relationship explicitly demonstrates the exact tuning of the local-resonance frequency to the Bragg conditions, which corresponds to the band-gap coupling conditions revealed in Refs. [[59]] and [[60]].

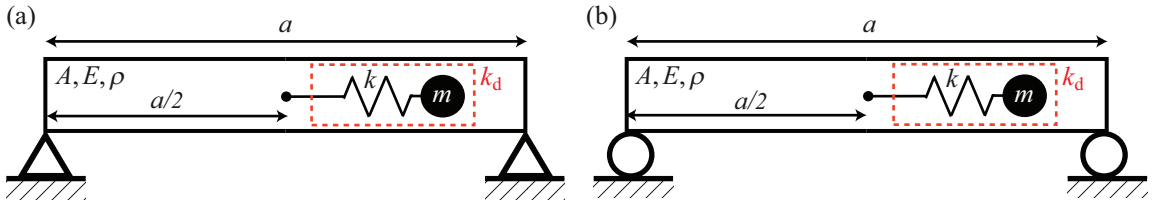

Figure 5.3: Finite rod with an attached spring-mass resonator and (a) fixed-fixed or (b) free-free boundaries.

A physical interpretation of these equations can be made by considering the natural frequencies of two corresponding finite structures representing the configuration of the 1D MM unit cell. The end boundary conditions of these two finite structures are fixed-fixed and free-free, respectively, as demonstrated in Fig. 5.3. Following Ref. [59], an analysis of these two structure yields the band-gap edge frequencies of the original infinite 1D MM, i.e., the same frequencies obtained from Eqs. (5.25) and (5.26), respectively. We consider a harmonic wave solution for the rod structures of Fig. 5.3,

$$u_{\mathrm{r}}(x,t) = \begin{cases} (\alpha_1 \sin \kappa^* x + \beta_1 \cos \kappa^* x)\mathrm{e}^{-\mathrm{i}\omega t}, & 0 \le x \le \dfrac{a}{2} \\ (\alpha_2 \sin \kappa^* (x - \dfrac{a}{2}) + \beta_2 \cos \kappa^* (x - \dfrac{a}{2}))\mathrm{e}^{-\mathrm{i}\omega t}, & \dfrac{a}{2} \le x \le a \end{cases}, \tag{5.31}$$

where u_{r} represent the longitudinal displacement within the strucutre, a is the length of structure (which is equal to the length of the unit cell in the infinite medium), and α and β are coefficients describing the wave amplitude. The governing equation of the resonator, located at $x = a/2$, is

$$m u_{\mathrm{m,tt}}(t) + k(u_{\mathrm{m}}(t) - u_{\mathrm{r}}(\frac{a}{2}, t)) = 0, \tag{5.32}$$

where $u_{\mathrm{m}}(t)$ is the displacement of the resonator mass. Assuming $u_{\mathrm{r}}(t) = U_0 e^{-i\omega t}$, Eq. (5.32) is solved for the amplitude U_0 to give

$$U_0 = \frac{k\beta_2}{k - m\omega^2}. \tag{5.33}$$

In both structures, applying the compatibility condition on Eq. (5.31) at $x = a/2$ gives

$$\alpha_1 \sin(\frac{\kappa^* a}{2}) + \beta_1 \cos(\frac{\kappa^* a}{2}) = \beta_2, \tag{5.34}$$

and enforcing axial force equilibrium at the same point gives

$$\alpha_1 \cos(\frac{\kappa^* a}{2}) - \beta_1 \sin(\frac{\kappa^* a}{2}) = \alpha_2 - \beta_2 V. \tag{5.35}$$

The boundary conditions of the structure showed in Fig. 5.3a are fixed-fixed, that is, $u_{\mathrm{r}}(0,t) = u_{\mathrm{r}}(a,t) = 0$. From Eq. (5.31), this produces

$$\begin{cases} \beta_1 = 0 \\ \alpha_2 \sin(\frac{\kappa^* a}{2}) + \beta_2 \cos(\frac{\kappa^* a}{2}) = 0 \end{cases}, \tag{5.36}$$

On the other hand, the boundary conditions of the structure showed in Fig. 5.3b are free-free, that is, $(u_{\mathrm{r}})_{,x}(0,t) = (u_{\mathrm{r}})_{,x}(a,t) = 0$; this yields

$$\begin{cases} \alpha_1 = 0 \\ \alpha_2 \cos(\frac{\kappa^* a}{2}) - \beta_2 \cos(\frac{\kappa^* a}{2}) = 0 \end{cases}. \tag{5.37}$$

We can represent Eqs. (5.34), (5.35) and (5.36) for the fixed-fixed structure in a matrix form as

$$\begin{bmatrix} \sin(\frac{\kappa^* a}{2}) & 0 & -1 \\ \cos(\frac{\kappa^* a}{2}) & -1 & V \\ 0 & \sin(\frac{\kappa^* a}{2}) & \cos(\frac{\kappa^* a}{2}) \end{bmatrix} \begin{bmatrix} \alpha_1 \\ \alpha_2 \\ \beta_2 \end{bmatrix} = \begin{bmatrix} 0 \\ 0 \\ 0 \end{bmatrix}, \tag{5.38}$$

and, similarly, for the free-free structure, Eqs. (5.34), (5.35) and (5.37) are represented as

$$\begin{bmatrix} \cos(\frac{\kappa^* a}{2}) & 0 & -1 \\ -\sin(\frac{\kappa^* a}{2}) & -1 & V \\ 0 & \cos(\frac{\kappa^* a}{2}) & -\sin(\frac{\kappa^* a}{2}) \end{bmatrix} \begin{bmatrix} \beta_1 \\ \alpha_2 \\ \beta_2 \end{bmatrix} = \begin{bmatrix} 0 \\ 0 \\ 0 \end{bmatrix}. \tag{5.39}$$

As in the dispersion analysis, the form of κ^* as a function of frequency is dependent on whether infinitesimal or finite strain is assumed.

The natural frequencies of each structure can be found by solving these sets of equations separately. For the fixed-fixed structure, we get

$$\sin\frac{\Omega\pi}{2}(V \sin\frac{\Omega\pi}{2} + 2\cos\frac{\Omega\pi}{2}) = 0, \tag{5.40}$$

which is identical to Eq. (5.24a). For the free-free structure, we obtain

$$\cos\frac{\Omega\pi}{2}(V\cos\frac{\Omega\pi}{2}-2\sin\frac{\Omega\pi}{2})=0, \tag{5.41}$$

which, on its part, is identical to Eq. (5.24b).

Now that the physical interpretation of Eqs. (5.25) and (5.26) is elucidated, it is worth pointing out, as done for the analogous string-based problem in Ref. [[59]], that Eqs. (5.25a) and (5.26a) represent the antisymmetric modes for a fixed-fixed and a free-free structure, respectively. Here, the central point of the rod, $x = a/2$, forms a node with zero displacement which causes the system to be independent of the resonator and represent simply a rod [63]. On the other hand, Eqs. (5.26a) and (5.26b) represent the symmetric modes for a fixed-fixed and a free-free structure, respectively, where in this case the displacement of the central point depends on the resonator parameters.

Moreover, we can find explicitly the influence of the resonator parameters, m and k, on the behaviour of the band-gap edge frequencies by substituting Eq. (5.20) into Eqs. (5.25b) and (5.26b) and solving for the mass and stiffness for Mode A and Mode B, respectively. For Mode A, we obtain

$$m=\frac{2Zk\cot(\frac{\Omega\pi}{2})}{\omega^2(2Z\cot(\frac{\Omega\pi}{2})+k)}, \tag{5.42a}$$

$$k=\frac{2Zm\omega^2\cot(\frac{\Omega\pi}{2})}{2Z\cot(\frac{\Omega\pi}{2})-m\omega^2}, \tag{5.42b}$$

and for Mode B we obtain

$$m=\frac{2Zk\tan(\frac{\Omega\pi}{2})}{\omega^2(2Z\tan(\frac{\Omega\pi}{2})-k)}, \tag{5.43a}$$

$$k=\frac{2Zm\omega^2\tan(\frac{\Omega\pi}{2})}{2Z\tan(\frac{\Omega\pi}{2})+m\omega^2}. \tag{5.43b}$$

5.3 Treatment of nonlinearity

In this section, we provide a theoretical treatment of finite-strain dispersion. As mentioned earlier, the process involves obtaining the dispersion relation for a 1D homogeneous medium (e.g., a homogeneous thin rod) and then using it in conjunction with the TM method to obtain a prediction of the dispersion relation for the 1D MM as a whole.

5.3.1 Finite-strain waves in a 1D homogeneous rod

The equation of motion and finite-strain dispersion relation is reviewed here for 1D plane wave motion in a bulk homogeneous medium without consideration of lateral effects. In principle, this problem is equivalent to that of a slender rod which is what we are interested in for the 1D MM derivations to follow. In the nonlinear formulation, all terms in the nonlinear strain tensor are retained and no high order terms emerging from the differentiations are neglected. The reader is referred to Ref. [[1]] for more details as well as a validation of the theoretical approach by means of a comparison with a standard finite-strain numerical simulation of a corresponding 1D model with finite dimensions.

5.3.1.1 Equation of motion

The exact complete Green-Lagrange strain field in our 1D model is given by

$$\epsilon = \frac{\partial u}{\partial s} + \frac{1}{2}(\frac{\partial u}{\partial s})^2, \tag{5.44}$$

where the first and second terms on the right-hand side represent the linear and nonlinear parts, respectively, and s denotes a Lagrangian longitudinal coordinate which is equal to x in Eq. (5.2).

Using Hamilton's principle, we write the equation of motion under longitudinal stress as

$$\int_0^t (\delta T - \delta U^e)\mathrm{d}t = 0, \tag{5.45}$$

where T and U^e denote kinetic and elastic potential energy, respectively. No external non-conservative forces and moments are permitted because of our interest in the free wave propagation problem.

The variation of kinetic energy is obtained using integration by parts and is given as

$$\delta T = -\rho A \int_0^l (u_{,tt}\delta u)\mathrm{d}s, \tag{5.46}$$

where l denotes the length of a portion of the 1D medium. Similarly, the variation of elastic potential energy is written as

$$\delta U^e = \int_0^l \int_A (\sigma \delta \epsilon)\mathrm{d}A\,\mathrm{d}s, \tag{5.47}$$

where σ is the longitudinal stress. We choose to base our analysis on the Cauchy stress and, as mentioned earlier, model the stress-strain relationship by Hooke's law, $\sigma = E\epsilon$. Using Eq. (5.47), and with the aid of integration by parts, we can now write the variation of elastic potential energy as

$$\delta U^e = \int_0^l \{\frac{1}{2}EAh(h^2-1)\delta u'\}\mathrm{d}s, \tag{5.48}$$

where $u' = du/ds = u_{,s}$, and h is an agent variable defined as

$$h = 1 + u'. \tag{5.49}$$

Substitution of Eqs. (5.48) and (5.46) into Eq. (5.45), and assuming constant cross-sectional area, produces the exact finite-strain equation of motion as

$$\rho u_{,tt} = \frac{1}{2}E(3h^2-1)u''. \tag{5.50}$$

If the longitudinal deformation is infinitesimal, then u' is small and from Eq. (5.49), $h \approx 1$. Substitution of $h = 1$ into Eq. (5.50) leads to

$$\rho u_{,tt} = Eu'', \tag{5.51}$$

which is the equation of motion describing infinitesimal longitudinal deformation and is identical to Eq. (5.2).

5.3.1.2 Dispersion relation

Using Eq. (5.49), we rewrite Eq. (5.50) as

$$u_{,tt} - c^2 u'' = \frac{1}{2}\Big[c^2[3(u')^2 + (u')^3]\Big]', \tag{5.52}$$

which upon differentiation with respect to s gives

$$(u_{,tt})' - c^2 u^{(3)} = \frac{1}{2}\Big[c^2[3(u')^2 + (u')^3]\Big]''. \tag{5.53}$$

Defining $\bar{u} = u'$ and $z = |\kappa^*|s + \omega t$, where ω in this context represents the wave frequency under finite strain, Eq. (5.53) becomes

$$\omega^2 \bar{u}_{,zz} - c^2(\kappa^*)^2 \bar{u}_{,zz} = \frac{1}{2}(\kappa^*)^2\Big[c^2[3\bar{u}^2 + \bar{u}^3]\Big]_{,zz}. \tag{5.54}$$

Integrating Eq. (5.54) twice leads to

$$[\omega^2 - c^2(\kappa^*)^2]\bar{u} - \frac{c^2(\kappa^*)^2}{2}[3\bar{u}^2 + \bar{u}^3] = 0, \tag{5.55}$$

where the nonzero constants of integration (in the form of polynomials in z) represent secular terms which we have set equal to zero in light of our interest in the dispersion relation. Selecting the positive root of Eq. (5.55) we get

$$\bar{u}(z) = \frac{-3 + \sqrt{1 + 8\omega^2/c^2(\kappa^*)^2}}{2}. \tag{5.56}$$

Since $\bar{u} = u_{,s}$, we recognize that $\bar{u} = |\kappa^*|u_{,z}$ and therefore Eq. (5.56) represents a first-order ordinary differential equation with z and u as the independent and dependent variables, respectively.

Now we return to Eq. (5.52) and consider for initial conditions a sinusoidal displacement field, with amplitude B and a zero phase in time, and a zero velocity field. This represents a fundamental harmonic signal for which we seek to characterize its dispersive behavior. In principle, any choice of the initial velocity field is permitted. Following the change of variables that have been introduced, these initial conditions correspond to the following restrictions at $z = 0$ on the $\bar{u}(z)$ function given in Eq. (5.56):

$$\bar{u}(0) = |\kappa^*|B, \quad \bar{u}_{,z}(0) = 0. \tag{5.57}$$

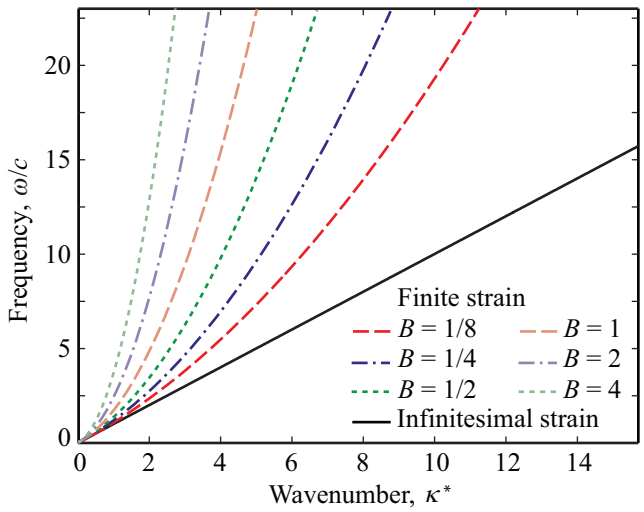

Figure 5.4: Frequency dispersion curves for a 1D homogeneous elastic medium [1]. The finite-strain dispersion relation is based on Eq. (5.58); the infinitesimal strain dispersion relation is based on Eq. (5.59).

These represent initial conditions in the wave phase, z, for Eq. (5.54) and allow for the introduction of the wave amplitude, B, into the formulation. Applying Eq. (5.57) to Eq. (5.56) enables us to use the latter to solve for ω for a given value of κ^*. This leads to the exact dispersion relation in the form of

$$\omega = \sqrt{\frac{2 + 3B|\kappa^*| + (B\kappa^*)^2}{2}} c|\kappa^*|, \tag{5.58}$$

which is a function of wavenumber and amplitude. We define this explicit finite-strain dispersion relation by the function g, i.e., $\omega_{\text{fin}} = g(\kappa^*; B)$, where ω_{fin} denotes the frequency under finite-strain conditions. By taking the limit, $\lim_{B\to 0} g(\kappa^*; B)$, we recover the standard linear dispersion relation for a 1D homogeneous elastic medium or a thin rod [6], that is,

$$\omega = c|\kappa^*|. \tag{5.59}$$

We will denote the explicit dispersion relation under infinitesimal strain conditions by the function h, i.e., $\omega_{\text{inf}} = h(\kappa^*)$. It is noteworthy that for the type of nonlinearity considered, the finite-stratin phase velocity, $c_{p,\text{fin}}$, is larger than the infinitesimal strain phase velocity, $c_{p,\text{inf}}$, and increases with

amplitude:

$$c_{p,\text{fin}} = \frac{\omega_{\text{fin}}}{|\kappa^*|} = \sqrt{\frac{2+3B|\kappa^*|+(B\kappa^*)^2}{2}}c > c = c_{p,\text{inf}}. \tag{5.60}$$

In Fig. 5.4, a set of amplitude-dependent finite-strain dispersion curves evaluated by Eq. (5.58) are shown. This figure demonstrates how the dispersion curve based on infinitesimal strain, i.e., Eq. (5.59), deviates with increasing wave amplitude under finite-strain. The reader is referred to Ref. [[1]] for a numerical validation of these results.

5.3.2 Finite-strain waves in a 1D elastic metamaterial

The TM method is now used to obtain a dispersion relation for the 1D MM when the base rod is exhibiting finite-strain motion. The outcome is an approximate overall dispersion relation since the construction of the transfer matrix is based on a linear strain-displacement relationship [see Eq. (5.6)]. While not exact, this approach provides a quantitative prediction of the effect of the nonlinearity on the location, size and character of the band gaps across the spectrum, all as a function of wave amplitude. The technique's accuracy reduces as the strength of the nonlinearity increases.

As mentioned in Section 5.2.1, the TM method is applicable in either the absence or presence of nonlinearity; the distinction is made in the definition of κ^* in Eq. (5.5) and thereafter. For the infinitesimal-strain problem, $\kappa^*_{\text{inf}} = \hat{h}(\omega) = \omega/c$ as outlined earlier in Eq. (5.21). An analogous function for κ^* can be found for the finite-strain problem, i.e., $\kappa^*_{\text{fin}} = \hat{g}(\omega; B)$. To derive this function, we recast Eq. (5.58) as the following fourth order characteristic equation for the bare rod's homogeneous medium in the unit cell:

$$\kappa^{*4} + \frac{3}{B}\kappa^{*3} + \frac{2}{B^2}\kappa^{*2} - \frac{2\omega^2}{B^2c^2} = 0. \tag{5.61}$$

This equation has the following four solutions:

$$\kappa^*_{1,2} = \frac{1}{12B}(-9+P \mp \sqrt{Q-R}), \tag{5.62a}$$

$$\kappa^*_{3,4} = -\frac{1}{12B}(9+P \pm \sqrt{Q+R}), \tag{5.62b}$$

where,

$$P = \sqrt{\frac{33cS + 12(S^2 + 4c^2 - 24B^2\omega^2)}{cS}}, \tag{5.63a}$$

$$Q = \frac{6(-2S^2 + 11cS - 8c^2 + 48B^2\omega^2)}{cS}, \tag{5.63b}$$

$$R = 54\sqrt{\frac{3cS}{4S^2 + 11cS + 16c^2 - 96B^2\omega^2}}, \tag{5.63c}$$

and

$$S = \left(8c^3 - 99cB^2\omega^2 + 3B\omega\sqrt{-48c^4 + 321c^2B^2\omega^2 + 1536B^4\omega^4}\right)^{\frac{1}{3}}. \tag{5.63d}$$

We define $\kappa^*_{\text{fin}} = \hat{g}(\omega; B) = \max\{\kappa^*_{\text{n}} : \text{n} = 1, 2, 3, 4\}$ and substitute it into the TM formalism of Section 5.2.1. This generates the finite-strain dispersion curves of the 1D MM.

5.4 Analysis of nonlinear dispersion behavior

In this section, the dispersive behavior of the 1D MM is investigated using the theoretical formulation developed above. First we define dimensionless values of mass, $m' = m\pi/\rho aA$, stiffness $k' = ka/EA\pi$, and wave amplitude $B' = B\pi/a$ and present, in Fig. 5.5, the finite-strain dispersion curve (obtained using function $\hat{g}$) for the following parameters: $a = 1$, $k' = 1$, $m' = 3$ and $B' = \pi/8$ (corresponding to $B/a = 1/8$). Superimposed, for comparison, are the dispersion curves on the basis of infinitesimal strain (obtained using function $\hat{h}$) and the corresponding dispersion curves for an equivalent statically homogenized medium (for which the long-wave static speed is equal to that of the 1D MM). We observe in the figure that the finite-strain dispersion curves asymptotically converge to the infinitesimal-strain curves at long wavelengths as expected. We also note that the finite strain causes the dispersion branches to rise and the band gap sizes to increase significantly−an attractive trait for many applications involving sound and vibration control. This behavior, however, is dependent on the type of nonlinearity considered as noted earlier.

In Fig. 5.6, we consider three examples, whereby the non-dimensional mass is $m' = 3$, the non-dimensional wave amplitude is $B' = 1/8$, and the non-dimensional stiffness is chosen to be

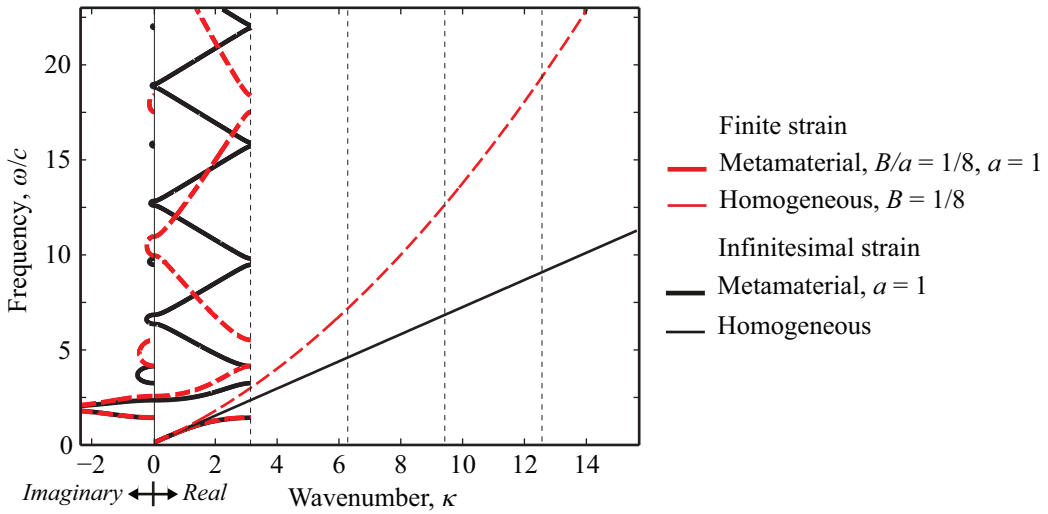

Figure 5.5: Frequency band structure for 1D MM under finite strain [obtained using Eqs. (5.13) and (5.62)]. The results shown are for $B/a = 1/8$. For comparison, the dispersion curves under infinitesimal strain are included. Also, corresponding dispersion curves for a statically equivalent 1D homogeneous elastic medium are overlaid.

$k' = 3.5,\ 3$ and 2.5, respectively. Superimposed, for comparison, are the dispersion curves based on infinitesimal strain. For all these cases, we observe the existence of Bragg-scattering band gaps as well as a hybridized local-resonance band gap [62]. As the value of k' decreases, the location of the local-resonance band gap drops. Furthermore, in the case of infinitesimal strain, we observe that the

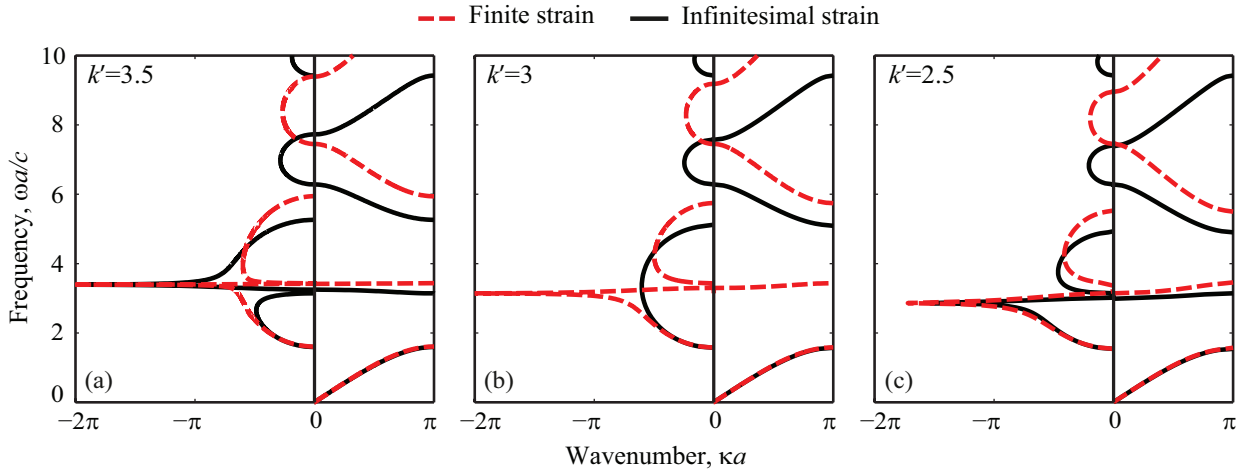

Figure 5.6: Frequency band structure for 1D MM with properties of $m' = 3$ and (a) $k' = 3.5$, (b) $k' = 3$, and (c) $k' = 2.5$. The results shown are for $B' = 1/8$.

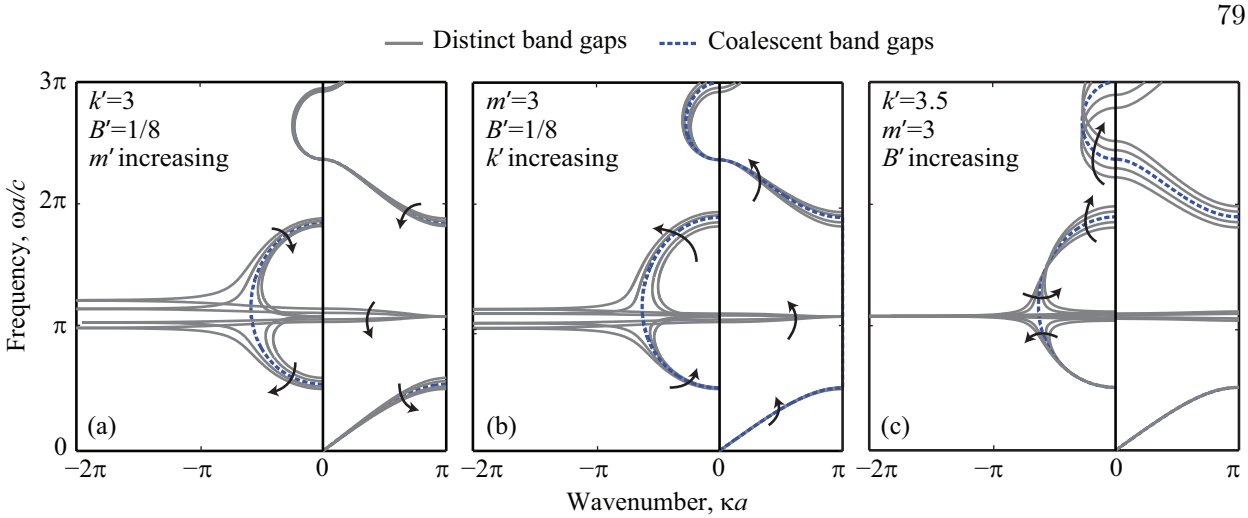

Figure 5.7: Demonstration of band-gap coalescence for 1D MM under finite-strain conditions. Changes in the band gaps opening mechanism are shown for (a) constant resonator stiffness ($k' = 3$), constant nonlinearity ($B' = 1/8$), and increasing resonator mass, (b) constant resonator mass ($m' = 3$), constant nonlinearity ($B' = 1/8$), and increasing resonator stiffness, and (c) constant resonator mass ($m' = 3$), constant resonator stiffness ($k' = 3.5$), and increasing nonlinearity. The coalescence happens at $m' = 2.5099$, $k' = 3.586$, and $B' = .107275$ for these cases, respectively, and the corresponding curves are represented by dashed blue lines.

local-resonance band gap interacts with a lower Bragg-scattering band gap leading to a complete coalescence at $k' = 3$ and eventually by-passes it. The coalescence condition may be predicted theoretically using Eq. (5.29), which in dimensionless parameters takes the form $k' = m'n^2$. In this specific case, $n = 1$ and the coalescence forms when $k' = m' = 3$. In the case of finite strain, on the other hand, we observe that a band-gap coalescence does not take place for the chosen values of k'.

In Fig. 5.7, we further demonstrate the significance of the nonlinearity in the context of the effects of the resonator's mass and stiffness on the band gaps. Increasing the mass of the resonator transforms the opening mechanism of the first band gap from Bragg scattering to local resonance; this takes effect due to the drop in the resonator's frequency (Fig. 5.7a). Conversely, increasing the stiffness of the resonator generates the opposite effect (Fig. 5.7b). The most intriguing case is the one shown in Fig. 5.7c, where it can be seen that increasing the nonlinearity, while keeping the resonator parameters constant, transforms the opening mechanism of the first band gap from

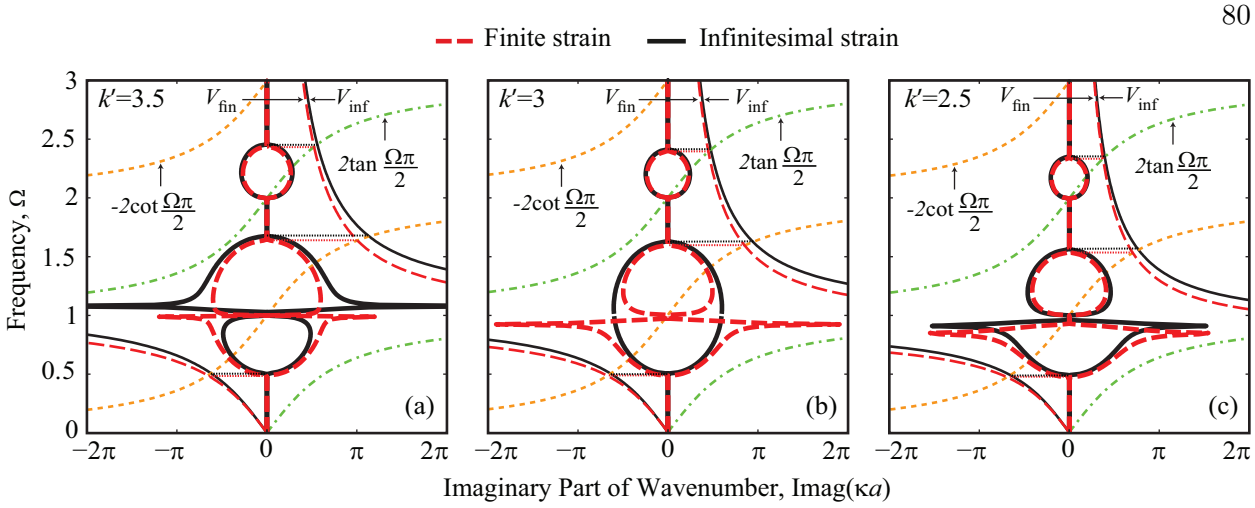

Figure 5.8: Prediction of dimensionless band-gap edges for 1D MM with properties of $m' = 3$ and (a) $k' = 3.5$, (b) $k' = 3$, and (c) $k' = 2.5$. The explicit band-gap edges relations are shown to provide exact predictions, compared to the curves pertaining to the direct dispersion relation. All finite-strain cases correspond to a dimensionless wave amplitude of $B' = 1/8$. The thick solid black and dashed red curves represent the imaginary part of infinitesimal and finite strain dispersions, respectively. The thin solid black and dashed red lines represent the non-dimensional dynamic stiffness, generated from Eq. (5.20), for the infinitesimal and finite strains, respectively. Finally, the dashed orange and dash-dotted green curves represent the left hand side of Eqs. (5.25b) and (5.26b), respectively.

Bragg scattering to local resonance. Exactly at the point of the transition, the first and the second band gaps coalesce, as highlighted in the figure. Thus, large deformation alone may cause a pair of isolated Bragg-scattering and local-resonance band gaps to coalesce to form a single wide band gap.

In Fig. 5.8, we present a dimensionless band-gap diagram for both the infinitesimal- and finite-strain models, using equations derived in Sections 5.2.1 and 5.2.2, for the corresponding cases featured in Fig. 5.6. In this diagram, we plot the imaginary part of the dispersion relation from Eq. (5.18) for the infinitesimal-strain ($\omega = \omega_{\text{inf}}$) and the finite-strain ($\omega = \omega_{\text{fin}}$) models, respectively. We also superimpose the infinitesimal cotangent and tangent curves of Eqs. (5.25b) and (5.26b), respectively, as well as the curves for the the infinitesimal ($V_{\text{inf}} = V(\omega_{\text{inf}})$) and finite ($V_{\text{fin}} = V(\omega_{\text{fin}})$) non-dimensional dynamic stiffnesses using Eq. (5.20). We observe that the intersection of the latter set of curves does indeed provide exact predictions of the band-gap edges, for both the infinitesimal-

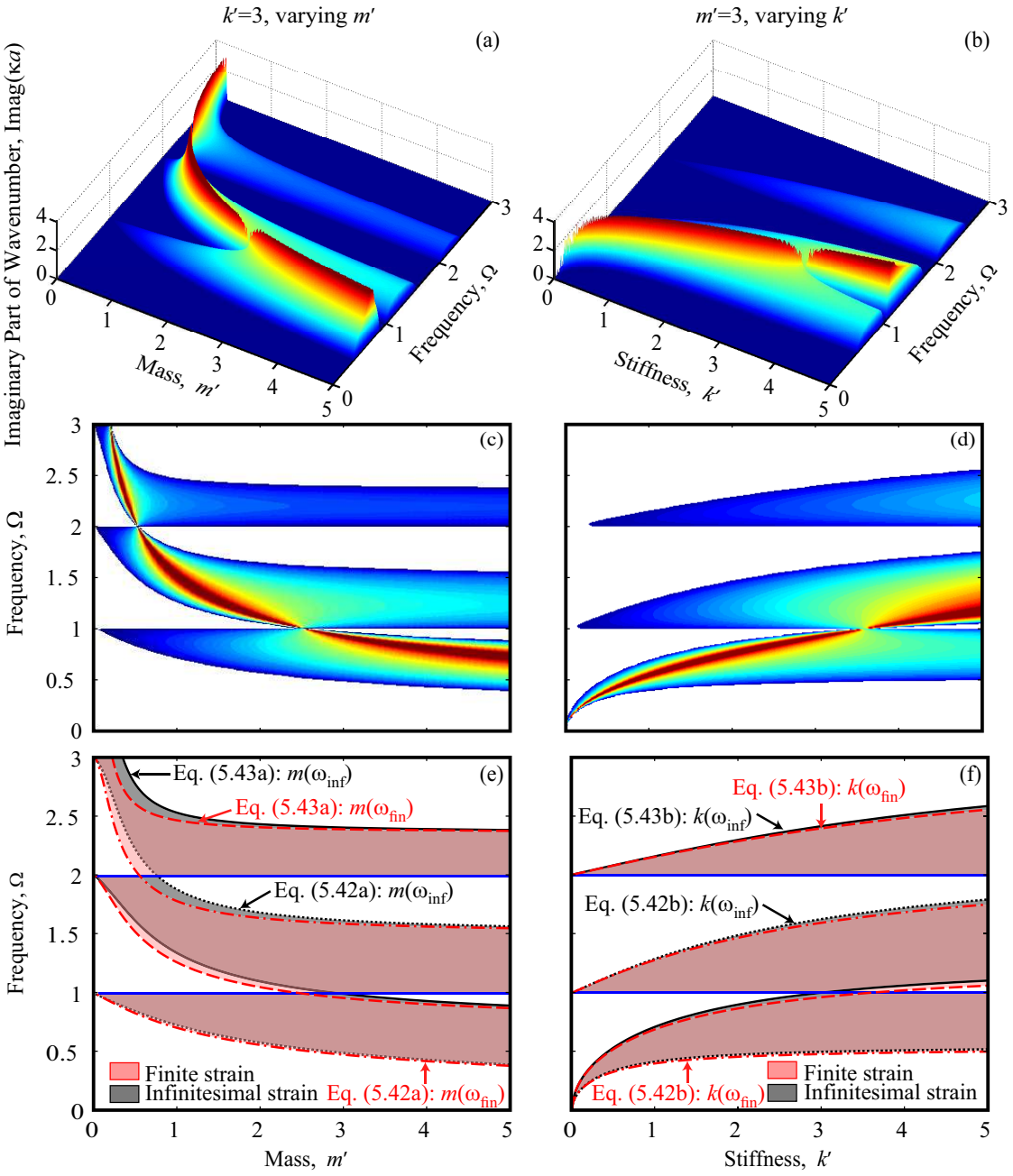

Figure 5.9: Dependency of 1D MM band-gap attenuation and transition characteristics on the resonator properties. Subfigures (a), (c) and (e) present the effect of varying m' while keeping the dimensionless stiffness fixed at $k' = 3$. Subfigures (b), (d) and (f) present the effect of varying k' while keeping the dimensionless mass fixed at $m' = 3$. The top row shows surface plots of the imaginary part of the dispersion relation for finite strain and the middle row shows the same results in the form of contour plots. The bottom row presents the curves for the frequencies of the band-gap edges for the cases of infinitesimal and finite strains, as predicted using Eqs. (5.42) and (5.43) as marked, as well as the band-gap edge frequencies (solid blue horizontal lines) corresponding to the Bragg conditions given in Eq. (5.27). The association of each curve with either Mode A or Mode B can be inferred from the marked equation numbers.

and finite-strain models.

Further analysis of the location, size and character of band gaps is presented in Fig. 5.9. In the top row of the figure, the imaginary part of the wavenumber for the finite-strain model is plotted the dimensionless frequency Ω for varying m' or k' and for a fixed wave amplitude of $B' = 1/8$. The same set of results is shown in the middle row as contour plots. In the bottom row, the band-gap edge curves are plotted for infinitesimal [$k = k(\omega_{\text{inf}})$, $m = m(\omega_{\text{inf}})$] and finite [$k = k(\omega_{\text{fin}})$, $m = m(\omega_{\text{fin}})$] strains for both Mode A and Mode B, from Eqs. (5.42) and (5.43), respectively. The band-gap edge curves plotted for the finite strain in the bottom row correspond to the boundaries of the contour plots in the middle row. The blue horizontal lines in the bottom subfigures correspond to the Bragg conditions of Eq. (5.27). The complete coalescence between a Bragg-scattering band gap and a local-resonance band gap can be seen at the intersection points. As in Fig. 5.6, the condition for this coalescence phenomenon can be obtained immediately. For example, for the case of infinitesimal strain, the two coalescence conditions in Fig. 5.9e are $m' = k'/1 = 3$ and $m' = k'/4 = 0.75$, respectively. And the coalescence condition in Fig. 5.9f is $k' = m'/1 = 3$. We note that Eq. (5.30) suggests that a higher wave speed in the host structure requires a higher tuned local-resonance frequency to achieve complete coalescence. Here we recall that the wave speed under finite strain is higher than under infinitesimal strain [see Eq. (5.60)]. As a result, for the case of finite strain, the tuned local-resonance frequency to achieve complete coalescence must be higher that the case of infinitesimal strain. In other words, if the other parameters are the same, the resonator mass, m', must be smaller (or the resonator stiffness, k', must be larger) to achieve coalescence when finite strain is accounted for, as observed in Fig. 5.9e Fig. 5.9f.

Finally we quantitatively examine the threshold beyond which the effect of nonlinearity on the dispersion characteristics is no longer negligible. Investigating this limitation is particularly important when linear theory is used to approximate the dynamical properties of nonlinear systems. Since we observe in the previous figures that the finite-strain dispersion curves begin their deviation from the corresponding infinitesimal dispersion curves within the sub-Bragg-scattering regime, this analysis has implications on the study of MMs with subwavelength band gaps.

In Fig. 5.10a, we plot the frequency band structure for the 1D MM with a subwavelength band-gap corresponding to approximately $\lambda/15$, where λ denotes the wavelength of the hybridizing wave. This condition is realized with $m' = 3$ and $k' = 0.03$. For different values of wave amplitude-to-unit-cell ratio, B/a, we calculate the location along the wavenumber access at which the finite-strain dispersion curve deviates by more than 5% from the corresponding infinitesimal-strain dispersion curve. From this value, we calculate the maximum unit-cell size, $a_{\max}$, beyond which the nonlinear effect is no longer negligible, and plot this quantity as a function of B/a in Fig. 5.10b. This result can be used to determine whether the characteristics of a particular subwavelength band gap may be approximated by linear theory without incurring a significant prediction error.

5.5 Conclusions

We have provided an analytical formulation for the calculation of the dispersion curves of a 1D locally resonant elastic metamaterial admitting finite-strain wave motion. We considered a

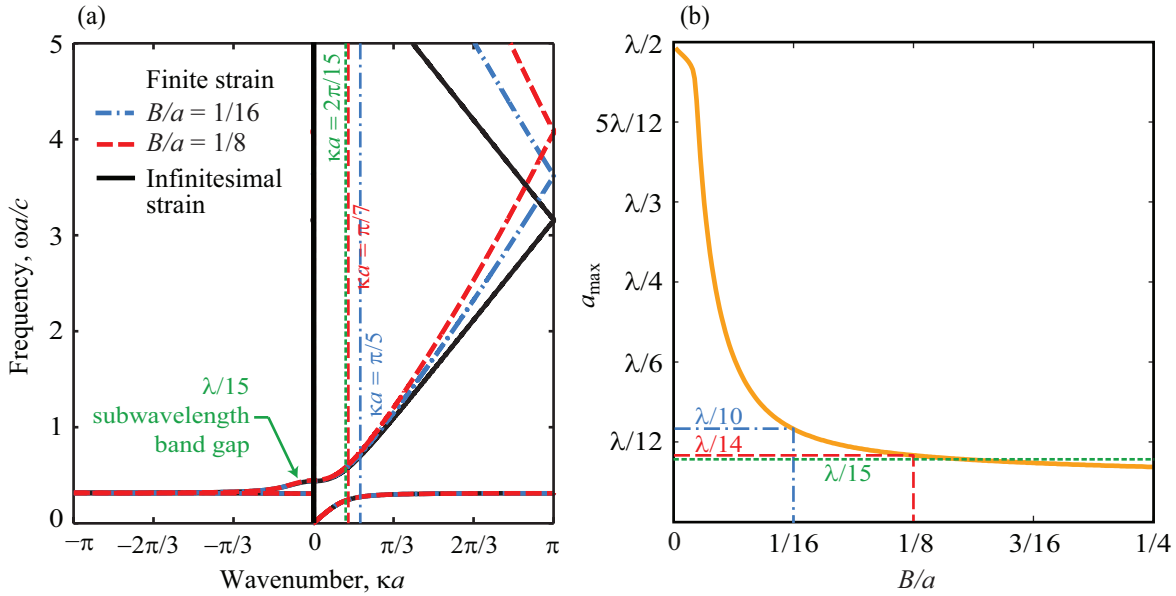

Figure 5.10: The effect of nonlinearity in the subwavelength regime. (a) Dispersion band structure for 1D MM with properties: $m' = 3$ and $k' = 0.03$. (b) Maximum unit cell size beyond which the effects of nonlinearity are no longer negligible (based on a 5% error threshold).

uniform thin rod with a periodic array of spring-mass resonators. The effect of the nonlinearity has been incorporated exactly at the bare rod level. Subsequently, the Transfer Matrix method has been applied to the unit cell to provide an approximate dispersion relation for the 1D MM as a whole. The approximation stems from the elimination of higher order strains in the TM method. However, since band gaps in locally resonant MMs are commonly designed to fall within the subwavelength regime, the results are relatively accurate especially for moderate values of wave amplitude.

Furthermore, we adopted the band-gap edge frequencies formulation of Xiao et al. [59] and extended it to the finite-strain regime. The analysis also examined the nonlinear vibration characteristics of equivalent finite structures.

In order to understand the effect of the nonlinearity on the band-gap formation behavior in the 1D MM considered, we have investigated several systems with a variety of resonator parameters. The results show that as the wave amplitude is increased, the location and size of the band gaps change, and under certain conditions it is possible for the character of a band gap (i.e., Bragg scattering versus hybridized local resonance) to change as well. Of particular interest is the observation that the nonlinearity alone could cause two band gaps, one of each character, to coalesce and form a combined wide band gap.

Finally we have shown that the error incurred by assuming linear elastic wave propagation theory increases rapidly as the wave amplitude is increased. We have provided a figure that determines the maximum unit-cell size permissible for a given wave amplitude beyond which ignoring the effects of finite strain would incur an error exceeding 5%. As an example, for a wave amplitude on the order of one-sixteenth of the unit cell size, the effect of the nonlinearity in the 1D MM considered is no longer negligible when the unit-cell size is one-tenth of the wavelength or larger.

Chapter 6

Summary and outlook

6.1 Summary of dissertation

This dissertation consists of two main parts; the first part investigates the effects of nonlinearities on the dispersion relation of a one-dimensional (1D) homogeneous medium when a large-amplitude elastic wave propagates through it. The second part extends this analysis to a continuous periodic thin rod - in one case a 1D phononic crystal constructed from several layers of different materials in its unit cell, and in another case, a 1D elastic metamaterial with a periodically placed local resonator.

Chapter 1 introduces the non-dispersive elastic wave equation and provides a few examples of physical problems that are governed by this equation. Selected sources of dispersion in an elastic solid medium are presented and common methods of treating them mathematically are introduced. A nonlinear elastic wave with the nonlinearity introduced in the form of large deformation is derived. Mathematical models for simplified periodic materials are formulated. A brief literature search is provided allowing the current work to be put in context. The chapter concludes with the thesis objectives and organization.

Chapter 2 starts by a brief derivation of a generalized form of the equation of motion incorporating a linear dispersive mechanism, lateral inertia, and two nonlinear dispersive mechanisms, the Green-Lagrange and Hencky finite strain measures. For 1D elastic media, the exact amplitude-dependent dispersion relations are derived without directly solving the governing equations. A numerical tool, the Fourier spectral method, followed by wavenumber-frequency spectrum analysis,

is developed to verify the analytical results. A brief formulation of this method can be found in Appendix A. Results comparing the theory with the simulation are plotted and a novel correlation between the nonlinear dispersion relation and the harmonic generation spectrum is established. It has been shown that the response of the spectrum is strongly related to the harmonic generations, establishing complete map connecting the space-time solution, the harmonic generations, and the nonlinear dispersion relation of the system.

Chapter 3 follows the same concept described in chapter 2 but for small amplitudes and through a perturbation method. This chapter formulates an expanded nonlinear dispersion relation for a 1D elastic rod under Green-Lagrange and Hencky finite strains. Benefiting from the exact nonlinear dispersion relations derived in chapter 2, the limitations of the perturbation theory are quantitatively determined. The chapter also shows a derivation of the second order spatial solution for the initial value problem introduced in chapter 2.

Chapter 4 discusses the theoretical treatment of elastic wave motion in a 1D elastic phononic crystal consisting of layers with alternating material properties in the presence of finite strains. The exact dispersion relation in each homogeneous layer is obtained and plugged into the familiar transfer matrix method to predict an amplitude-dependent dispersion relation. The dispersion relation that we obtain for the overall 1D phononic crystal represents an approximate solution. We then verify the derived dispersion relation using brute-force space-time simulations followed by a wave number-frequency spectrum analysis. The simulations are used to determine the upper limit of wave amplitude per unit-cell length for which the theory is accurate, which turns out to be 0.125. Finally, we use our formulation to investigate the effects of geometric nonlinearity on the elastic band structure and Bloch mode shapes as a function of the wave amplitude and shed some light on the possibility of balancing the linear and nonlinear contributions to the dispersion relation to yield a spatially invariant wave profile.

Chapter 5 discusses the dispersion characteristics of a 1D elastic metamaterial under large deformation. It starts with a TM method formulation which is slightly different that the one presented in section 1.2.1. An explicit formulation for band-gap edge frequencies calculations is

derived. A physical interpretation of the derived equation pertaining to the boundary conditions of a corresponding finite structure is given. The band structure exhibiting large deformation effects in a 1D elastic metamaterial is obtained and its behavior is analyzed.

In chapter 6, after a brief summery of the previous chapters, several directions for future research are proposed. Some preliminary results from these possible research tracks, namely, generalization of the work presented in Chapter 2 considering a nonlinear constitutive law, is presented.

6.2 Future work

While the results in Chapter 2 are restricted to two forms of finite-strain measures, the framework will be extended to include nonlinearities sourced from nonlinear constitutive laws. Generalization of this framework allows us to study the effects of each dispersive mechanism individually and collectively. This analysis framework will also be extended to 2D elastic waves and other problems in applied physics that can be analyzed using the developed approach.

In the following we present a first step in generalizing the theoretical treatment of dispersive elastic waves in a homogeneous medium considering a nonlinear constitutive law in the governing equation. Similar to the derivations in Chapter 1, we can derive the equation of motion for a 1D elastic media considering a nonlinear constitutive law, i.e., material nonlinearity. In this case, the kinetic and strain energy densities are

$$\mathcal{T} = \frac{1}{2}\rho(\frac{\partial u}{\partial t})^2, \tag{6.1}$$

and

$$\mathcal{U} = \frac{1}{2}E(\frac{\partial u}{\partial x})^2 + \frac{1}{2}\bar{E}(\frac{\partial u}{\partial x})^3 + \frac{1}{2}\bar{\bar{E}}(\frac{\partial u}{\partial x})^4, \tag{6.2}$$

where constitutive relation complies $\sigma = E\epsilon + \bar{E}\epsilon^2 + \bar{\bar{E}}\epsilon^3$. In this constitutive relation, $\bar{E}$ and $\bar{\bar{E}}$ are corrective terms. Upon substitution of these densities in Hamilton's principle, the equation of motion is

$$\frac{\partial^2 u}{\partial t^2} = c^2\frac{\partial^2 u}{\partial x^2} + \frac{1}{2}\frac{\partial}{\partial x}(3\bar{c}^2\frac{\partial u}{\partial x}^2 + 4\bar{\bar{c}}^2\frac{\partial u}{\partial x}^3). \tag{6.3}$$

Here $\bar{c}$ and $\bar{\bar{c}}$ denote higher order longitudinal velocities, defined by $\bar{c} = \sqrt{\bar{E}/\rho}$ and $\bar{\bar{c}} = \sqrt{\bar{\bar{E}}/\rho}$. Following the same steps introduced in the previous chapters, the amplitude-dependent dispersion relation is

$$\omega(\kappa; B) = c\kappa\sqrt{1 + \frac{3\bar{c}^2}{2c^2}B\kappa + \frac{2\bar{\bar{c}}^2}{c^2}B^2\kappa^2}. \tag{6.4}$$

This framework can be extended to a 1D elastic medium with both linear and nonlinear dispersive mechanisms, e.g., lateral inertia and material nonlinearity or lateral inertia and geometric nonlinearity.

Bibliography

[1] M. H. Abedinnasab and M. I. Hussein, "Wave dispersion under finite deformation," Wave Motion, vol. 50, no. 3, pp. 374 – 388, 2013.

[2] F. Bloch, "Über die quantenmechanik der elektronen in kristallgittern," Z. Phys., vol. 52, no. 7-8, pp. 555–600, 1929.

[3] M. G. Faulkner and D. P. Hong, "Free vibrations of a mono-coupled periodic system," J. Sound Vib., vol. 99, pp. 29–42, 1985.

[4] R. Esquivel-Sirvent and G. H. Cocoletzi, "Band-structure for the propagation of elastic-waves in superlattices," J. Acoust. Soc. Am., vol. 95, pp. 86–90, 1994.

[5] M. I. Hussein, G. M. Hulbert, and R. A. Scott, "Dispersive elastodynamics of 1D banded materials and structures: Analysis," J. Sound Vib., vol. 289, no. 4, pp. 779–806, 2006.

[6] J. Billingham and A. C. King, Wave Motion. Cambridge University Press, 2000.

[7] M. I. Hussein, M. J. Leamy, and M. Ruzzene, "Dynamics of phononic materials and structures: Historical origins, recent progress, and future outlook," Appl. Mech. Rev., vol. 66, p. 040802, 2014.

[8] G. B. Whitham, Linear and nonlinear waves. John Wiley & Sons, 1974.

[9] P. Yoon, R. Gaelzer, T. Umeda, Y. Omura, and H. Matsumoto, "Harmonic langmuir waves. i. nonlinear dispersion relation," Physics of Plasmas (1994-present), vol. 10, no. 2, pp. 364–372, 2003.

[10] J.-H. Huang, R. Chang, P.-T. Leung, and D. P. Tsai, "Nonlinear dispersion relation for surface plasmon at a metal–kerr medium interface," Optics Communications, vol. 282, no. 7, pp. 1412–1415, 2009.

[11] I. V. Shadrivov, A. A. Sukhorukov, Y. S. Kivshar, A. A. Zharov, A. D. Boardman, and P. Egan, "Nonlinear surface waves in left-handed materials," Phys. Rev. E, vol. 69, p. 016617, 2004.

[12] D. S. Montgomery, R. J. Focia, H. A. Rose, D. A. Russell, J. A. Cobble, J. C. Fernández, and R. P. Johnson, "Observation of stimulated electron-acoustic-wave scattering," Phys. Rev. Lett., vol. 87, p. 155001, Sep 2001.

[13] E. Herbert, N. Mordant, and E. Falcon, "Observation of the nonlinear dispersion relation and spatial statistics of wave turbulence on the surface of a fluid," Phys. Rev. Lett., vol. 105, p. 144502, 2010.

[14] R. Hager and K. Hallatschek, "Nonlinear dispersion relation of geodesic acoustic modes," Phys. Rev. Lett., vol. 108, p. 035004, 2012.

[15] G. Düring, C. Josserand, and S. Rica, "Weak turbulence for a vibrating plate: Can one hear a kolmogorov spectrum?," Phys. Rev. Lett., vol. 97, p. 025503, 2006.

[16] N. Mordant, "Are there waves in elastic wave turbulence?," Phys. Rev. Lett., vol. 100, p. 234505, 2008.

[17] P. Cobelli, P. Petitjeans, A. Maurel, V. Pagneux, and N. Mordant, "Space-time resolved wave turbulence in a vibrating plate," Phys. Rev. Lett., vol. 103, p. 204301, 2009.

[18] W. Lee, G. Kovačič, and D. Cai, "Generation of dispersion in nondispersive nonlinear waves in thermal equilibrium," Proc. Natl Acad. Sci., vol. 110, no. 9, pp. 3237–3241, 2013.

[19] Y. Liu, P. Ghaderi, and A. J. Dick, "High fidelity methods for modeling nonlinear wave propagation in one-dimensional waveguides," in ASME IMECE, pp. 741–750, 2012.

[20] R. Ganesh and S. Gonella, "Spectro-spatial wave features as detectors and classifiers of nonlinearity in periodic chains," Wave Motion, vol. 50, no. 4, pp. 821–835, 2013.

[21] A. S. Phani, J. Woodhouse, and N. A. Fleck, "Wave propagation in two-dimensional periodic lattices," J. Acoust. Soc. Am., vol. 119, no. 4, pp. 1995–2005, 2006.

[22] M. I. Hussein, G. M. Hulbert, and R. A. Scott, "Dispersive elastodynamics of 1D banded materials and structures: Design," J. Sound Vib., vol. 307, no. 3, pp. 865–893, 2007.

[23] S. Yang, J. H. Page, Z. Liu, M. L. Cowan, C. T. Chan, and P. Sheng, "Focusing of sound in a 3D phononic crystal," Phys. Rev. Lett., vol. 93, no. 2, p. 024301, 2004.

[24] J. Zhu, J. Christensen, J. Jung, L. Martin-Moreno, X. Yin, L. Fok, X. Zhang, and F. Garcia-Vidal, "A holey-structured metamaterial for acoustic deep-subwavelength imaging," Nat. Phys., vol. 7, no. 1, pp. 52–55, 2010.

[25] S. A. Cummer and D. Schurig, "One path to acoustic cloaking," New J. Phys., vol. 9, no. 3, p. 45, 2007.

[26] D. Torrent and J. Sánchez-Dehesa, "Acoustic metamaterials for new two-dimensional sonic devices," New J. Phys., vol. 9, no. 9, p. 323, 2007.

[27] A. J. H. McGaughey, M. I. Hussein, E. S. Landry, M. Kaviany, and G. M. Hulbert, "Phonon band structure and thermal transport correlation in a layered diatomic crystal," Phys. Rev. B, vol. 74, p. 104304, 2006.

[28] B. L. Davis and M. I. Hussein, "Thermal characterization of nanoscale phononic crystals using supercell lattice dynamics," AIP Adv., vol. 1, no. 4, p. 041701, 2011.

[29] B. L. Davis and M. I. Hussein, "Nanophononic metamaterial: Thermal conductivity reduction by local resonance," Phys. Rev. Lett., vol. 112, p. 055505, Feb 2014.

[30] M. I. Hussein, S. Biringen, O. R. Bilal, and A. Kucala, "Flow stabilization by subsurface phonons," Proc. Roy. Soc. A, vol. 471, p. 20140928, 2015.

[31] N. Li, J. Ren, L. Wang, G. Zhang, P. Hänggi, and B. Li, "Colloquium: Phononics: Manipulating heat flow with electronic analogs and beyond," Rev. Mod. Phys., vol. 84, no. 3, p. 1045, 2012.

[32] P. A. Deymier, Acoustic Metamaterials and Phononic Crystals, vol. 173. Springer, 2013.

[33] M. I. Hussein and I. El-Kady, "Preface to special topic: Selected articles from Phononics 2011: The first international conference on phononic crystals, metamaterials and optomechanics, 29 May–2 June 2011, Santa Fe, New mexico, USA," AIP Adv., vol. 1, p. 041301, 2011.

[34] M. I. Hussein, M. J. Leamy, and M. Ruzzene, "Editorial: Special issue on dynamics of phononic materials and structures," J. Vib. Acoust., vol. 135, pp. 040201–040201, 2013.

[35] M. M. Sigalas and E. N. Economou, "Elastic and acoustic wave band structure," J. Sound Vib., vol. 158, no. 2, pp. 377–382, 1992.

[36] M. S. Kushwaha, P. Halevi, L. Dobrzynski, and B. Djafari-Rouhani, "Acoustic band structure of periodic elastic composites," Phys. Rev. Lett., vol. 71, no. 13, p. 2022, 1993.

[37] M. Sigalas and E. N. Economou, "Band structure of elastic waves in two dimensional systems," Solid State Commun., vol. 86, no. 3, pp. 141–143, 1993.

[38] Z. Liu, X. Zhang, Y. Mao, Y. Zhu, Z. Yang, C. Chan, and P. Sheng, "Locally resonant sonic materials," Science, vol. 289, no. 5485, pp. 1734–1736, 2000.

[39] J. Li and C. Chan, "Double-negative acoustic metamaterial," Phys. Rev. E, vol. 70, no. 5, p. 055602, 2004.

[40] Y. Ding, Z. Liu, C. Qiu, and J. Shi, "Metamaterial with simultaneously negative bulk modulus and mass density," Phys. Rev. Lett., vol. 99, no. 9, p. 093904, 2007.

[41] Y. Cheng, J. Y. Xu, and X. J. Liu, "One-dimensional structured ultrasonic metamaterials with simultaneously negative dynamic density and modulus," Physical Review B, vol. 77, no. 4, p. 045134, 2008.

[42] S. Yao, X. Zhou, and G. Hu, "Experimental study on negative effective mass in a 1D mass–spring system," New J. Phys., vol. 10, no. 4, p. 043020, 2008.

[43] R. V. Craster and S. Guenneau, Acoustic Metamaterials: Negative Refraction, Imaging, Lensing and Cloaking, vol. 166. Springer, 2013.

[44] B. R. Mace, "Discussion of dynamics of phononic materials and structures: Historical origins, recent progress and future outlook (Hussein, M. I., Leamy, M. J., and Ruzzene, M., 2014, ASME Appl. Mech. Rev., 66(4), p. 040802)," Appl. Mech. Rev., vol. 66, p. 045502, 2014.

[45] M. I. Hussein, M. J. Leamy, and M. Ruzzene, "Closure to discussion of dynamics of phononic materials and structures: Historical origins, recent progress, and future outlook (2014, ASME Appl. Mech. Rev., 66(4), p. 040802)," Appl. Mech. Rev., vol. 66, p. 046002, 2014.

[46] G. Wang, X. S. Wen, J. H. Wen, L. H. Shao, and Y. Z. Liu, "Two-dimensional locally resonant phononic crystals with binary structures," Phys. Rev. Lett., vol. 93, p. 154302, 2004.

[47] Y. Pennec, B. Djafari-Rouhani, H. Larabi, J. O. Vasseur, and A.-C. ladky Hennion, "Low-frequency gaps in a phononic crystal constituted of cylindrical dots deposited on a thin homogeneous plate," Phys. Rev. B, vol. 78, p. 104105, 2008.

[48] T. T. Wu, Z. G. Huang, T. C. Tsai, and T. C. Wu, "Evidence of complete band gap and resonances in a plate with periodic stubbed surface," Appl. Phys. Lett., vol. 93, p. 111902, 2008.

[49] O. R. Bilal and M. I. Hussein, "Trampoline metamaterial: Local resonance enhancement by springboards," Appl. Phys. Lett., vol. 103, no. 11, p. 111901, 2013.

[50] R. Zhu, X. N. Liu, G. K. Hu, C. T. Sun, and G. L. Huang, "A chiral elastic metamaterial beam for broadband vibration suppression," J. Sound Vib., vol. 333, pp. 2759–2773, 2014.

[51] D. Krattiger, R. Khajehtourian, C. L. Bacquet, and M. I. Hussein, "Anisotropic dissipation in lattice metamaterials," AIP Adv., vol. 6, no. 12, p. 121802, 2016.

[52] G. Wang, D. Yu, J. Wen, Y. Liu, and X. Wen, "One-dimensional phononic crystals with locally resonant structures," Physics Letters A, vol. 327, no. 5, pp. 512–521, 2004.

[53] D. Yu, Y. Liu, H. Zhao, G. Wang, and J. Qiu, "Flexural vibration band gaps in Euler-Bernoulli beams with locally resonant structures with two degrees of freedom," Phys. Rev. B, vol. 73, p. 064301, 2006.

[54] D. Yu, Y. Liu, G. Wang, H. Zhao, and J. Qiu, "Flexural vibration band gaps in Timoshenko beams with locally resonant structures," J. Appl. Phys., vol. 100, p. 124901, 2006.

[55] J. Chen, B. Sharma, and C. Sun, "Dynamic behaviour of sandwich structure containing spring-mass resonators," Composite Structures, vol. 93, no. 8, pp. 2120–2125, 2011.

[56] Y. Pennec, B. Djafari-Rouhani, C. Li, J. M. Escalante, A. Martinez, S. Benchabane, V. Laude, and N. Papanikolaou, "Band gaps and cavity modes in dual phononic and photonic strip waveguides," AIP Adv., vol. 1, p. 041901, 2011.

[57] Y. Yao, Z. Hou, F. Wu, and X. Zhang, "Low-frequency band gaps in one-dimensional thin phononic crystal plate with periodic stubbed surface," Physica B, vol. 406, pp. 2249–2253, 2011.

[58] M. Nouh, O. Aldraihem, and A. Baz, "Vibration characteristics of metamaterial beams with periodic local resonances," J. Vib. Acoust., vol. 136, p. 061012, 2014.

[59] Y. Xiao, B. R. Mace, J. Wen, and X. Wen, "Formation and coupling of band gaps in a locally resonant elastic system comprising a string with attached resonators," Physics Letters A, vol. 375, no. 12, pp. 1485–1491, 2011.

[60] Y. Xiao, J. Wen, and X. Wen, "Longitudinal wave band gaps in metamaterial-based elastic rods containing multi-degree-of-freedom resonators," New J. Phys., vol. 14, no. 3, p. 033042, 2012.

[61] Y. Xiao, J. Wen, D. Yu, and X. Wen, "Flexural wave propagation in beams with periodically attached vibration absorbers: Band-gap behavior and band formation mechanisms," J. Sound Vib., vol. 332, pp. 867–893, 2013.

[62] L. Liu and M. I. Hussein, "Wave motion in periodic flexural beams and characterization of the transition between bragg scattering and local resonance," J. Appl. Mech., vol. 79, no. 1, p. 011003, 2012.

[63] K. F. Graff, Wave Motion in Elastic Solids. Dover Publications, 1991.

[64] J. Achenbach, Wave Propagation in Elastic Solids. Elsevier, 1984.

[65] P. L. Bhatnagar, Nonlinear Waves in One-dimensional Dispersive Systems. Oxford University Press, 1979.

[66] R. W. Ogden, Non-linear Elastic Deformations. Courier Corporation, 1997.

[67] A. N. Norris, "Finite amplitude waves in solids," in Nonlinear Acoustics (M. F. Hamilton and D. T. Blackstock, eds.), pp. 263–277, Academic Press, New York, 1998.

[68] A. Porubov, Amplification of Nonlinear Strain Waves in Solids. World Scientific, 2003.

[69] V. I. Erofeev, Wave Processes in Solids with Microstructure. World Scientific, 2003.

[70] G. Whitham, "Non-linear dispersion of water waves," J. Fluid Mech., vol. 27, no. 02, pp. 399–412, 1967.

[71] H. Hasimoto and H. Ono, "Nonlinear modulation of gravity waves," J. Phys. Soc. Jap., vol. 33, no. 3, pp. 805–811, 1972.

[72] D. G. Swanson, Plasma Waves. IOP Publishing, 2003.

[73] P. K. Shukla and B. Eliasson, "Nonlinear interactions between electromagnetic waves and electron plasma oscillations in quantum plasmas," Phys. Rev. Lett., vol. 99, no. 9, p. 096401, 2007.

[74] C. Daraio, V. F. Nesterenko, E. B. Herbold, and S. Jin, "Tunability of solitary wave properties in one-dimensional strongly nonlinear phononic crystals," Phys. Rev. E, vol. 73, no. 2, p. 026610, 2006.

[75] R. K. Narisetti, M. J. Leamy, and M. Ruzzene, "A perturbation approach for predicting wave propagation in one-dimensional nonlinear periodic structures," J. Vib. Acoust., vol. 132, p. 031001, 2010.

[76] L. L. Bonilla and S. W. Teitsworth, Nonlinear Wave Methods for Charge Transport. John Wiley & Sons, 2009.

[77] V. Berger, "Nonlinear photonic crystals," Phys. Rev. Lett., vol. 81, no. 19, p. 4136, 1998.

[78] I. V. Andrianov, V. V. Danishevskyy, O. I. Ryzhkov, and D. Weichert, "Dynamic homogenization and wave propagation in a nonlinear 1D composite material," Wave Motion, vol. 50, pp. 271–281, 2013.

[79] A. F. Vakakis and M. E. King, "Nonlinear wave transmission in a monocoupled elastic periodic system," J. Acoust. Soc. Am., vol. 98, p. 1534, 1995.

[80] K. Manktelow, M. J. Leamy, and M. Ruzzene, "Multiple scales analysis of wave–wave interactions in a cubically nonlinear monoatomic chain," Nonlinear Dynam., vol. 63, no. 1-2, pp. 193–203, 2011.

[81] N. Z. Swinteck, K. Muralidharan, and P. A. Deymier, "Phonon scattering in one-dimensional anharmonic crystals and superlattices: Analytical and numerical study," J. Vib. Acoust., vol. 135, p. 041016, 2013.

[82] G. Chakraborty and A. Mallik, "Dynamics of a weakly non-linear periodic chain," Int. J. Nonlinear Mech., vol. 36, no. 2, pp. 375–389, 2001.

[83] B. S. Lazarov and J. S. Jensen, "Low-frequency band gaps in chains with attached non-linear oscillators," Int. J. Nonlinear Mech., vol. 42, no. 10, pp. 1186–1193, 2007.

[84] R. K. Narisetti, M. Ruzzene, and M. J. Leamy, "Study of wave propagation in strongly nonlinear periodic lattices using a harmonic balance approach," Wave Motion, vol. 49, no. 2, pp. 394–410, 2012.

[85] K. Manktelow, M. J. Leamy, and M. Ruzzene, "Comparison of asymptotic and transfer matrix approaches for evaluating intensity-dependent dispersion in nonlinear photonic and phononic crystals," Wave Motion, vol. 50, no. 3, pp. 494–508, 2013.

[86] N. Li and B. Li, "Thermal conductivities of one-dimensional anharmonic/nonlinear lattices: renormalized phonons and effective phonon theory," AIP Adv., vol. 2, p. 041408, 2012.

[87] E. B. Herbold, J. Kim, V. F. Nesterenko, S. Y. Wang, and C. Daraio, "Pulse propagation in a linear and nonlinear diatomic periodic chain: effects of acoustic frequency band-gap," Acta Mech., vol. 205, no. 1-4, pp. 85–103, 2009.

[88] C. Daraio, V. F. V. F. Nesterenko, E. B. Herbold, and S. Jin, "Energy trapping and shock disintegration in a composite granular medium," Phys. Rev. Lett., vol. 96, p. 058002, 2006.

[89] A. Spadoni and C. Daraio, "Generation and control of sound bullets with a nonlinear acoustic lens," P. Natl. Acad. Sci. USA, vol. 107, pp. 7230–7234, 2010.

[90] N. Boechler, G. Theocharis, and C. Daraio, "Bifurcation-based acoustic switching and rectification," Nat. Mater., vol. 10, pp. 665–668, 2011.

[91] K. L. Manktelow, M. J. Leamy, and M. Ruzzene, "Analysis and experimental estimation of nonlinear dispersion in a periodic string," J. Vib. Acoust., vol. 136, no. 3, p. 031016, 2014.

[92] M. I. Hussein, R. Khajehtourian, and M. H. Abedinnasab, "Finite-strain bloch wave propagation by the transfer matrix method," pp. arXiv:1412.2131v1 [cond–mat.mtrl–sci], 2014.

[93] R. Khajehtourian and M. I. Hussein, "Dispersion characteristics of a nonlinear elastic metamaterial," AIP Adv., vol. 4, no. 12, p. 124308, 2014.

[94] R. Khajehtourian and M. I. Hussein, "Unified theory of nonlinear dispersion and harmonic generation," In prepration.

[95] M. I. Hussein and R. Khajehtourian, "Nonlinear elastic waves in solids: Deriving simplicity from complexity," Bulletin of the American Physical Society, vol. 60, 2015.

[96] R. Khajehtourian and M. I. Hussein, "Spatial evolution of nonlinear elastic waves in a 1d thin rod by high-order perturbation theory," In prepration.

[97] G. B. Whitham, Linear and nonlinear waves. John Wiley & Sons, 1974.

[98] J. H. Huang, R. Chang, P. T. Leung, and D. P. Tsai, "Nonlinear dispersion relation for surface plasmon at a metal–kerr medium interface," Opt. Commun., vol. 282, no. 7, pp. 1412–1415, 2009.

[99] P. C. di Leoni, P. Cobelli, and P. Mininni, "Wave turbulence in shallow water models," Phys. Rev. E, vol. 89, no. 6, p. 063025, 2014.

[100] P. Yoon, R. Gaelzer, T. Umeda, Y. Omura, and H. Matsumoto, "Harmonic langmuir waves. i. nonlinear dispersion relation," Phys. Plasmas, vol. 10, no. 2, pp. 364–372, 2003.

[101] M. Onorato, A. Osborne, and M. Serio, "Modulational instability in crossing sea states: A possible mechanism for the formation of freak waves," Phys. Rev. Lett., vol. 96, no. 1, p. 014503, 2006.

[102] P. K. Shukla, I. Kourakis, B. Eliasson, M. Marklund, and L. Stenflo, "Instability and evolution of nonlinearly interacting water waves," Phys. Rev. Lett., vol. 97, no. 9, p. 094501, 2006.

[103] A. Samsonov, G. Dreiden, A. Porubov, and I. Semenova, "Longitudinal-strain soliton focusing in a narrowing nonlinearly elastic rod," Phys. Rev. B, vol. 57, no. 10, p. 5778, 1998.

[104] M. J. Ablowitz, Nonlinear dispersive waves: asymptotic analysis and solitons. Cambridge University Press, 2011.

[105] S. W. Shaw and C. Pierre, "Normal modes for non-linear vibratory systems," J. Sound Vib., vol. 164, no. 1, pp. 85–124, 1993.

[106] G. Kerschen, K. Worden, A. F. Vakakis, and J.-C. Golinval, "Past, present and future of nonlinear system identification in structural dynamics," Mech. Syst. Signal Pr., vol. 20, no. 3, pp. 505–592, 2006.

[107] P. Gumbsch and H. Gao, "Dislocations faster than the speed of sound," Science, vol. 283, no. 5404, pp. 965–968, 1999.

[108] A. Rosakis, O. Samudrala, and D. Coker, "Cracks faster than the shear wave speed," Science, vol. 284, no. 5418, pp. 1337–1340, 1999.

[109] M. K. Sen and P. L. Stoffa, "Nonlinear one-dimensional seismic waveform inversion using simulated annealing," Geophysics, vol. 56, no. 10, pp. 1624–1638, 1991.

[110] L. Ostrovsky and P. Johnson, "Dynamic nonlinear elasticity in geomaterials," Riv. Nuovo Cimento, vol. 24, no. 7, pp. 1–46, 2001.

[111] Y. Zheng, R. G. Maev, and I. Y. Solodov, "Review/sythèse nonlinear acoustic applications for material characterization: a review," Can. J. Phys., vol. 77, no. 12, pp. 927–967, 2000.

[112] B. Ward, A. Baker, and V. Humphrey, "Nonlinear propagation applied to the improvement of resolution in diagnostic medical ultrasound," J. Acoust. Soc. Am., vol. 101, no. 1, pp. 143–154, 1997.

[113] V. Sánchez-Morcillo, I. Pérez-Arjona, V. Romero-García, V. Tournat, and V. Gusev, "Second-harmonic generation for dispersive elastic waves in a discrete granular chain," Phys. Rev. E, vol. 88, no. 4, p. 043203, 2013.

[114] M. C. Remillieux, R. A. Guyer, C. Payan, and T. Ulrich, "Decoupling nonclassical nonlinear behavior of elastic wave types," Phys. Rev. Lett., vol. 116, no. 11, p. 115501, 2016.

[115] "See appendix a for the details on stability analysis, the fourier spectral method, and recovering linear dispersion relation from a nonlinear one.."

[116] G. P. Agrawal, Nonlinear fiber optics. Academic press, 2007.

[117] A. H. Nayfeh, Introduction to perturbation techniques. John Wiley & Sons, 2011.

[118] S. A. Cummer and J. Christensen, "Controlling sound with acoustic metamaterials," Nature Rev. Mat., vol. 1, p. 16001, 2016.

[119] V. Laude, Phononic Crystals: Artificial Crystals for Sonic, Acoustic, and Elastic waves. Walter de Gruyter, 2015.

[120] A. Khelif and A. Adibi, Phononic Crystals: Fundamentals and Applications. Springer, 2016.

[121] A. N. Norris and M. R. Haberman, "Introduction to the special issue on acoustic metamaterials," J. Acoust. Soc. Am., vol. 132, p. 2783, 2012.

[122] M. I. Hussein, I. El-Kady, B. Li, and J. Sánchez-Dehesa, "Preface to special topic: Selected articles from Phononics 2013: The second international conference on phononic crystals/metamaterials, phonon transport and optomechanics, 2-7 June 2013, Sharm El-Sheikh, Egypt," AIP Adv., vol. 4, p. 124101, 2014.

[123] M. I. Hussein, B. Bonello, A. Khelif, and B. Djafari-Rouhani, "Preface to special topic: Selected articles from Phononics 2015: The third international conference on phononic crystals/metamaterials, phonon transport and phonon coupling, 31 May–5 June 2015, Paris, France," AIP Adv., vol. 6, p. 121501, 2016.

[124] A. N. Norris and M. R. Haberman, "Introduction to the special issue on acoustic metamaterials," J. Acoust. Soc. Am., vol. 139, p. 3239, 2016.

[125] M. I. Hussein, D. Torrent, and O. R. Bilal, "Editorial for the focus issue on "Frontiers of mechanical metamaterials," Extreme Mech. Lett, vol. 12, p. 1, 2017.

[126] R. Ganesh and S. Gonella, "Spectro-spatial wave features as detectors and classifiers of nonlinearity in periodic chains," Wave Motion, vol. 50, no. 4, pp. 821–835, 2013.

[127] B. Yousefzadeh and A. S. Phani, "Energy transmission in finite dissipative nonlinear periodic structures from excitation within a stop band," J. Sound Vib., vol. 354, pp. 180–195, 2015.

[128] R. K. Pal, J. Villa, M. J. Leamy, and M. Ruzzene, "Amplitude-dependent topological edge states in nonlinear phononic lattices," arXiv:1705.01118 [cond-mat.mes-hall], 2017.

[129] J. Pendry, "Photonic band structures," J. Mod. Optic., vol. 41, no. 2, pp. 209–229, 1994.

[130] A. H. Nayfeh and D. T. Mook, Nonlinear Oscillations. John Wiley & Sons, 2008.

[131] A. N. Norris, "Finite amplitude waves in solids," In: M. F. Hamilton and D. T. Blackstock (Eds.), Nonlinear Acoustics, 263–277, Academic Press, San Diego, 1999.

[132] D. Mead, "Wave propagation and natural modes in periodic systems: I. mono-coupled systems," J. Sound Vib., vol. 40, no. 1, pp. 1–18, 1975.

[133] D. H. Johnson and D. E. Dudgeon, Array signal processing: concepts and techniques. Simon & Schuster, 1992.

Appendix A

Supplemental material: Unified theory of nonlinear dispersion and harmonic generation

A.1 Nondispersive wave WFS analysis

To verify the computational approach, we study the system at the limits of $B \to 0, r \to 0$ to recover the linear dispersion relation $\omega_{\text{inf}} = c\kappa$ from Eqs. (3) and (4). We set $r = 0$ and choose a small amplitude in specific $B = 0.0005$ to avoid numerical instabilities in the numerical simulations. The profile is defined the same as the one in Fig. (3). This condition generates a non-dispersive wave in an almost non-dispersive medium, as it is shown in the top panels of Fig. A.1. The space-time solution is shown in Fig. SA.1(a) followed by the WFS analysis results in Fig. SA.1(b) where the spectrum perfectly falls along the infinitesimal dispersion relation.

A.2 Stability Analysis

The stability of nonlinear thin rod can be locally evaluated using eigenvalues of Eq. (A.1) which is the equivalent first order system of Eq. (2) ignoring effects of lateral inertia,

$$\begin{aligned} \partial_\xi \bar{u} &= \bar{v}, \\ \partial_\xi \bar{v} &= \frac{\kappa^2}{\omega^2} \partial_{\xi\xi} (\alpha \bar{u} + \beta \mathcal{N}(\bar{u})). \end{aligned} \tag{A.1}$$

By analyzing this system, we find two distinct real eigenvalues, one negative, and one positive which collide to each other on $\bar{v} = 0$. The positive eigenvalue indicates that the system is unstable and

solutions are in the form of breaking waves.

A.3 Computational method: Fourier spectral method

We simulate the propagation of Eq. (1) using a spectral method for the spatial variable in conjunction with an efficient explicit time stepping method. The nonlinear PDEs are discretized with the discrete Fourier transform (DFT) in space and marched in time using a numerical integration scheme. We consider $\bar{u}$ as a discrete function on N-point spatial grid x_j, $j = 1, \ldots, N$. The DFT is defined by $\widehat{u}_k = h \sum_j \mathrm{e}^{-\mathrm{i}kx_j} \bar{u}_j$, for $k = -N/2 + 1, ..., N/2$, and the inverse discrete Fourier transform (IDFT) by $\bar{u}_j = \frac{1}{2\pi} \sum_k \mathrm{e}^{\mathrm{i}kx_j} \widehat{u}_k$, for each point. Here, $h = 2\pi/N$, $x_j = jh$, h is the spacing of the grid points, and k is the Fourier wave numbers. We apply $\partial_t \bar{u} = \bar{v}$ followed by

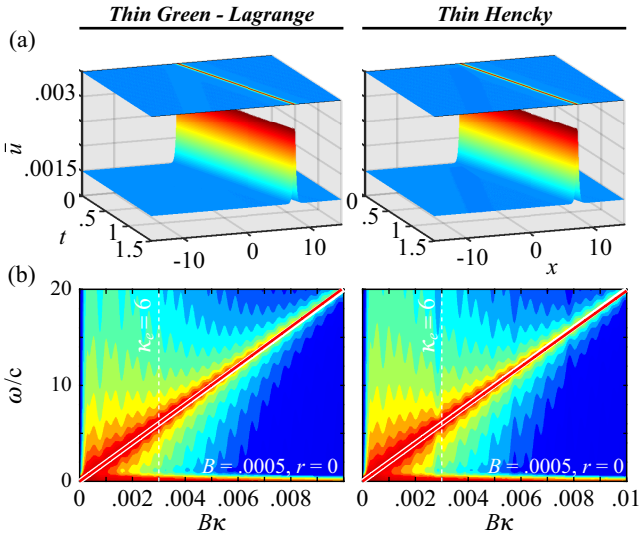

Figure A.1: (color). Wave propagation and its corresponding WFS analyses (GLS measure at left and HS measure at right columns).(a) Infinitesimal strain space-time solution. Here we have used $B = 0.0005$ and $\kappa_e = 6$ to form the initial wave profile. (b) The WFS analysis of the infinitesimal strain space-time solution represented by the logarithmic spectrum S. Corresponding dispersion curves from Eqs. (3) and (4) are overlaid as solid lines. Time and space units are [ms] and [m], respectively.

the DFT on Eq. (1) to form the corresponding first order system

$$\partial_t \begin{bmatrix} \widehat{u} \\ \\ \widehat{v} \end{bmatrix} = \begin{bmatrix} 0 & 0 \\ \\ -\frac{\alpha k^2}{1+\gamma k^2} & 0 \end{bmatrix} \begin{bmatrix} \widehat{u} \\ \\ \widehat{v} \end{bmatrix} + \begin{bmatrix} \widehat{v} \\ \\ -\frac{\beta k^2}{1+\gamma k^2}\mathcal{F}(\mathcal{N}) \end{bmatrix}, \tag{A.2}$$

where $\mathcal{F}(.)$ denotes the Fourier transform of the considered function. Differentiating the transformation $[\widetilde{u},\widetilde{v}]^{\mathrm{T}} = \mathbf{\Gamma}\,[\widehat{u},\widehat{v}]^{\mathrm{T}}$ with respect to time, with $\mathbf{\Gamma} = [I, 0; \alpha k^2 \Delta t, I]$ being the integral factor of Eq. (A.2), followed by the substitution of the $\partial_t \widehat{u}$ and $\partial_t \widehat{v}$ values from Eq. (A.2) and $\widehat{u}$ and $\widehat{v}$ from the inverse transformation $[\widehat{u},\widehat{v}]^{\mathrm{T}} = \mathbf{\Gamma}^{-1}\,[\widetilde{u},\widetilde{v}]^{\mathrm{T}}$, produces the following numerically integrable system,

$$\begin{aligned} \partial_t \widetilde{u} &= -\frac{\alpha k^2 \Delta t}{1+\gamma k^2}\widetilde{u} + \widetilde{v}, \\ \partial_t \widetilde{v} &= \frac{\alpha k^2 \Delta t}{1+\gamma k^2}(-\frac{\alpha k^2 \Delta t}{1+\gamma k^2}\widetilde{u} + \widetilde{v}) - \frac{\beta k^2}{1+\gamma k^2}\mathcal{F}(\mathcal{N}). \end{aligned} \tag{A.3}$$

We use the fourth-order explicit Runge-Kutta time stepping scheme to integrate Eq. (A.3). Then the inverse transformation is applied followed by IDFT on $[\widetilde{u},\widetilde{v}]^{\mathrm{T}}$ to obtain $\bar{u}(x,t)$. Now that we have the space-time solution, we expand the concept of Fourier analysis to the spatio-temporal wave-field data $\bar{u}_{p,q}, p = 0, 1, ..., N-1, q = 0, 1, ..., T-1$ by $s_{l,n} = \frac{1}{NT}\sum_p \sum_q \mathrm{e}^{-2\pi \mathrm{i}(lp/N + nq/T)}\bar{u}_{p,q}$, for $l = 0, 1, ..., N$ and $n = 0, 1, ..., T$ defining T as the number of time steps, to reveal the wave number-frequency spectrum $s(\kappa, \omega)$ [20, 133].

Appendix B

Nonlinear dispersion verification by the finite-element method

A finite element method is used to simulate the wave propagation in elastic media under finite deformation. The following formulation is presented for the Green-Lagrange strain measure, but it can be reformulated for any other strain measure. The governing equation of un-damped free vibration is

$$\mathbf{M}\ddot{\mathbf{u}} + \mathbf{f} = \mathbf{0}. \tag{B.1}$$

In order to capture the effect of large deformation in 1D, a two-node element with length l, consisting of the following 4 degrees of freedom (DOF) is defined

$$\mathbf{u}^e = [u_{x1}, \theta_{z1}, u_{x2}, \theta_{z2}]^T. \tag{B.2}$$

We derive the mass matrix through a variational formulation by taking the kinetic energy as part of the governing functional. The kinetic energy of an element of mass density ρ and velocity field $\dot{u}^e$ is

$$T^e = \frac{1}{2}\rho A \int (\dot{u}^e)^T \dot{u}^e dx. \tag{B.3}$$

The element velocity field is interpolated using shape functions defined by

$$\mathbf{N}^e = \left[\frac{1}{l^3}(2x+l)(x-l)^2, \frac{1}{l^2}x(x-l)^2, -\frac{1}{l^3}x^2(2x-3l), \frac{1}{l^2}x^2(x-l)\right], \tag{B.4}$$

as $\dot{u}^e(x) = du^e(x)/dt = \mathbf{N}^e\dot{\mathbf{u}}^e$. Substituting Eq. (B.4) into Eq. (B.3) and taking the node velocities out of the integral gives

$$T^e = \frac{1}{2}\rho A \dot{\mathbf{u}}^{e^T} \int (\mathbf{N}^e)^T \mathbf{N}^e dx \dot{\mathbf{u}}^e. \tag{B.5}$$

The mass matrix is derived from the Hessian of T^e

$$\mathbf{M} = \frac{\partial^2 T}{\partial \dot{\mathbf{u}}^e \partial \dot{\mathbf{u}}^e} = \frac{1}{2}\rho A \int (\mathbf{N}^e)^T \mathbf{N}^e dx. \tag{B.6}$$

If in the in static equilibrium, the internal forces, $\mathbf{p}$, balance the external forces, $\mathbf{f}$, the residual forces $\mathbf{r} = \mathbf{p} - \mathbf{f}$ becomes zero. The internal force vector can be obtained by taking the first variation of the internal energy with respect to the node displacements as

$$\mathbf{f} = \mathbf{p} = \frac{\partial U^e}{\partial \mathbf{u}^e}, \tag{B.7}$$

in which U^e is the internal energy and is defined by

$$U^e = \frac{1}{2} A \int \sigma \epsilon dx. \tag{B.8}$$

We introduce the Green-Lagrange strain as

$$\epsilon = u_x + \frac{1}{2} {u_x}^2 = \mathbf{B}\mathbf{u}^e + \frac{1}{2}(\mathbf{B}\mathbf{u}^e)^2, \tag{B.9}$$

where $\mathbf{B}$ is the deformation matrix and upon substitution in Eq. (B.8) we get

$$U^e = \frac{1}{2} AE(\dot{\mathbf{u}}^{e^T} \int \mathbf{B}^T \mathbf{B} dx \mathbf{u}^e + \dot{\mathbf{u}}^{e^T} \int \mathbf{B}^T \mathbf{B}\mathbf{B} dx \mathbf{u}^{e2} + \dot{\mathbf{u}}^{e^{T^2}} \int \frac{1}{4} \mathbf{B}^T \mathbf{B}\mathbf{B}^T \mathbf{B} dx \mathbf{u}^{e^2}). \tag{B.10}$$

The internal force vector becomes

$$\begin{aligned} \mathbf{f} = \frac{1}{2} AE(&\int \mathbf{B}^T \mathbf{B} dx \mathbf{u}^e + \dot{\mathbf{u}}^{e^T} \int \mathbf{B}^T \mathbf{B} dx + \int \mathbf{B}^T \mathbf{B}\mathbf{B} dx \mathbf{u}^{e^2} + \\ &\dot{\mathbf{u}}^{e^T} \int \mathbf{B}^T \mathbf{B}\mathbf{B} dx \mathbf{u}^e + \dot{\mathbf{u}}^{e^T} \int \frac{1}{2} \mathbf{B}^T \mathbf{B}\mathbf{B}^T \mathbf{B} dx \mathbf{u}^{e^2} + \dot{\mathbf{u}}^{e^{T^2}} \int \frac{1}{2} \mathbf{B}^T \mathbf{B}\mathbf{B}^T \mathbf{B} dx \mathbf{u}^e). \end{aligned} \tag{B.11}$$

Now that the mass matrix and the force vector are formed we can integrate Eq. (B.1) by any integration method and find the displacement field and its gradient at every point in time.